SYNTHESIS AND CHARACTERIZATION OF CARBON NANOTUBES USING SCANNING PROBE BASED NANO-LITHOGRAPHIC TECHNIQUES

A Thesis

by

ROHIT VASANT GARGATE

Submitted to the Office of Graduate Studies of
Texas A&M University
in partial fulfillment of the requirements for the degree of

MASTER OF SCIENCE

December 2008

Major Subject: Mechanical Engineering

SYNTHESIS AND CHARACTERIZATION OF CARBON NANOTUBES USING SCANNING PROBE BASED NANO-LITHOGRAPHIC TECHNIQUES

A Thesis

by

ROHIT VASANT GARGATE

Submitted to the Office of Graduate Studies of
Texas A&M University
in partial fulfillment of the requirements for the degree of

MASTER OF SCIENCE

Approved by:

Chair of Committee,	Debjyoti Banerjee
Committee Members,	Nagamangala Anand
	Kamran Entesari
Head of Department,	Dennis L. O'Neal

December 2008

Major Subject: Mechanical Engineering

ABSTRACT

Synthesis and Characterization of Carbon Nanotubes Using Scanning Probe Based Nano-Lithographic Techniques. (December 2008)

Rohit Vasant Gargate, B.E., Pune University

Chair of Advisory Committee: Dr. Debjyoti Banerjee

A novel process which does not require the traditional Chemical Vapor Deposition (CVD) synthesis techniques and which works at temperatures lower than the conventional techniques was developed for synthesis of carbon nanotubes (CNT). The substrates used for this study involved MEMS (Micro Electrical Mechanical Systems) elements and passive elements. These were coated with Fullerene using Physical Vapor Deposition or through a solution in an organic solvent. Catalyst precursors were deposited on these Fullerene coated substrates using “wet processes”. These substrates were then heated using either the integrated microheaters or external heaters in an inert atmosphere to obtain CNT. Thus, in this process we tried to obviate the Chemical Vapor Deposition (CVD) process for synthesis of CNT (SWCNT and MWCNT). The synthesized CNT will be characterized using Scanning Electron Microscopy and Raman spectroscopy techniques. Also, conductivity measurements were carried out for the synthesized tubes using Dry (contact based) and Wet (electro-chemical) methods. This work also proves the concept for the feasibility for a portable hand held instrument for synthesis of CNT with tunable “on demand” chirality.

DEDICATION

This thesis is dedicated to the Almighty for his blessings, my loving parents and my younger sister for their caring support, my elder sister and my brother in law for their motivation, to my wonderful friends for their unconditional help and to Dr. Debjyoti Banerjee for constant inspiration and guidance.

ACKNOWLEDGEMENTS

First and foremost I offer my sincerest gratitude to my advisor, Dr Debjyoti Banerjee, who has supported and guided me throughout my research with his patience and knowledge whilst trusting me to work in my own way. Without his inspiration, this thesis would not have been completed or written.

I would like to express my gratitude to Dr. Kamran Entesari and Dr. N. K. Anand for being a part of my thesis committee.

I would also like to thank Dr. Liang, Dr. Jingyi Shen and Dr. Orla Wilson at the Material Characterization Facility, Mike Pendleton and Tom Stephens at the Microscopy and Imaging Center, Brian Bachmeyer from the Instrumentation room for allowing me to use the laboratory equipments and helping me in any possible way whenever I needed. I also want to extend my gratitude to DARPA (Defense Advanced Research Projects Agency) for funding this research.

Finally, thanks to my parents and my family members, my labmates Vijay, Navdeep and Stephen, and my friends – Matthew, Tarun, Harshawardhan, Rajat, Manoj, Ranil, Sayak, Parikshit, Jared, Kevin, Chris, Andron and Roston for believing in me and being there for me whenever I needed. Special thanks to David Huitink for helping me get started with my research.

I am grateful to everyone who has helped me in some way or another throughout this entire duration.

NOMENCLATURE

CNT	Carbon Nanotube
SWCNT	Single Walled Carbon Nanotube
MWCNT	Multi Walled Carbon Nanotube
CVD	Chemical Vapor Deposition
DPN	Dip Pen Nanolithography
Si	Silicon
PdCl2	Palladium Chloride
CoCl2	Cobalt Chloride
NiCl2	Nickel Chloride
FeCl2	Ferrous Chloride
C60	Fullerene
AFM	Atomic Force Microscope
LFM	Lateral Force Microscope
SEM	Scanning Electron Microscope
FIB/SEM	Focused Ion Beam/ Scanning Electron Microscope
TEM	Transmission Electron Microscope
HR-TEM	High Resolution Transmission Electron Microscopy
XPS	X-ray Photo Electron Spectroscopy
RBM	Radial Breathing Modes
D	Defect Band

G	Graphite Band
EDS	Energy Dispersion Spectroscopy
XDS	X-Ray Dispersion Spectroscopy
d	CNT Diameter in mm
ω	Raman Shift in cm^{-1}
$\hat{C}_h$	Chiral Vector
n, m	Integers
$\hat{a}_1$, $\hat{a}_2$	Basis Unit Vectors
fn	Natural Frequency
K	Stiffness of the Spring/Beam
M	Mass of the Beam
f_1, f_2	Resonant Frequencies before and after Chemical Deposition Respectively
N	A Constant Having Values Depending on the Beam Shape.
Δm	Change in Mass of the Cantilever

TABLE OF CONTENTS

Page

ABSTRACT iii

DEDICATION iv

ACKNOWLEDGEMENTS v

NOMENCLATURE vi

TABLE OF CONTENTS viii

LIST OF FIGURES xi

LIST OF TABLES xvi

CHAPTER

I INTRODUCTION 1

1.1 Background and Motivation 1
1.2 Need for a Novel Approach 3
1.3 Carbon Nanotube - Types and Natures 4
1.3.1 Chirality 5
1.3.2 Single Walled Carbon Nanotubes (SWCNT) 8
1.3.3 Multi Walled Carbon Nanotubes (MWCNT) 9
1.4 Carbon Nanotube Synthesis Theory 9
1.4.1 Chemical Vapor Deposition (CVD) 11
1.4.2 Arc Discharge 13
1.4.3 Laser Ablation 14
1.5 Carbon Nanotube Characterization Techniques 15
1.5.1 Direct Imaging Techniques 16
1.5.1 Spectroscopy Characterization Techniques 17
1.5.2 Other Techniques 20
1.6 Introduction to Fullerenes 25
1.7 Introduction to Dip Pen Nanolithography 26
1.8 Proposed Novel Approach 29
1.8.1 Conductivity Measurements 30

II EXPERIMENTAL APPARATUS 31

CHAPTER Page

2.1 Substrates 31
2.1.1 SINDEX Chips 31
2.1.2 PIMTEM Chips 32
2.1.3 Silicon Wafers 35
2.2 Deposition and Manipulation 35
2.2.1 AFM Pens 35
2.2.2 Active Pens 37
2.2.3 Inkwell 39
2.2.4 Denton Thermal Evaporator 40
2.2.5 DPN/AFM Instrument 41
2.2.6 Focused Ion Beam (FIB) 41
2.3 Experimental Setup 42
2.4 Verification and Evaluation 45
2.4.1 XPS Instrument 45
2.4.2 Raman Spectroscopy Instrument 46
2.4.3 Scanning Electron Microscope 46
2.4.4 Transmission Electron Microscope 47

III EXPERIMENTAL PROCEDURE 49

3.1 Sample Preparation 49
3.1.1 Fullerene Deposition 49
3.1.2 Metal Catalyst Preparation 50
3.1.3 Passive Pen Bulk Deposition 51
3.1.4 Active Pen and Passive Pen Inkwell 51
3.1.5 PIMTEM Chips Bulk Deposition 53
3.1.6 DPN Pen Preparation (Double Dipping) 54
3.1.7 Substrate Patterning Using DPN Pens 55
3.2 Synthesis Experiment 58
3.2.1 Synthesis on DPN Nscriptor 58
3.2.2 Synthesis at Ambient Conditions 60
3.3 Conductivity Measurements 62
3.3.1 Dry Method 62
3.3.2 Wet Method 62
3.4 Uncertainty Analysis 64
3.5 Evaluation and Characterization 65
3.5.1 X-Ray Photoelectron Spectroscopy 65
3.5.2 Scanning Electron Microscopy 65
3.5.3 Transmission Electron Microscopy 68
3.5.4 Raman Spectroscopy 69
3.5.5 Resonance 69

CHAPTER Page

IV RESULTS AND DISCUSSION 71

4.1 Active Pen Results (Method I) 71
4.1.1 Raman 72
4.1.2 SEM 73
4.1.3 Uncertainty Analysis 74
4.2 Active Pen Results (Method II) 75
4.2.1 Raman 75
4.2.2 SEM 76
4.2.3 Resonance 77
4.2.4 Uncertainty Analysis 78
4.3 PIMTEM Chip and Si-Wafer Results (Method I) 78
4.3.1 SEM 79
4.3.2 Raman Spectroscopy 80
4.4 PIMTEM Chip and Si-Wafer results (Method II) 85
4.4.1 SEM 86
4.4.2 Raman Spectroscopy 87
4.5 Uncertainty Analysis 88
4.6 Patterned Deposition Results 88
4.7 Passive Probes Results 89
4.7.1 SEM 90
4.7.2 Raman 91
4.8 Conductivity Results 93
4.8.1 Wet Method 93

V CONCLUSION AND FUTURE DIRECTION 96

REFERENCES 99

APPENDIX I: EXTRA IMAGES 106

APPENDIX II: MATLAB CODE 119

APPENDIX III: PIMTEM CHIPS FABRICATION PROCESS 122

VITA 128

LIST OF FIGURES

Page

Figure 1: Images of a Damascus sword, at various magnifications. Top left: Damascus sword. Top right: magnified SEM image. Bottom: HR-TEM images of the blade structure, showing the presence of MWCNT's. Scale bar is 5 nm. 2

Figure 2: Schematic showing the vector diagram for the hexagonal structure of a nanotube. 5

Figure 3: The three types of carbon nanotubes, based on the chirality. 7

Figure 4: Model of a SWCNT (left) and MWCNT (right) 8

Figure 5: Schematic showing the catalytic CNT growth mechanism by the root growth and folded growth modes (Left and Right branch respectively.)....10

Figure 6: Top: Picture of a CVD apparatus. Bottom: simple schematic of the CVD apparatus....12

Figure 7: Schematic of the 'Arc Discharge' method apparatus. 13

Figure 8: Schematic of the 'Laser Ablation' method apparatus....14

Figure 9: Schematic of Raman Spectroscopy principle. Raman shift is the difference between the frequencies of incident light and inelastically scattered light. 18

Figure 10: Top – An AFM cantilever with the pyramid probe on the left, and its equivalent spring mass model on the right. Bottom – coated cantilever and the equivalent increase in the mass of model after coating. The deposition of additional mass by coating is shown in the schematic in transparent green. 22

Figure 11: X-Ray Photoelectron Spectroscopy principle. 24

Figure 12: The spherical structure of fullerenes is similar to the weave pattern of a soccer-ball. (Image Source: http://www.physics.uc.edu/~pkent/pictures/c60.html; Kroto et al., 1985) 26

Figure 13: Schematic of the DPN process. (Source: Banerjee et al., 2005)....27

Page

Figure 14: Magnified images of Sindex chip. Left: Sindex chip image taken under an optical microscope. Right: magnified SEM image showing the mesa's on the chip. 32

Figure 15: Top: AutoCAD design in the preliminary stages on the left and low magnification SEM image of the actual fabricated chip on the right. Top: design I, Bottom: design II. 33

Figure 16: Left: Backside of the chips showing the square opening etched in silicon for exposing the membrane at the center. Right: AutoCAD image showing the cross-section diagram. 34

Figure 17: Magnified image of cantilever showing the pyramid shaped tip of the scanning probe.....36

Figure 18: Left: Magnified image of the micro-cantilever array, with pyramid probes at the free end and serpentine heaters at the base. Right: lower magnification image showing the electrical connections extending towards the integrated circuit board. 38

Figure 19: Left: A low magnification image of an inkwell. Right: magnified image showing the reservoir, microchannels and the 3 wells connected to it. It also shows the inkwell label 'B' for easy identification. 39

Figure 20: A high magnification SEM image showing an individual inkwell.....40

Figure 21: A screen capture of the interface software on the FEI SEM/FIB computer interface showing the assigned pattern and the resulting pattern (overlaid next to each other for convenience). 42

Figure 22: Schematic model of the experimental setup. 44

Figure 23: Kratos Axis Ultra Imaging XPS 45

Figure 24: JY Horiba LabRam IR Raman Spectrometer 46

Figure 25: The JEOL 6400 (left) and the FEI Strata (right) Scanning Electron Microscopes. 47

Figure 26: JEOL 2010 Transmission Electron Microscope 48

Page

Figure 27: Sequence of images showing the inkwell dipping (coating) operation for a scanning probe tip in the ActivePen™ array. 52

Figure 28: A schematic showing a microcantilever with the pyramid probe dipped into a microwell of the Inkwell. 53

Figure 29: A snapshot of the InkCAD window with the CAD Pattern. The faint squares in the background are 1 µm in size. 56

Figure 30: Top: Lateral Force Microscopy scans of the deposited pattern in forward (left) and reverse (right) directions. 57

Figure 31: A line analysis of the same image in 2D, showing a X-Z axis plot. Note the colors of the graph and the corresponding positions in the LFM image. 58

Figure 32: Photograph of the experimental apparatus for synthesis at ambient conditions. 60

Figure 33: Top - Experimental setup for conductivity measurement using the wet method. Bottom – bubble formation is seen at the copper electrode in the right image. 63

Figure 34: SEM images showing charge trapping effects and the remedies that were developed in this study. Top left: Distortion of cantilevers causing damage to an active probe array. Middle Left: Vibration of an individual nanotube. Top and Middle Right: too much illumination in the charge trapped area (arrow indicates charge trapping). Bottom: samples mounted using Copper tape, sputter coating and silver paint to minimize charge trapping. 66

Figure 35: SEM image of a sample before and after sputter coating. 67

Figure 36: XPS Spectra shows a peak at ~285 eV confirming fullerene deposition 71

Figure 37: Micro-Raman spectra in the RBM mode, and D and G mode of the fullerene-coated scanning probe tip (dipped in $PdCl_2$), before (red) and after (blue) the synthesis experiment. 72

Page

Figure 38: SEM images of a microcantilever before and after the synthesis experiments, at different magnifications. The figure shows carbon nanotube bundles, which appear as hair or wire shaped material synthesized at the base of the scanning probe. 73

Figure 39: Micro-Raman spectra in the RBM mode, and D and G mode of the fullerene-coated scanning probe tip (dipped in NiCl2*)*, before (faint) and after (dark) the synthesis experiment. 75

Figure 40: SEM image of the cantilevers after the experiment showing charge trapping. 76

Figure 41: Images from the first experiment (successful with method I and Palladium catalyst) showing samples under SEM at various magnifications. 79

Figure 42: Raman spectra from the experiment. Top Row: samples with NiCl2 catalyst, second row: CoCl2 catalyst, Bottom rows: PdCl2 Catalyst..... 81

Figure 43: SEM images from the repeated experiments (with method I and Palladium catalyst) at various magnifications, showing straight CNTs..... 82

Figure 44: SEM images from the experiments using direct palladium catalyst through sputter coating at various magnifications, showing straight CNTs 83

Figure 45: Raman spectra from the method I repeated experiments showing the desired D and G peaks. 84

Figure 46: SEM images from the experiments (Pd Catalyst, Method II) at various magnifications, showing smooth and curved CNTs..... 86

Figure 47: Raman Spectra from the method II repeated experiments showing the desired D and G peaks. 87

Figure 48: SEM images of the PIMTEM chip showing the patterned deposition locations in red circles, and magnified image of each location showing successful CNT synthesis. 89

Page

Figure 49: SEM images from the experiments on passive probes as substrates (Pd Catalyst, method I) at various magnifications. 90

Figure 50: EDS micrograph obtained from the passive probe samples shows Silicon and Carbon presence. The first peak seen at 0 KeV does not mean anything. 91

Figure 51: Raman spectra from the passive probe samples. 92

Figure 52: SEM images of the passive probes obtained after doing the Raman Spectroscopy, showing the ablation of nanotubes. 93

Figure 53: Variation of current w.r.t. voltage for the two samples, showing increased currents for same voltage on the CNT coated Chips. 94

Figure 54: Logarithmic Variation of current w.r.t. voltage for two samples, showing increased currents for same voltage on the CNT coated Chips. 95

LIST OF TABLES

Page

Table I: Specifications of the 4 cantilevers of the Veeco probes. (Source: https://www.veecoprobes.com/probe_detail.asp?ClassID=17).....36

Table II: Mass of the respective components calculated using resonance techniques on the DPN platform. 77

Table III: Comparison of popular commercial methods for CNT synthesis against the novel approach. 97

CHAPTER I

INTRODUCTION

1.1 Background and Motivation

In 1991, Sumio Ijima, noticed unusual nanoscopic threads suspended in soot when observed under an electron microscope after using the arc-discharge process. (Ijima 1991). These threads of nanometer dimensions were recognized as Carbon Nanotubes (CNT). This marked the beginning of a new technology – Nanotechnology. Recent reports in literature have shown the existence of CNT (and Carbon Nano-Fibers or "CNF") being synthesized naturally at locations like volcanoes (Su and Chen, 2007).

CNTs are invisible to the naked human eye. Theoretical studies indicate that CNT can handle 1,000 times the current density of conventional conductive materials like copper or silver. CNT materials are also the strongest and stiffest materials on earth, in terms of tensile strength and elastic modulus respectively. Carbon nanotubes have been a subject of curiosity and wide investigations owing to these unique thermal (Small *et al*., 2003), electrical **(**Collins *and* Avouris, 2000**)**, and mechanical (Salvetat 1999; Treacy *et al.,* 1996) properties. This has allowed scientists to propose novel applications of nanotubes in superconductors, microelectronics, nano/micro sensors and MEMS (Micro Electro Mechanical Systems).

This thesis follows the style of *Scanning.*

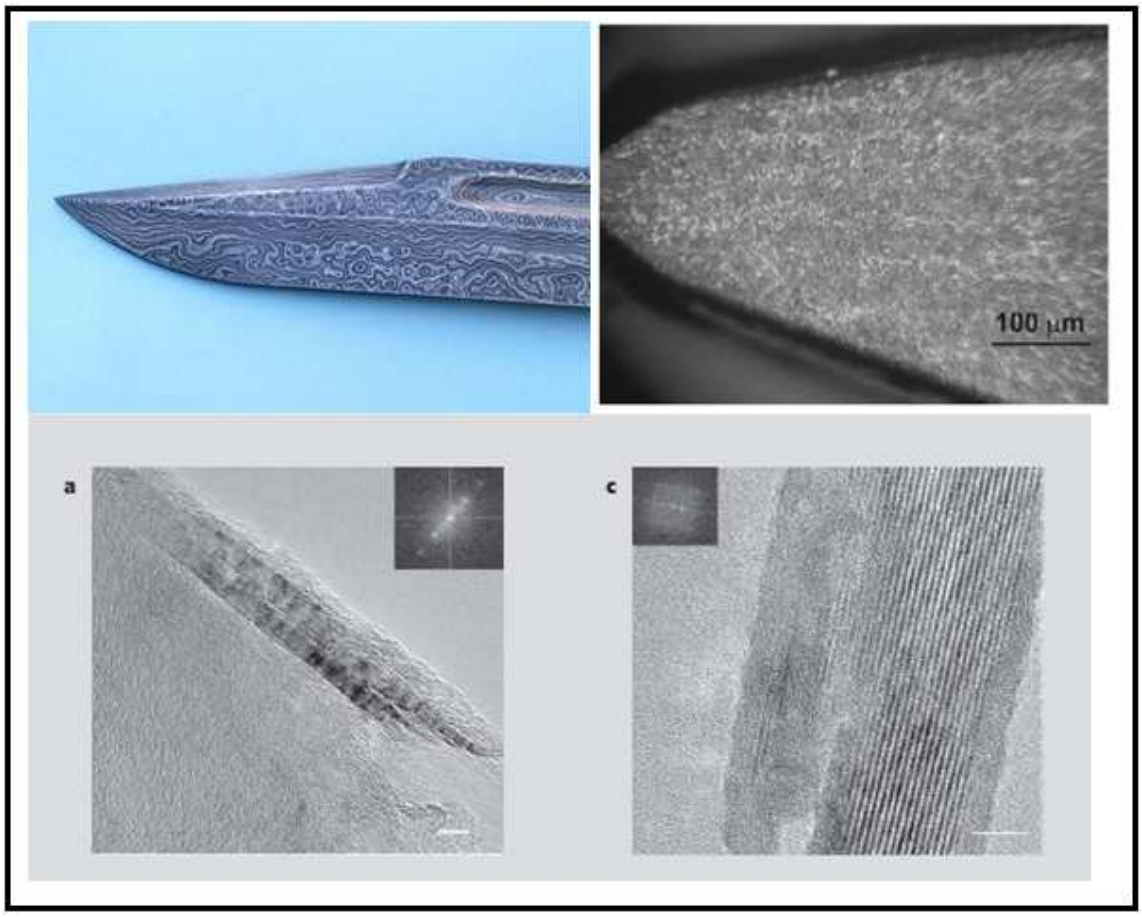

Figure 1: Images of a Damascus sword, at various magnifications. Top left: Damascus sword. Top right: magnified SEM image. Bottom: HR-TEM images of the blade structure, showing the presence of MWCNT's. Scale bar is 5 nm.
(Image source: Levin et al., 2005; Brief Communications, 2006)

Research on legendary swords having their origin in 17th century, was carried out using modern day characterization techniques. These swords have extra ordinary durability, sharpness and strength, which were shown to be due to the presence of CNT/CNF in their blade structure in High Resolution Transmission Electron Microscopy as seen in Figure 1. (National Geographic News, 2006; Brief Communications, 2006;

Levin et al., 2005). By empirically optimizing their blade-treatment procedure, craftsmen ended up making nanotubes more than 400 years ago.

1.2 Need for a Novel Approach

Since their discovery, several processes were devised for the synthesis of CNTs. These processes were aimed at 'bulk production' of carbon nanotubes, and to exploit their properties to the fullest. The original arc discharge technique was refined in 1992 (Ebbesen and Ajayan, 1992). Several other processes were developed - such as the Chemical Vapor Deposition (CVD) process and the High Pressure Carbon Monoxide Conversion Process (HiPCo) process (Ouellette *et al*., 2002).

However, irrespective of the process being used, the resultant yield is a mixture of small proportions of MWCNT (Multi-walled Carbon Nanotubes) and SWCNT (Multi-walled Carbon Nanotubes) while the major proportions of the reaction products are carbon fibers and soot. Also, in these processes the synthesized SWCNT is obtained as a mixture of metallic and semi-conducting type. Hence, conventional techniques require expensive separation processes, which are an impediment to their implementation in novel commercial devices that have been envisioned for decades.

Microelectronic applications require precise location and chirality of synthesized CNTs with high spatial density, hence successful implementation of SWCNT in nano-electronic circuits has not been possible. Some major primary challenges preventing commercial applications of CNTs in nanoelectronics are:

1. The inability to pattern SWCNT at a precise location,

2. The inability to precisely control the chirality of the synthesized SWCNT, i.e. metallic or semiconducting type (separation of SWCNT mixtures is expensive and complicated).
3. The inability to synthesize SWCNT with high spatial number density.
4. Requirement of high synthesis temperatures (of the order of 800 °C), which prevent direct synthesis of CNTs on Micro/Nano applications.

These problems motivate us to attempt a novel method for the synthesis of CNTs, wherein we aim at attaining the following goals:

1. No CVD is required.
2. Synthesis temperatures are low.
3. Precise positioning of the synthesized CNT is managed.
4. Nature of the CNTs synthesized is controlled.

The objectives of this research, thus, are to try and eliminate bulky traditional apparatus for low temperature CNT synthesis, characterize the synthesized CNTs and measure their electrical conductivity. This technique, if successful, would obviate some of the significant impediments presented by other methods that prevent the commercial application of CNT in electronic devices.

1.3 Carbon Nanotube - Types and Natures

CNT's can be basically described as seamless rectangular sheets of graphite, which are rolled in different orientations to obtain a cylindrical configuration (tube). The nature of roll angle controls the physical and chemical properties of the nanotube (Rao *et*

al., 2001). Having a length to diameter ratio of over 1000, CNT's are sometimes treated as a one dimensional structure. The structure and the orientation of the Carbon atoms within these graphitic sheets in a CNT (also called "chirality") determine the nature of the nanotube. Chirality defines the electrical and mechanical properties of the tube. Thus, the arrangement of carbon atoms and the defectiveness present in the sheet define the mechanical behavior of the nanotubes.

1.3.1 Chirality

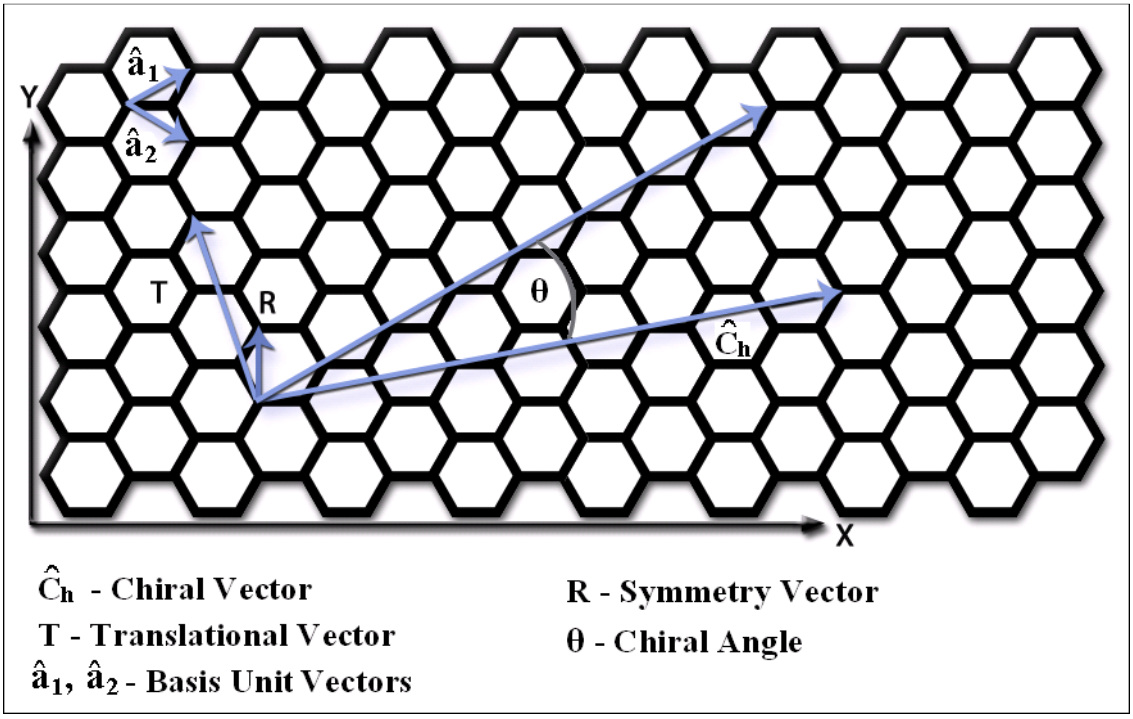

Figure 2: Schematic showing the vector diagram for the hexagonal structure of a nanotube.

Chirality of the CNTs is obtained from the description of the angle of hexagonal carbon bond pattern i.e. the angle of twist (or the wrapping angle) with respect to the central axis of the nanotube. The formula for the chiral vector is

$$\hat{C}_h = m.\hat{a}_1 + n.\hat{a}_2 \ \ (0 \leq \ m \leq n)$$

Where $\hat{a}_1$, $\hat{a}_2$ are the unit vectors in directions as seen on the figure and m and n are integers. The Chiral angle (θ) is the angle between vector a1 and the Chiral vector $\hat{C}_h$. Because of hexagonal symmetry, the chiral angle has a minimum value of 0° and maximum value of 30°. **(**Dresselhaus *et al*., 1995), where *n* and *m* are integers, and $\hat{a}_1$and $\hat{a}_2$ are the basis unit vectors shown in the hexagonal carbon network in Figure 2. As seen from the above equation, the Chiral vector depends on (n,m), and this represents chirality of the nanotubes. There are three different types of chiralities, shown in Figure 3. These can be explained as:

Armchair

For these orientations n = m or (n-m) is a multiple of 3; hence the Chiral angle (θ) is 30°. These are metallic and hence conducting in nature.

Zigzag

Here, the value of either n or m is zero, and hence the Chiral angle (θ) is 0°. These can either be conducting or semi-conducting. For zigzag CNT, one third of the (n,m) combinations are conducting, while two thirds of the (n,m) combinations are semi-conducting.

Intermediate

In this case, n and m take values other than those mentioned above, with respect to the relation$0 \leq m \leq n$, and the chiral angle (θ) ranges from 0° to 30°. These are semi conducting in nature. (Wilder *et al*., 1998)

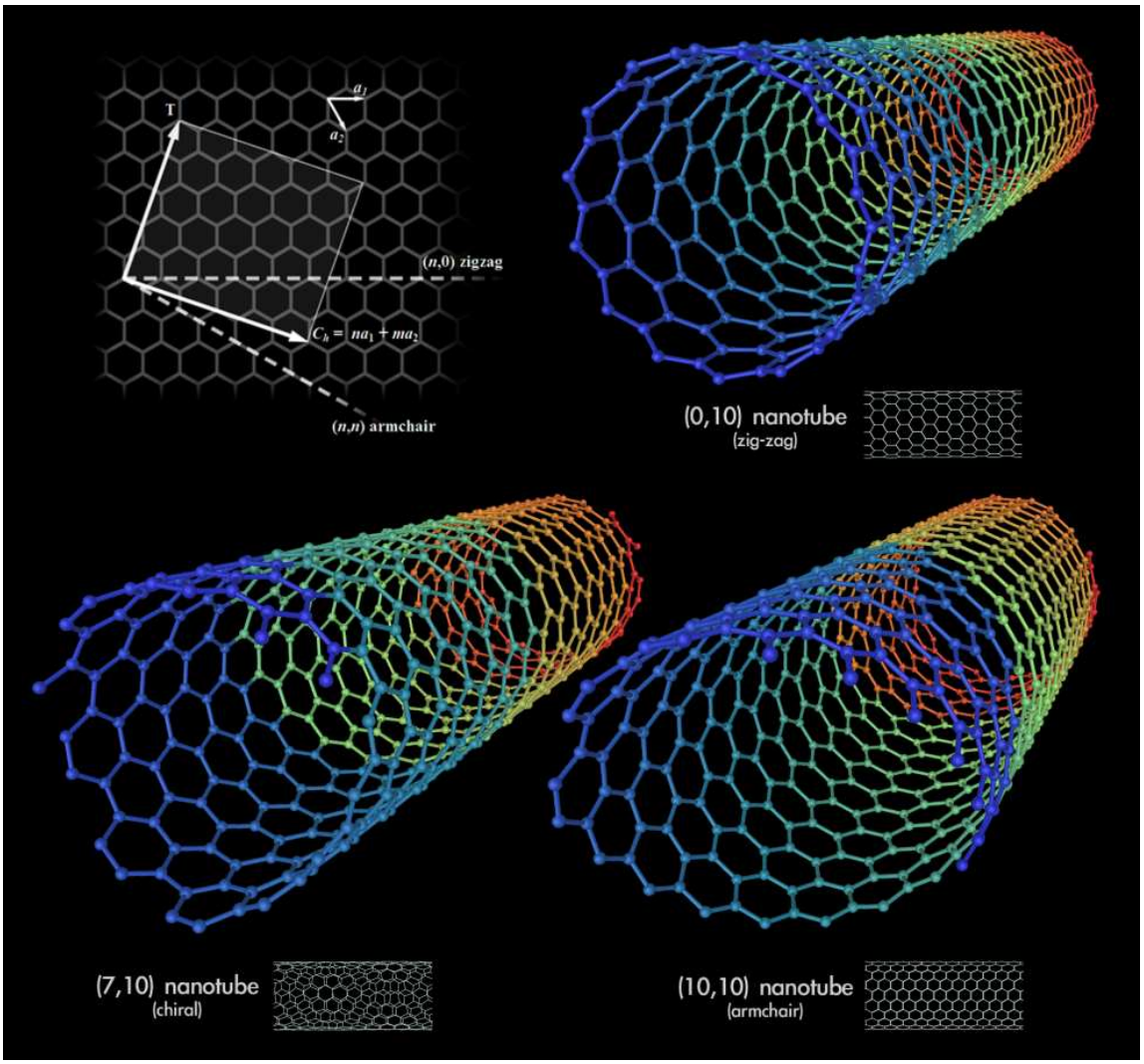

Figure 3: The three types of carbon nanotubes, based on the chirality.
(Image Source: http://www.nanoscienceworks.org/Members/siebo/657px-types_of_carbon_nanotubes.png/view)

Also, the diameter of the carbon nanotube is given by:

$$d = \frac{a_{cc}}{\pi}.\sqrt{3(n^2 + m^2 + n.m)}$$

Where, a_{cc} is the average carbon – carbon bond length (e.g. 1 Å).

Carbon nanotubes are also classified as Single walled and Multi walled, based on the number of concentric layers of graphitic sheets in the nanotube. Structure of a SWCNT and a MWCNT is shown in Figure 4.

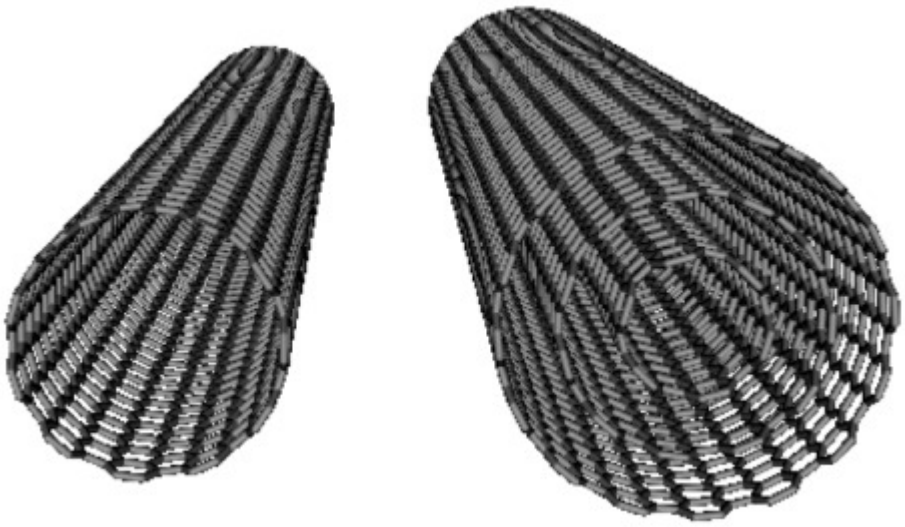

Figure 4: Model of a SWCNT (left) and MWCNT (right).
(Image Source: www-ibmc.u-strasbg.fr/ict/images/ SWNT_MWNT.jpg)

1.3.2 Single Walled Carbon Nanotubes (SWCNT)

These nanotubes are composed of a single layer of graphitic sheet. These can be conducting or semi-conducting in nature.

1.3.3 Multi Walled Carbon Nanotubes (MWCNT)

These nanotubes are composed of multiple graphitic sheets arranged concentrically in the order of increasing diameters, along the axis of the nanotube. Since these are a number of SWCNT's together, MWCNT's may have a large number defects. Depending upon the configuration a MWCNT nanotube can demonstrate structural formations like herringbone and bamboo type.

1.4 Carbon Nanotube Synthesis Theory

There are many methods reported in the literature on the synthesis of CNTs. Three major commercial methods are: Chemical Vapor Deposition (CVD) process, Arc Discharge Process and Laser Ablation Process. Despite the diversity of these techniques, the basic chemistry behind each of the synthesis processes remains the same, and so do the basic ingredients:

1. A carbon source.
2. A catalyst, which initiates the nanotube formation.
3. A heat source, to provide the enthalpy of formation.

These components may be used in solid, liquid or gaseous forms depending on the specific method.

Alternate synthesis methods have been developed which do not require catalysts, but these are not fully optimized and therefore are not used for industrial manufacturing (Journet and Bernier, 1998). The mechanism of CNT growth is not yet completely explained or understood. 'Catalytic growth model' is a popular model which explains to

a major extent the CNT formation in these synthesis processes. The nanotube formation depends on various factors such as the geometry of the catalyst particle, temperature of the process, viscous forces, structural properties of the catalysts, strength of interaction between the substrate and the particle, etc. (Vinciguerra *et al.*, 2003). Still the basic process behind the formation is explained as follows:

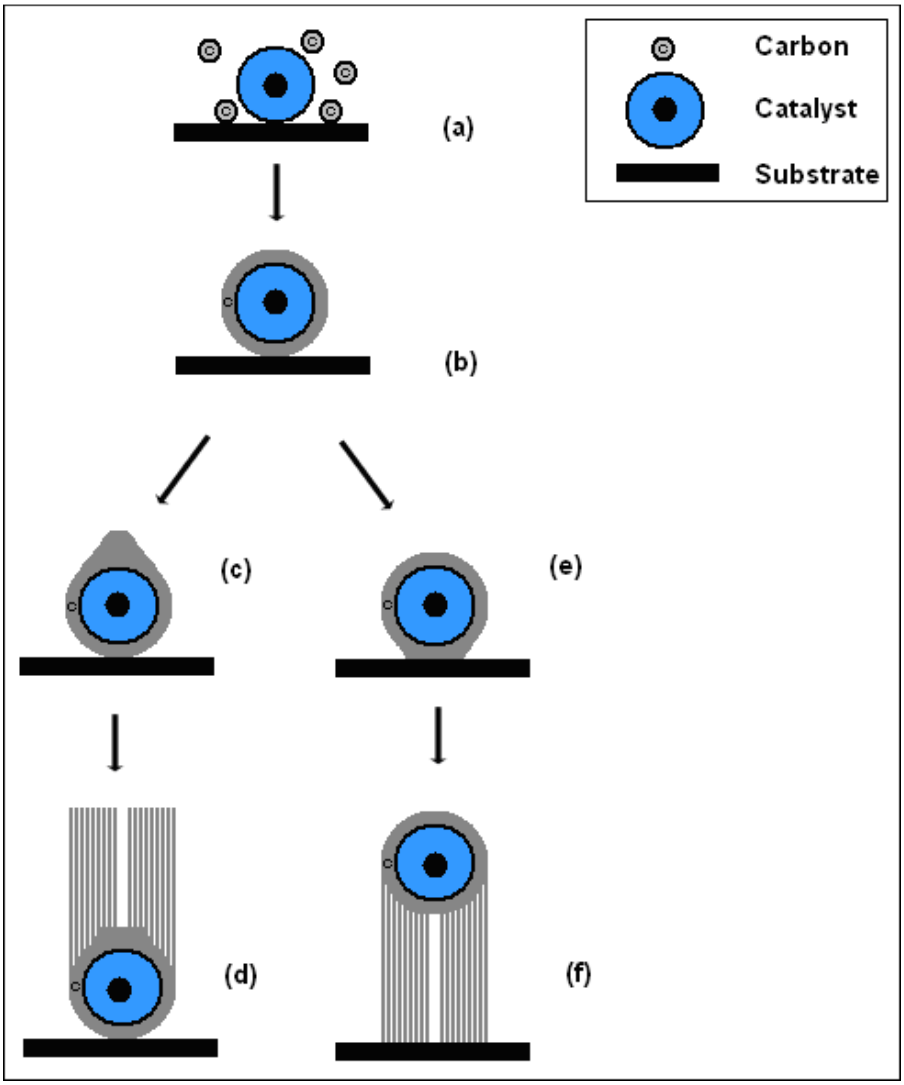

Figure 5: Schematic showing the catalytic CNT growth mechanism by the root growth and folded growth modes (Left and Right branch respectively).

The catalyst nano-particles on the substrate surface are surrounded by carbon atoms which come from the carbon source. As temperature increases, the carbon atoms diffuse and eventually saturate the catalyst particle. The tube formation takes place around this saturated catalyst particle in an inert or reducing atmosphere in one of possibly two models. The concept is illustrated in Figure 5.

In the "Root Growth" mode **(**Dai *et al*., 1996) (left branch in figure 1), a carbon wall thrusts up, the catalyst particle being its root or foundation.

In the "Folded Growth" mode (Louchev *et al*., 2003) (right branch in figure 1), carbon nano-tubes grow from beneath the catalyst particles, supporting it while the nanotube evolves.

These models are differentiated based on the position of the catalyst particle. In both the cases, if a single wall is structurally too weak to support the entire length of the nanotubes (or the catalyst particle is larger), multiple wall formation may occur. Hence the formation of SWCNTs or MWCNTs is explained using these models.

1.4.1 Chemical Vapor Deposition (CVD)

This is the most popular method due to its simplicity. This process uses a carbon source in a gaseous form, unlike the other two methods. Gases like Methane and Acetylene are used for the purpose. The decomposition of these hydrocarbons is then carried out, with the use of external energy source like a heated coil.

The substrate is placed in a reactor or a furnace. Figure 6 shows an actual CVD furnace and its schematic. The process gases flow into the furnace. The organic process

gas cracks into the carbon particles at high temperatures. The carbon particles diffuse into the catalysts (as explained earlier to eventually form CNTs). An inert gas prevents the oxidation of the synthesized CNT.

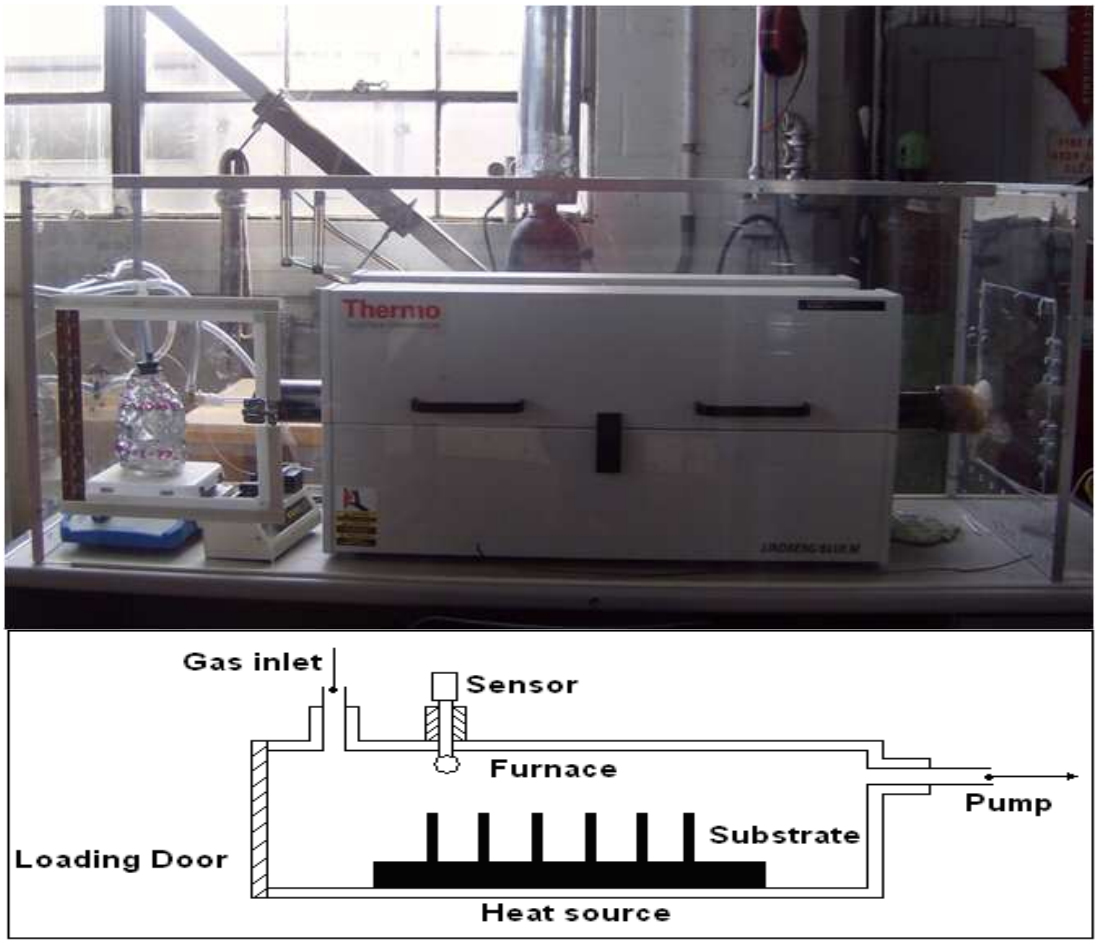

Figure 6: Top: Picture of a CVD apparatus. Bottom: simple schematic of the CVD apparatus.

The temperature is monitored by a thermocouple and valves are used to control the gas flow from the storage cylinder. The apparatus is placed in a sealed chamber which is maintained at negative pressure using exhaust gases.

1.4.2 Arc Discharge

In this process, controlled vaporization of solid carbon is carried out in inert atmosphere in presence of a catalyst (Journet et al., 1997).

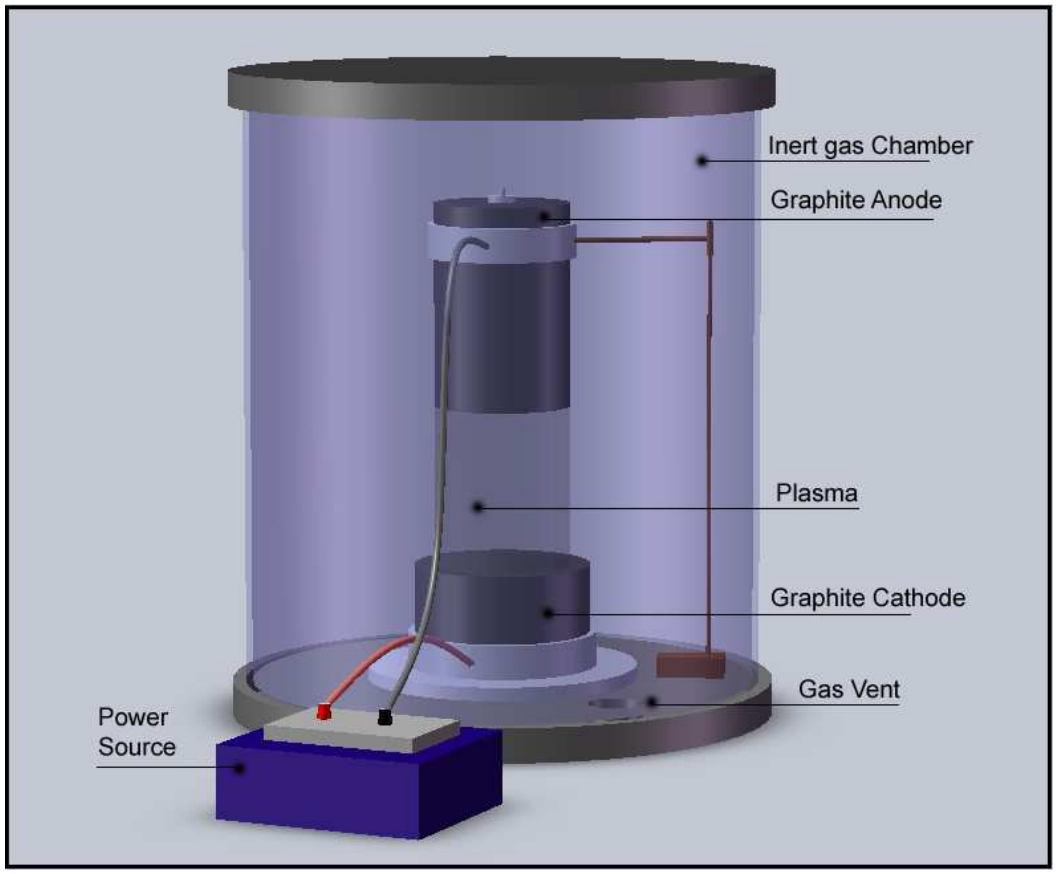

Figure 7: Schematic of the 'Arc Discharge' method apparatus.

There are two carbon rods in the apparatus as seen in Figure 7. These rods act as anode and cathode. The arc is produced between these two electrodes by applying voltage of the order of kilovolts across them. The catalyst is introduced into the gas streams through a hole drilled in the anode. This results in formation of plasma, which is

a mixture of the vaporized carbon, catalyst and inert gas. The very high temperature of the arc leads to CNT soot formation of soot and CNT. The reaction products are deposited on the electrode i.e. the cathode. To sustain the plasma arc, this process is typically performed at reduced pressures.

1.4.3 Laser Ablation

Similar to the Arc Discharge process, this method utilized solid carbon source, and its vaporization in controlled atmosphere (Guo et al., 1995). Figure 8 illustrates the Laser Ablation apparatus.

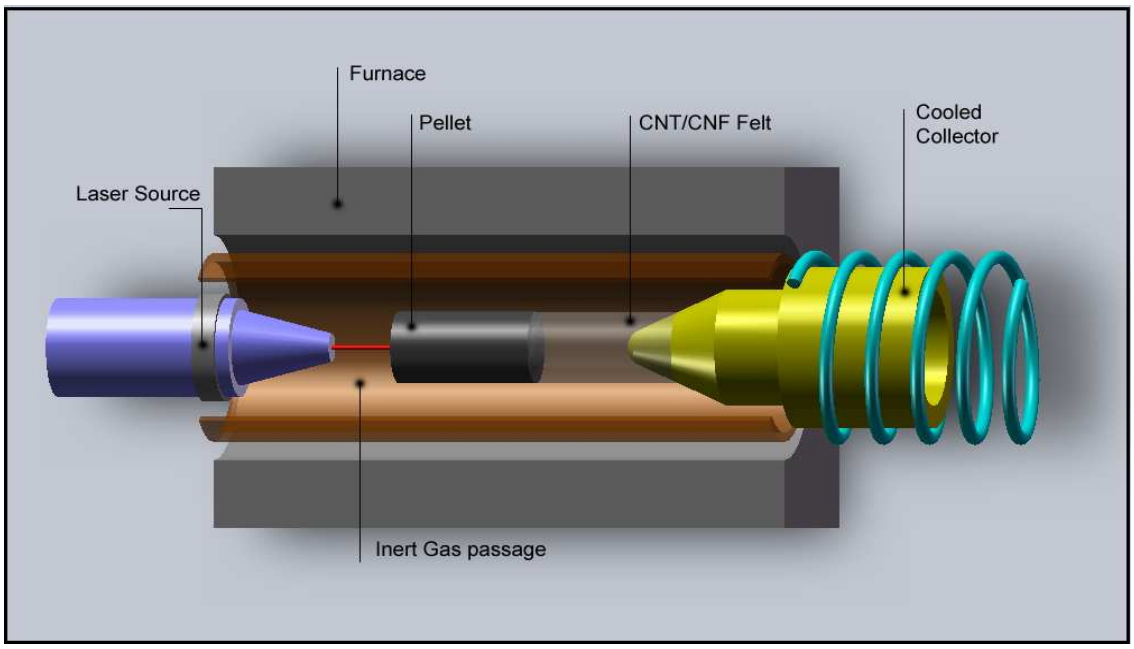

Figure 8: Schematic of the 'Laser Ablation' method apparatus.

Here, a laser source is used, which provides energy in the form of laser radiation for the CNT synthesis. A graphite pellet is used as the source and the substrate. This pellet is doped with a catalyst. This pellet is heated in a furnace to a temperature of around 1200 °C followed by directed irradiation with a laser. After the CNT formation takes place, and these CNTs which are suspended in soot are carried away using inert gas flow and are deposited on a cooled copper surface.

CNT's produced using laser and arc discharge method are of a higher quality than that in the CVD with respect to the percentage yield of tubes, compared to soot and amorphous carbon. Also the high temperature in these two cause annealing effects in nanotubes, thus reducing the defects in CNT. However, the cost is higher than that in CVD.

1.5 Carbon Nanotube Characterization Techniques

After the synthesis of CNTs, the next important step is to confirm its presence and determine their type and characteristics, i.e. 'characterize' the CNTs. The characterization of CNT is a significant component for qualifying the process. Hence Carbon nanotubes are characterized using a variety of different methods. Some of the commonly used techniques today are:

Microscopic Characterization Techniques:

1. Scanning Electron Microscopy (SEM).
2. Transmission Electron Microscopy (TEM).
3. Atomic Force microscopy (AFM).

Spectroscopy Techniques:

4. Raman Spectroscopy.
5. Absorption Spectroscopy.
6. X-Ray/Energy Dispersion Spectroscopy (EDS/XDS).
7. Infrared Spectroscopy.

Other Techniques:

8. Thermal Analysis.
9. Resonance Analysis.
10. Neutron Diffraction.
11. X-Ray Photoelectron Spectroscopy (XPS) (Eichhorn and Stolle, 2007).

The techniques proposed for this research are mainly Raman spectroscopy, Scanning Electron Microscopy and Transmission Electron microscopy. These are very widely used and reliable methods for CNT characterization. SEM and Raman are used as complementary characterization techniques, for validating the results mutually.

1.5.1 Direct Imaging Techniques

Scanning Electron Microscopy and Tunneling Electron Microscopy are direct visual imaging techniques, where the synthesized CNTs can be imaged at various ranges of magnification.

In SEM, the image of the sample surface is formed by scanning the surface with a high-energy electron beam in a raster scan pattern. These electrons are reflected by the nucleus of the atoms in the sample. These are known as Backscatter electrons. Also

electrons from the atoms of sample itself get dislodged under intense electric field. These are known as secondary electrons. Signals are thus produced which contain information about the sample's surface topography in terms on intensity of the electrons. These signals are then gathered by a detector, and rendered as high magnification images in 3D (using electrons instead of light). In case of TEM, a beam of electrons is made incident on a thin sample; and the beam transmitted on the other side of the sample is collected on a phosphor screen. This beam is of varying intensity due to filtering of electrons with respect to its cross section because of the sample, thus rendering a through image of the sample.

The SEM provides an outer visual image of the nanotubes, including the topography and depth, whereas the TEM, due to its ‘tunneling’ provides information about the ‘structure’ of the nanotubes. In TEM, MWCNTs show a number of concentric tubes and SWCNTs show a single walled hollow tube, thus easily distinguishing them from each other and also from the carbon nanofibers.

1.5.1 Spectroscopy Characterization Techniques

Raman Spectroscopy is popular contemporary technique to characterize the structure of carbon nanotubes. This technique is used to confirm the presence of carbon nanotube, even in situations where direct imaging techniques cannot be employed due to problems like charge trapping.

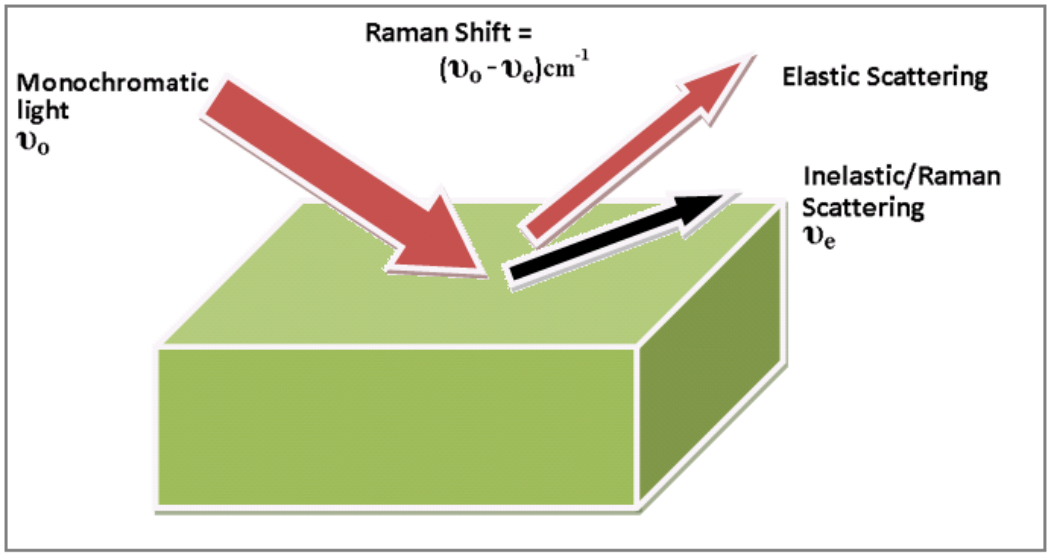

Figure 9: Schematic of Raman Spectroscopy principle. Raman shift is the difference between the frequencies of incident light and inelastically scattered light.

In Raman spectroscopy, when light is scattered from a molecule most photons are elastically scattered (same energy i.e. frequency and wavelength, as the incident photons), and a very small amount of photons scatter in-elastically (at optical frequencies different from the frequency of the incident photons). This process is the Raman Effect. This concept is illustrated in Figure 9. Raman scattering occurs due to change in vibrational energy of a molecule. The difference in energy between the incident photon and the Raman scattered photon is equal to the energy of a vibration of the molecule. A graph of intensity of scattered light versus energy difference (Raman shift) is a Raman spectrum.

When a CNT sample is excited with a laser beam, three definite categories of resonant vibrational peaks are exhibited in the resultant spectra. The resonant frequency peaks in the 1400-1700 cm^{-1} range where the G-Peaks are observed around 1600 cm^{-1} are observed. This peak arises from a graphitic mode of vibration which is a

consequence of the longitudinal vibration of the tubes. Secondly peaks in the domain ranging from 1100 to 1400 cm^{-1} ("D-Peak") is observed, which quantifies the degree of defects in the CNT sample. The low frequency range (~100-300 cm^{-1}) shows the Radial breathing Mode (RBM) peaks, (Lefrant et al., 2004) which can be used to estimate the diameter of the CNT in the sample. The RBM peaks are due to the radial pulsation of the tube cylinder. It is well known that these peaks have a monotonic relation to its diameter (Zhao *et al*., 2002).

Usually, SWCNTs have diameters up to 2 nm, and display all the three categories of peaks mentioned above. In samples containing MWCNTs, only D and G peaks are visible. In rare cases even MWCNTs display RBM peaks which can be related to the innermost tube diameters. (Zhao *et al*., 2002).

Dresselhaus developed the following empirical correlation for the determination of SWCNT diameters (diameters up to 2 nm) from Raman information, due to the relationship seen between the shift location of the RBM peak and the diameter of the tube. (Jorio *et al*., 2001)

$$d = \frac{248}{\omega}$$

where, d = Nanotube diameter in nm.

ω = Raman shift in cm^{-1}

Prior to Dresselhaus, Eklund calculated the numerator in this equation to be 223.8 nm/cm, while predicting the theoretical behavior of the rolled graphitic structure (Bandow *et al*., 1998). Other authors have noted the use of 234 nm/cm as well (Saito *et*

al., 2002); however, the value of 248 nm/cm found by Dresselhaus has been the popular choice in contemporary literature reports.

In case of SWCNT's the G peak is more dominant relative to D. The size of these peaks is a statistical representation of the concentration of the corresponding features in the tubes. MWCNT's have diameters above this range and exhibit a spectra which is similar to graphite, showing only the D and G peaks, both of which are usually of comparable intensity, owing to the larger number of defects in a MWCNT, as compared to a SWCNT (Eklund *et al*., 1995, Jorio *et al.*, 2001; Jorio *et al.*, 2004**;** Thomsen *et al*., 2004). Thus Raman spectroscopy also allows a clear identification of the structure (and type) of CNT.

The conventional synthesis techniques yield a mixture of different types of CNTs with diameters varying in some particular range. So Raman spectra is often used to find a statistical distribution of diameter of the nanotubes (and hence their chiralities).

All these aspects of Raman spectroscopy renders it as very powerful characterization technique for CNT.

1.5.2 Other Techniques

Mass based resonance analysis is not a typical characterization technique as such, but it is a technique which enables us to calculate the mass of the CNT's synthesized. It is more applicable for samples which can be vibrated at their resonant frequency, during *in-situ* synthesis of CNT. For example scanning probes can be easily vibrated at resonant frequencies using an AFM platform, in the scanning probe tapping mode.

The scanning probe tips are cantilevers which are usually rectangular or triangular in shape. These are modeled as a simple spring mass system, as shown in the Figure 10. The mass of the probe increases after the deposition of the respective chemicals, and also after the synthesis process takes place, as seen in the bottom half of the figure. Natural frequency of vibration and mass of a cantilever beam are directly related by the relation:

$$f_n = \sqrt{\frac{K}{M}}$$

where,

f_n = Natural frequency

K = Stiffness of the spring/beam

M = Mass of the beam.

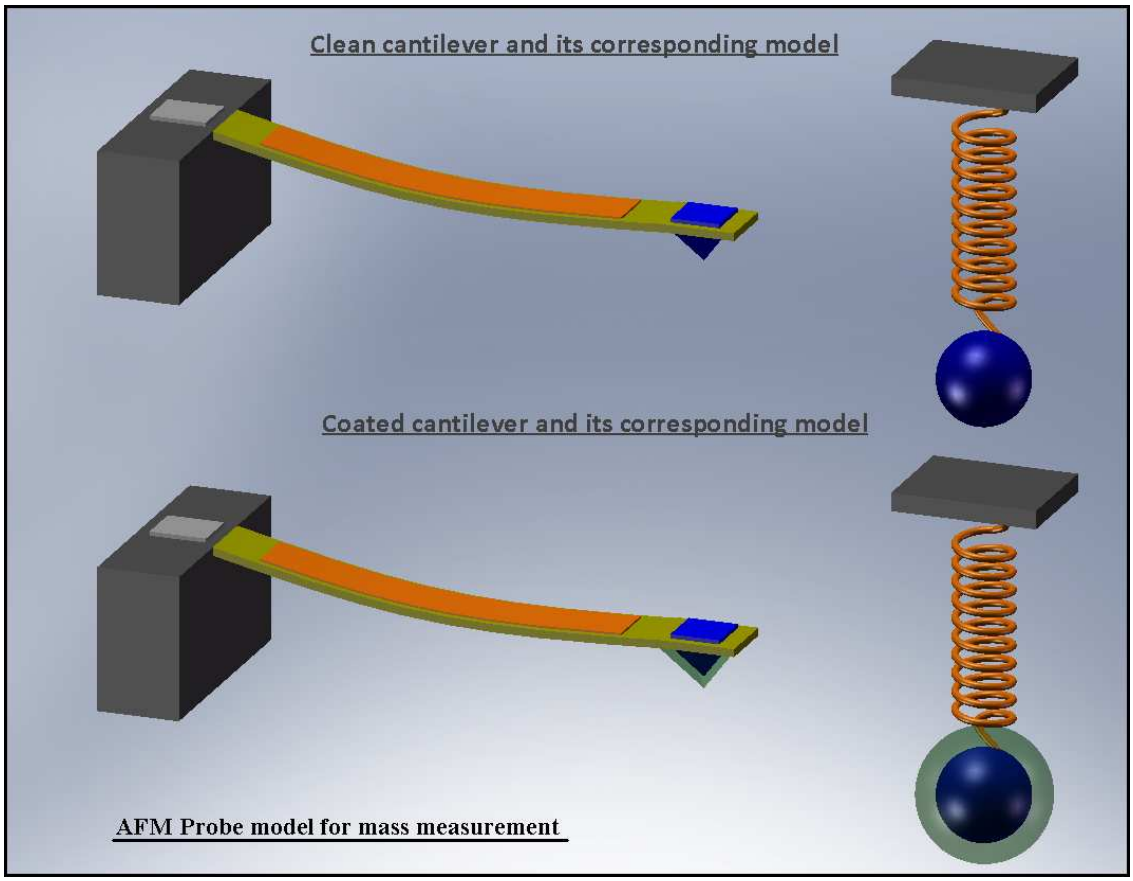

Figure 10: Top – An AFM cantilever with the pyramid probe on the left, and its equivalent spring mass model on the right. Bottom – coated cantilever and the equivalent increase in the mass of model after coating. The deposition of additional mass by coating is shown in the schematic in transparent green.

Hence, because of the increase in mass of the cantilever, the frequency decreases. Thus, if the natural frequencies for the beam are monitored at two different points in a process, the difference in the masses of the can be estimated to reasonable accuracy. In these calculations, the shift in the stiffness can be assumed negligible (Cleveland *et al*., 1993). Hence, the change in mass is given by the relation:

$$\Delta m = \frac{1}{N} . \frac{K}{4\pi^2} . \left(\frac{1}{{f_1}^1} - \frac{1}{{f_2}^1} \right)$$

where,

K = Stiffness of the spring/beam

f_1, f_2 = resonant frequencies before and after the process.

Δm = change in mass.

N = A constant, which has values depending on the beam shape.

(0.137-0.2 for V shaped, 0.24 for rectangular) (Chen *et al.,* 1994).

This method can be employed very effectively to calculate the change in mass during chemical synthesis of CNT.

X-Ray Photoelectron Spectroscopy (XPS)

XPS is a quantitative spectroscopic technique which is used to determine the elemental composition on the surface of a substrate. The process works by irradiating a sample with x-rays, resulting in the emission of photoelectrons (electrons escaping from atoms in the sample after absorbing energy from incident X-Rays).

The energies of these emitted electrons are detected using an energy analyzer. A typical XPS output is a spectrum which is a plot of the Intensity i.e. the number of electrons detected on the vertical axis against the binding energy of electrons detected on the Horizontal axis. The principle is shown in Figure 11.

All elements have known distinct spectra, with peaks at known values of binding energies.

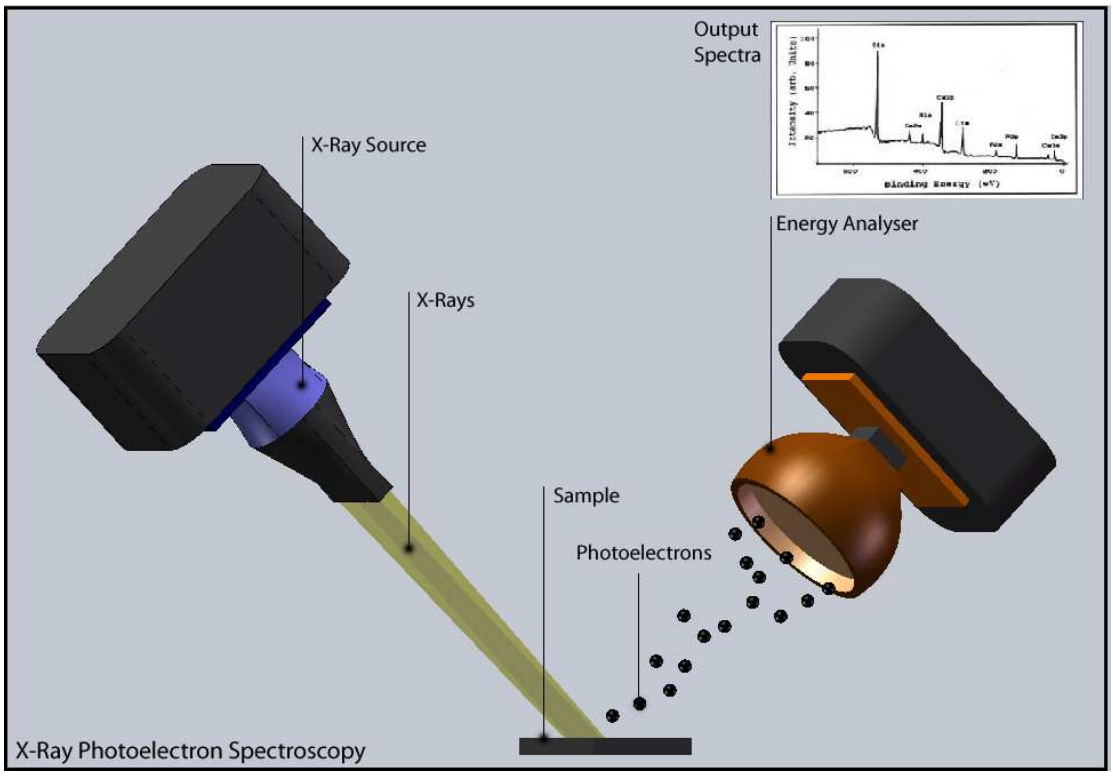

Figure 11: X-Ray Photoelectron Spectroscopy principle.

XPS systems provide the option to survey the sample for all the elements or check for a particular element. The value of the binding energies at the peaks is used to identify the particular element. XPS is not usually used as a characterization technique for CNT's specifically, but is used in the synthesis experiments to ensure the chemical deposition, detect sample compositions, contaminations etc.

Energy Dispersive Spectroscopy (EDS)

Scanning Electron Microscopes usually come with an inbuilt EDS unit. Energy dispersive spectroscopy (EDS) measures the number of x-rays produced by a solid sample when irradiated by electrons versus the energy of these x-rays. Thus it is used for rapid identification and quantification of the elemental composition of the sample.

Electron Diffraction (ED)

Electron diffraction of solid samples is usually performed in a Transmission Electron Microscope (TEM) where the electrons pass through a thin film of the material to be studied. The resulting diffraction pattern is then observed on a fluorescent screen and recorded. AD helps to determine whether the sample is crystalline, amorphous or fibrous in nature. This technique helps to distinguish CNT from CNF's.

1.6 Introduction to Fullerenes

Fullerenes (also called "Buckyballs") were discovered in 1985 by Robert Curl, Harold Kroto and Richard Smalley at the University of Sussex and Rice University, and are named after Richard Buckminster Fuller. Like diamonds, Fullerenes are stable allotropes of Carbon. Due to their spherical structure consisting of 60 carbon atoms, they are also called as C-60 **(**Kroto *et al*., 1985**)**.

The structure of carbon nanotubes is very similar to the buckyballs (seen in Figure 12), except that CNT have elongated, cylindrical structure.

Thus Fullerenes are an ideal choice as organic source for synthesis of carbon nanotubes. MWCNT formation from fullerenes has been observed before in experiments at relatively low temperatures at about 500 ºC (Czerwosz *et al*., 1999). This temperature is lower than the temperatures recorded in the synthesis experiments which used other carbon sources as discussed earlier.

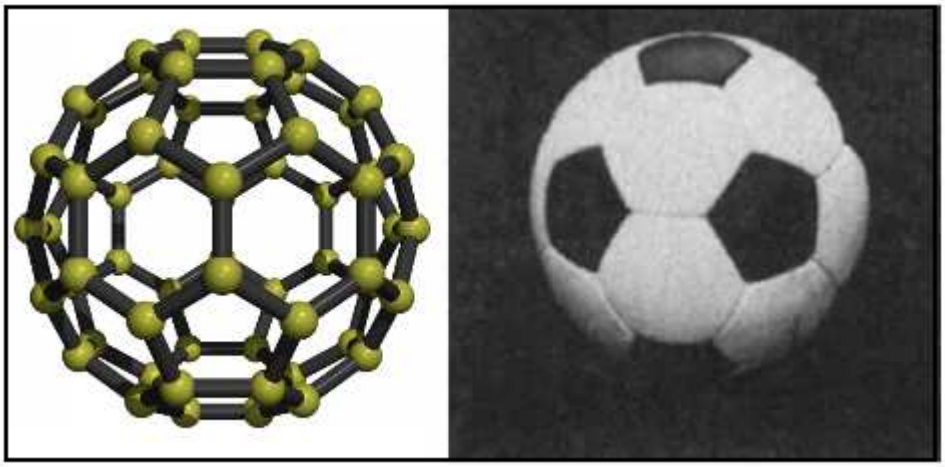

Figure 12: The spherical structure of fullerenes is similar to the weave pattern of a soccer-ball. (Image Source: http://www.physics.uc.edu/~pkent/pictures/c60.html; Kroto et al., 1985)

All these properties therefore make fullerene an ideal candidate for CNT synthesis.

1.7 Introduction to Dip Pen Nanolithography

DPN (Dip-Pen Nano-Lithography) is a lithographic technique, in which various material (ink) coated on a sharp object is transported to a substrate (paper) via capillary mechanisms. The sharp object typically used is the tip of a scanning probe, e.g., AFM (Atomic Force Microscopy) probe. This probe is chemically coated using standard procedures, and then made to contact the substrate surface. The substrate is a smooth surface on which the probe is moved when in contact, in a controlled fashion with nanometer precision. Under ambient conditions, a water meniscus is formed between the probe tip and the substrate. This capillary condenses water from the humidity present in the atmosphere forming a water meniscus around the tip. During the lithography, the

molecules of the coated chemical get transferred from the probe tip to the substrate, thus leaving a deposit 'trail' of the chemical wherever the tip moves on the substrate. The process is demonstrated in Figure 13 (Piner *et al*., 1999).

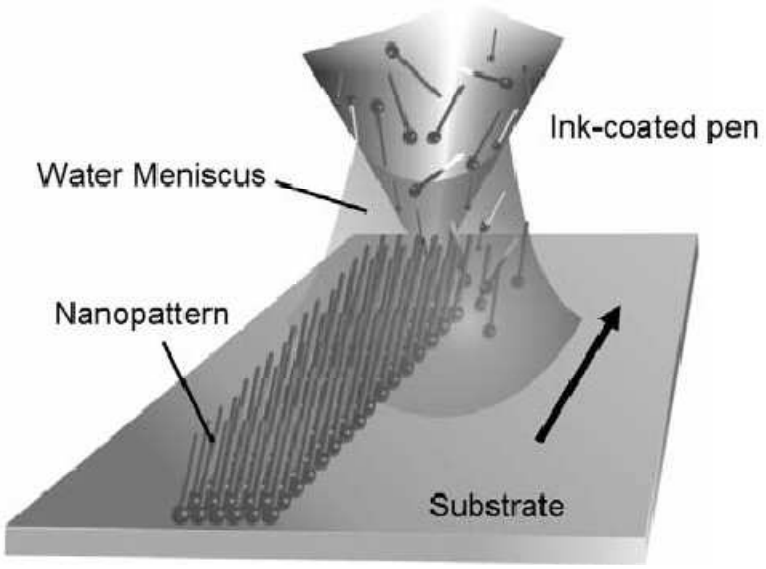

Figure 13: Schematic of the DPN process. (Source: Banerjee et al., 2005)

Conventionally, DPN is used to pattern and deposit materials on the nanometer scale, leading to improved and novel applications. Applications of DPN are envisioned for novel devices such as advanced chemical and biological sensors. (Diegoli *et al*., 2007). Furthermore, using multi-tipped pens, several symmetrical nanostructures can be created simultaneously and at precisely defined positions at regular intervals.

DPN offers a rapid method of producing chemical templates with customized chemical composition and structure, which provides a great way of investigating and characterizing nanoscale phenomenon. Using this technique surfaces properties can be directly 'altered' at a fine resolution. Various combinations of materials can be added resulting in a range of patterns, with different shapes and sizes. DPN has been used for

patterning biological molecules like DNA (Demers *et al*., 2002), peptides (Cho and Ivanisevic, 2005, Cho and Ivanisevic, 2004, Jiang and Stup, 2005), proteins (Lee *et al*., 2003; Lim *et al*., 2003), viruses (Cheung et al., 2003) and bacteria (Rozhock *et al.,* 2005) into nanoarrays for studying their behavior and various other aspects.

In a similar approach, IBM has developed a prototype called Millipede which is a nano-storage device. This device utilizes scanning probe techniques using multiple cantilevers. It can store 20 times more data than any currently available magnetic storage medium. The prototype's capacity would enable the storage of 25 DVDs on a small area, the size of a postage stamp (Vettiger *et al*., 2000).

This research is an extension of work done earlier where science of dip pen nanolithography was shown to be viable means of producing CNTs in a controlled fashion when used in conjunction with CVD synthesis processes. DPN was used as a means of controlled delivery of catalyst materials, allowing “nano-gardening” of tubes in specified locations. Results from this research indicated that the tubes grown using this process can be designed as metallic or semiconducting in type, based on the selection of catalyst (Huitink *et al*., 2007). Another part of this research demonstrated use of a specially designed and fabricated microfluidic device called Centiwells, which further enhances the DPN process by allowing the coating of multiple scanning probes with different chemicals by using the 96 microwells embedded in it. Thus this device makes it possible to deposit different chemicals at desired locations simultaneously (Rivas-Cardona and Banerjee, 2007).

We thus try to consolidate the previous studies in this research and explore this direct-write technique which offers high-resolution patterning capabilities for deposition of number of chemicals on a variety of substrates, which is then utilized for CNT synthesis.

1.8 Proposed Novel Approach

Based on the requirements itemized in sections 1.2 and 1.6, in this study Fullerenes as the source of Carbon for the CNT synthesis. In this study, Fullerenes were deposited on the MEMS elements either in the form of a solution, by using direct/physical thermal vapor deposition (PVD). Over this, a layer of catalysts was deposited using dip pen and wet techniques. Various catalysts were used for the synthesis, such as Fe, Ni, Pt, Pd, etc. **(**Li *et a*l., 2001**).** The synthesis was performed on these substrates by heating the substrates. Various parameters like temperature, catalyst layer thickness and fullerene deposition thickness were altered to optimize the process. Bulk deposition of the catalysts was performed to probe the novel synthesis concepts. Dip Pen Nanolithography techniques were explored for controlled deposition of the catalysts as a means for patterned growth of CNT. Materials characterization was performed after the synthesis to evaluate the effect of the various approaches on the synthesized CNT.

1.8.1 Conductivity Measurements

The conductivity of synthesized nanotubes were measured using dry and wet methods. The dry method involves a direct contact based approach, wherein the substrate with the synthesized CNTs was part of an electrical circuit which includes a power supply across it with an Ammeter in series and Voltmeter in parallel. This circuit was devised on an AFM platform, and conductive AFM probe was used to make contact with the CNTs. LFM images provide accurate measurements of nanotube positions on the substrate and the AFM controller allows nano-scale movements for precise positioning of the probe. The current and voltage readings were noted on the Ammeter and Voltmeter, and compared with the readings from a bare conducting substrate to find the conductivity on the synthesized CNTs.

The wet method involved an electro-chemical approach for the conductivity measurements. Here, an “Electrolytic Cell” apparatus was assembled. A salt solution in de-ionized water was used as electrolyte. The substrate with CNTs on it served as one electrode while another regular copper electrode was used as the complementary electrode. Again the voltage and current readings from the substrate-electrode was compared to readings from a bare electrode to obtain the conductivity measurements for nanotubes.

CHAPTER II

EXPERIMENTAL APPARATUS

The elements and features produced as a result of this of this research are far smaller than the optical wavelength in the visible spectrum. Hence several nanoscopic precision techniques for experimentation, visualization, measurement and characterization were used in this study.

2.1 Substrates

The choice of substrates is significant as they serve as the base for CNT growth. These substrates need to be thermally conductive, and have low thermal inertia as well for rapid response to temperature increase to enable efficient transfer of heat from the source to the substrate surface, in order to facilitate synthesis and growth of CNT on the patterned catalysts on the surface of the substrates. Four types of substrates were used for this research: PIMTEM™, SINDEX™, Active Probes™, and Passive scanning probes. The last two are discussed in the next section, since they also serve additional metrology functions.

2.1.1 SINDEX Chips

The SINDEX™ substrates are shown in Figure 14 and are commercially available from Bioforce Nanosciences, Ames, Iowa. These are gold coated - silicon substrates. They have a 15 x 15 array of square etched Mesas. The material is thermally

conductive so it acts as a good base for CNT growth. The chips are highly planar and have surface roughness ~ 0.5 nm. This quality makes them an ideal candidate for DPN, allowing patterned growth of CNTs using DPN.

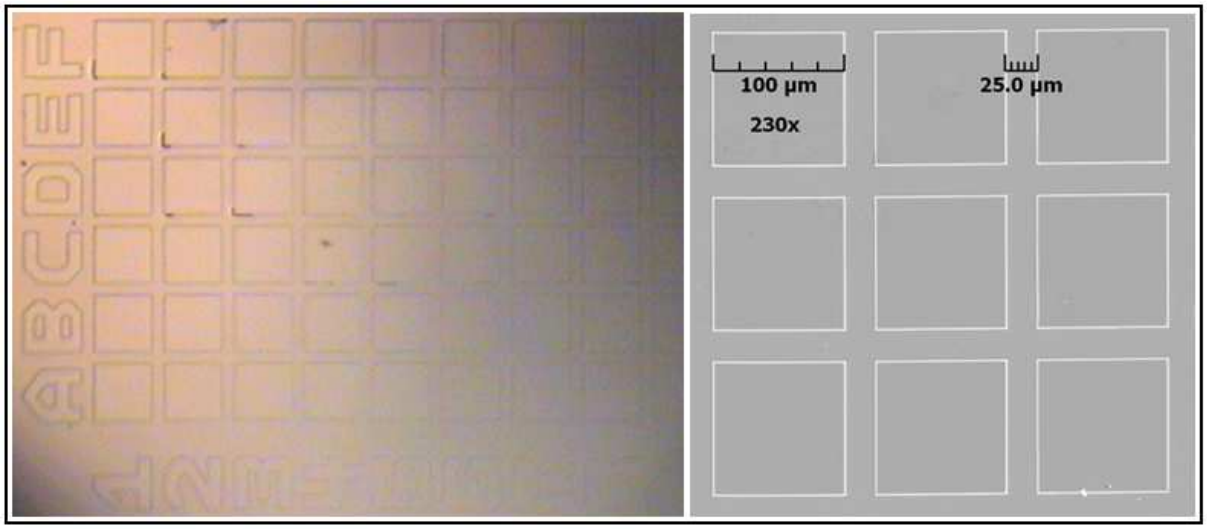

Figure 14: Magnified images of Sindex chip. Left: Sindex chip image taken under an optical microscope. Right: magnified SEM image showing the mesa's on the chip.

The mesa array is numbered vertically and horizontally using alphabets and numerals for easy re-location of any particular mesa used.

2.1.2 PIMTEM Chips

These MEMS (Micro Electro Mechanical System) substrates were designed at Texas A&M University by the author and were custom manufactured for this study and fabricated by MEMS Exchange Inc, Reston, VA. PIMTEM stands for Platform for In-situ Microscopy and Transmission Electron Microscopy. The platforms were in the form of square chips, the dimensions being 3.5 x 3.5 x 0.5 mm. The substrate material is

Silicon, and it has a thin Silicon Nitride membrane at its center. This membrane is surrounded by two serpentine microheaters made of Titanium. The fabricated PIMTEM chip is shown with its corresponding AutoCAD model in Figure 15.

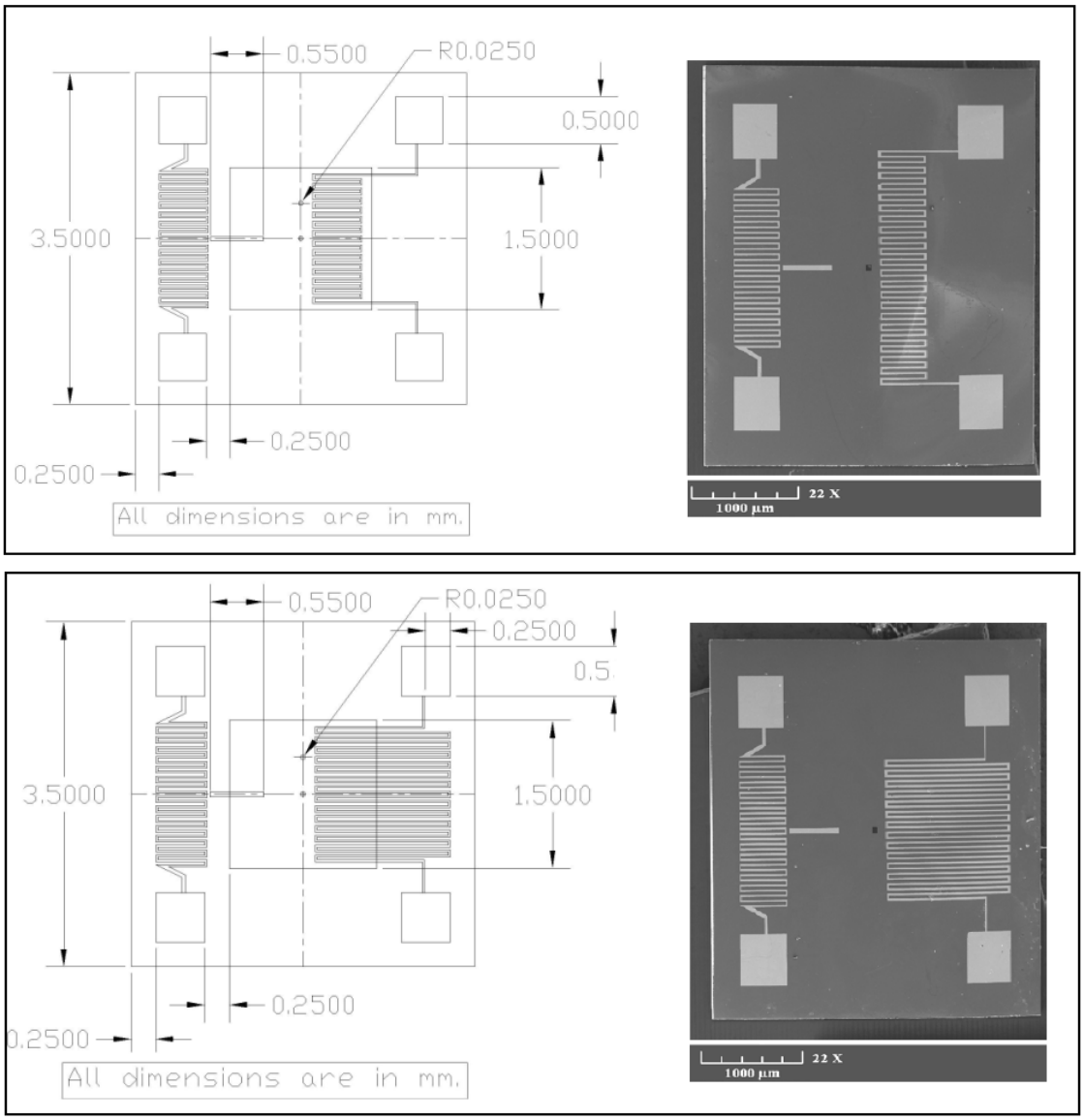

Figure 15: Top: AutoCAD design in the preliminary stages on the left and low magnification SEM image of the actual fabricated chip on the right. Top: design I, Bottom: design II.

Three different types of heaters with variation in length and orientation were used on the substrate. The lengths of the microheaters are 18 mm, 19 mm and 42 mm. The thickness of the heater elements is 100nm. The idea of integrated heaters was to eliminate external heating sources, such as the furnace in the setup, and making it more compact. A metal pad was deposited near the edge of the square membrane and perpendicular to the heaters - using “lift-off” process to serve as an ‘alignment mark’.

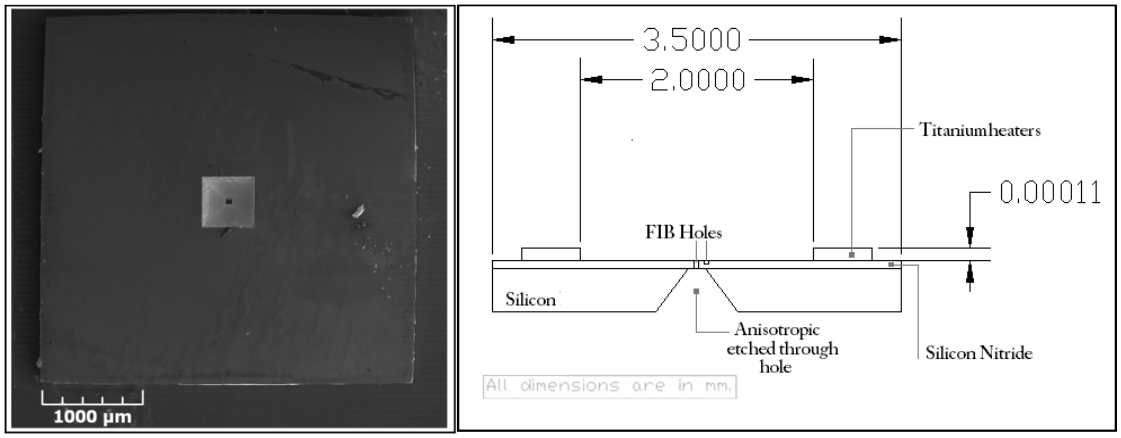

Figure 16: Left: Backside of the chips showing the square opening etched in silicon for exposing the membrane at the center. Right: AutoCAD image showing the cross-section diagram.

The alignment mark served as a locator for precise positioning of catalyst for deposition and subsequent characterization. The idea of having a thin membrane was to make this platform directly usable under the TEM. Figure 16 shows the back side of the chip with the etched membrane at the center and the side view of its AutoCAD model. The fabrication process of these chips is explained in appendix III of this thesis.

2.1.3 Silicon Wafers

These are bare silicon wafers. These were broken in smaller pieces to be used as substrates.

2.2 Deposition and Manipulation

These consist of various equipments required for depositions, scanning and various other things at a nano-scale level.

2.2.1 AFM Pens

The passive AFM probes used were the DNP - NP Series Probes manufactured by Veeco Inc, Plainview, NY. These are Triangular type passive AFM pens, and an AFM/DPN platform is necessary for using these.

There are four triangular cantilevers of different thickness and stiffness on a single probe. These are made up of Silicon Nitride. Each Cantilever has a pyramid shaped probe at its free end. This probe comes in contact with the surface during the DPN and is used for scanning for the AFM or deposition for the DPN.

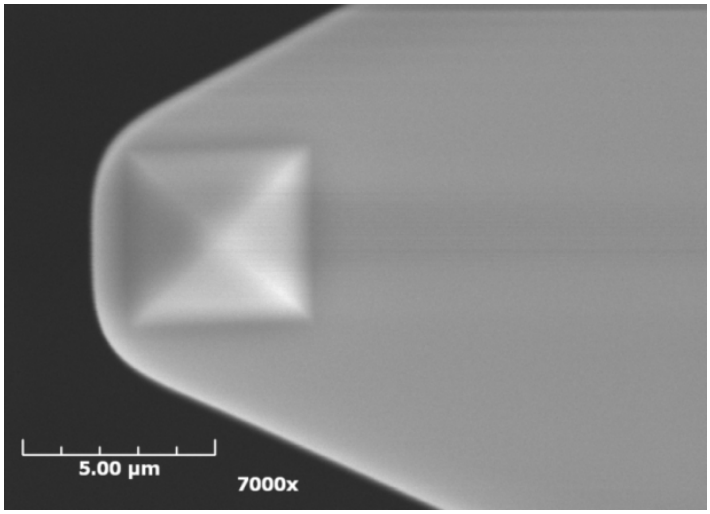

Figure 17: Magnified image of cantilever showing the pyramid shaped tip of the scanning probe.

The nominal diameter of the probe tip is 20 nm. Sharper tips provide better the resolution for scanning or deposition on a surface. Subsequently these pens were also used as substrates to grow CNTs. The aim was to make the probe tips sharper by synthesizing CNT on the tips. A magnified image of a single tip is shown in Figure 17. Some specifications are given in the Table I.

Table I: Specifications of the 4 Cantilevers of the Veeco probes. (Source: https://www.veecoprobes.com/probe_detail.asp?ClassID=17)

	Length (µm)			Width (µm)			Frequency (KHz)			Stiffness (N/m)
Tip	Nom	Min	Max	Nom	Min	Max	Nom	Min	Max	
A	115	100	115	25	20	30	57	40	75	0.58
B	196	180	196	41	33	49	20	14	26	0.12
C	115	100	115	17	13	21	56	40	75	0.32
D	196	180	196	23	18	28	18	12	24	0.06

2.2.2 Active Pens

These are similar in construction to the passive pen, with an integrated circuit, which enables passing of current and applying voltage through the probe tips (Active Pen™ System, Manufactured by NanoInk Inc, Skokie, IL). These probes are used on a Dip Pen Nanolithography™ (DPN™) instrument (NScriptor™, by NanoInk Inc.). The probe system consists of an array of 8 silicon nitride cantilevers; each cantilever is 100 microns long, 20 microns wide and with a pitch of 40 microns. At the base of each cantilever a serpentine gold microheater is micro fabricated *in situ*. A gold heat spreader extends along the length of the cantilever for facilitating uniform temperature distribution. The electrical interconnects from each microheater extends into a circuit board on which the cantilever array is packaged. The circuit board also houses a connector which plugs into the DPN instrument. At the free end of each cantilever is a pyramid shaped tip, on which the dip coating operations are performed as well as serves as the site for synthesis of CNT. The probe tips are shown in the Figure 18.

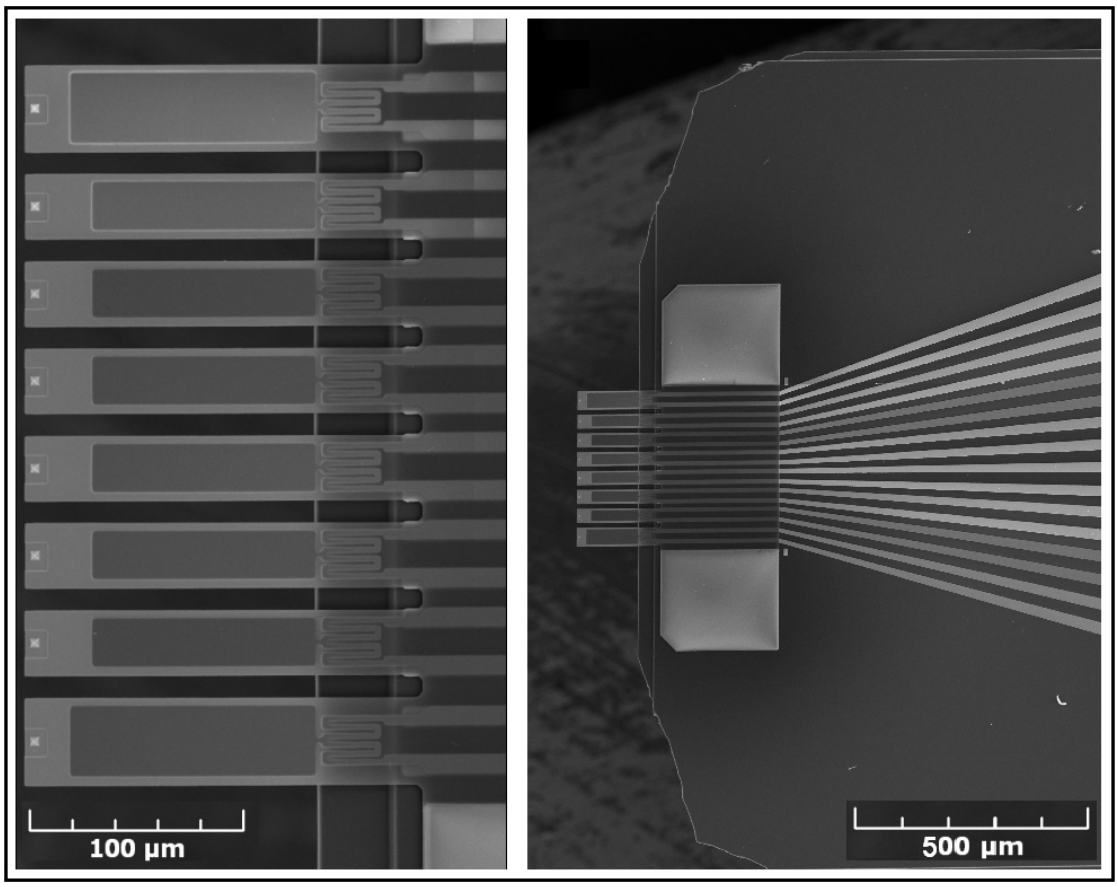

Figure 18: Left: Magnified image of the micro-cantilever array, with pyramid probes at the free end and serpentine heaters at the base. Right: lower magnification image showing the electrical connections extending towards the integrated circuit board.

The electrical connections allow us to actuate the cantilevers individually and heat them by passing current through them. Because of this feature, the active probes were also used as a substrate for CNT growth.

2.2.3 Inkwell

The inkwells consist of microwells which are connected individually to 6 reservoirs through microchannels. Figure 19 shows an inkwell with a magnified view of its reservoir, microchannel and connected wells.

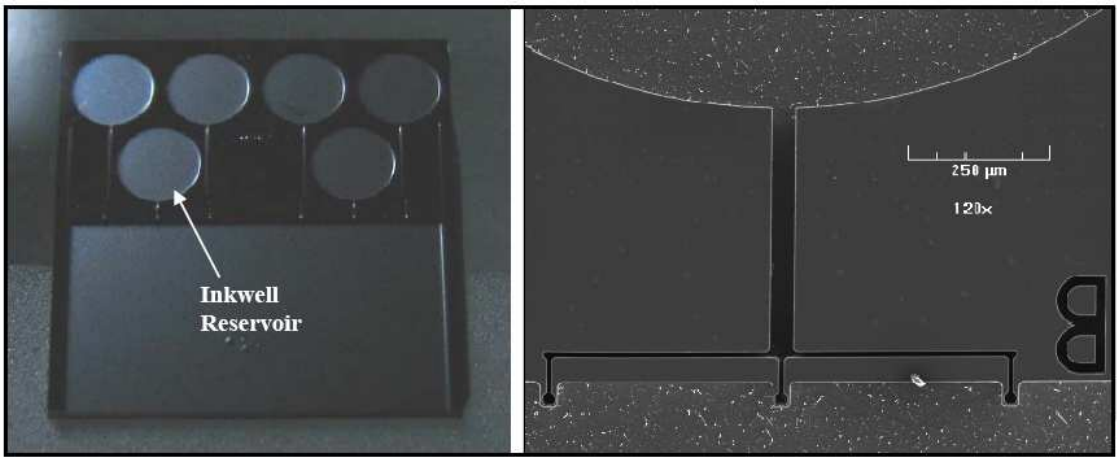

Figure 19: Left: A low magnification image of an inkwell. Right: magnified image showing the reservoir, microchannels and the 3 wells connected to it. It also shows the inkwell label 'B' for easy identification.

Different chemical solutions can be conveniently used in different wells at the same time. This enables the dipping of the different tips of an array into different chemical solutions. A single magnified well is shown in Figure 20 below.

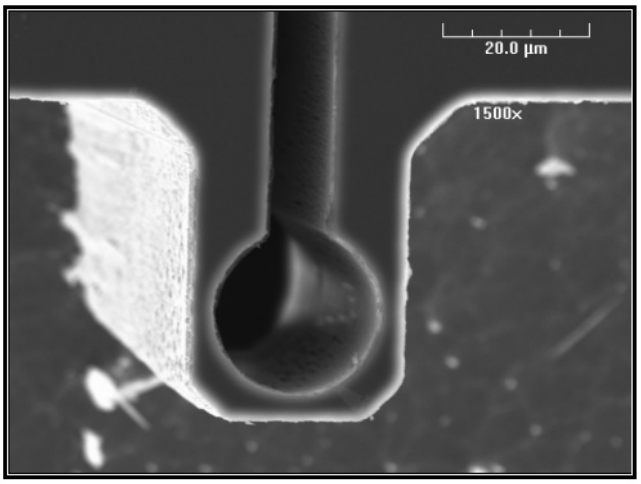

Figure 20: A high magnification SEM image showing an individual inkwell.

Use of inkwell dipping for catalyst deposition helps with localizing the area of deposition of the chemical solution. The top of the Inkwell substrate has a coating of hydrophobic material which prevents cross contamination of these different solutions.

2.2.4 Denton Thermal Evaporator

The Denton evaporator is a device used for deposition of thin films onto substrates (located at the Center for Nano-manufacturing, University of Texas at Austin). The source material is placed into a metallic boat at the bottom. By applying a high voltage across the boat, it is heated which causes evaporation or sublimation of the source material. This evaporated substance then condenses onto the target which is placed in an inverted position on the roof of the chamber. Parameters like voltage and time are adjusted to obtain the desired thickness and deposition rate. There is a provision to rotate the target to ensure a uniform deposition.

2.2.5 DPN/AFM Instrument

The DPN/AFM Instrument used for this research is the Nanoink NScriptor™ System (Nanoink Inc.) located at the Material Characterization Facility (MCF) in the Chemical Engineering Dept. at Texas A&M University. This System enables dedicated DPN experiments based on a fully functional scanning probe microscope (SPM/AFM) system. Leveraging these scanning probe capabilities, the NSCRIPTOR is optimized for both nanolithography and subsequent image acquisition. NSCRIPTOR includes a PC with the interfacing software, real-time instrument controllers, and controlled environmental chamber. This machine also has ability to resonate and measure the frequency of the AFM cantilevers, thus it's also used as a metrology platform instrument.

2.2.6 Focused Ion Beam (FIB)

The dual beam SEM/FIB system (FEI Inc, Hillsboro, OR) located at University of Texas at Austin was used. This focused Ion Beam (FIB) systems utilize a finely focused beam of gallium ions operated at low-beam currents for imaging and at high-beam currents for site-specific milling.

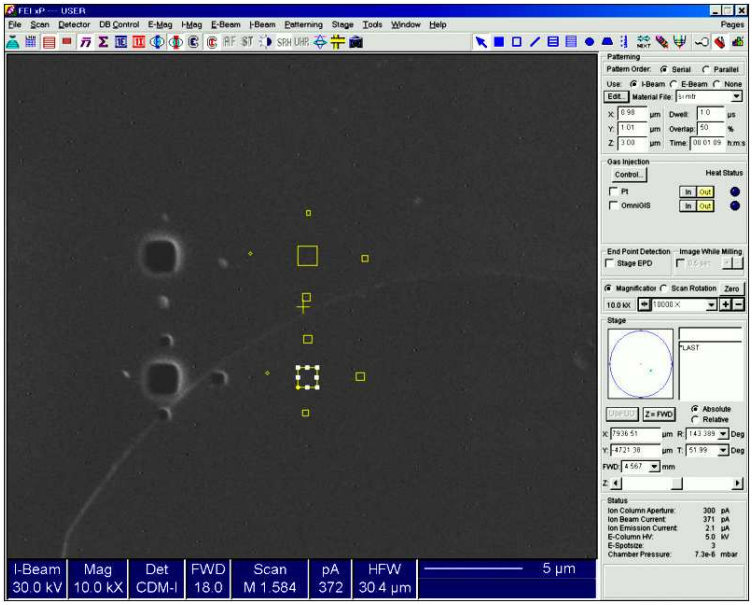

Figure 21: A screen capture of the interface software on the FEI SEM/FIB computer interface showing the assigned pattern and the resulting pattern (overlaid next to each other for convenience).

FIB was used to drill through and partial holes of varying depth on the silicon nitride membrane. The Figure 21 shows the assigned machining pattern and the resulting machined pattern. The aim of the FIB drilling was to use these specific locations to grow CNTs for convenient deposition and characterization.

2.3 Experimental Setup

Keeping in mind the objectives of this research, a separate simple apparatus was devised. The schematic of the apparatus is shown in the Figure 22.

It consists of a dessicator, which is an airtight vessel. This served as the chamber inside which the substrates were placed for the synthesis. It has two openings, one of the opening was connected to a Nitrogen Cylinder (high purity grade) and the other one was

used as a vent as well as the inlet for electrical connections for the substrates placed inside the dessicator.

A thermal insulator support platform was placed inside the dessicator with the aid of alligator clamps. The substrates/MEMS elements were placed on the platform. This prevents the heated substrates from touching any surface of the container which is not resistant to high temperatures. Electrical connections were made to these substrates/MEMS elements, taken from a DC power supply. An industrial grade humidity sensor was used to monitor the humidity. The probe was placed inside the dessicator, and the sensor display was placed outside of the dessicator. For avoiding any possible damage to the probe from high temperature, a separate casing was used to cover the probe, enabled the sensor be exposed to the atmosphere inside the dessicator. This casing was made of a low thermal conductivity material like Pyrex glass, wood or steel. An Ammeter was connected in series with the substrate, and a Voltmeter was connected in parallel, to measure the current and voltage in the electrical circuit. A wire thermocouple was used for the temperature measurement on the substrate. A thermocouple reader was used to monitor the temperature outside the dessicator.

The supporting platform was later replaced by an external heater in case of the passive substrates, and the electrical connections from the power supply were made to this heater.

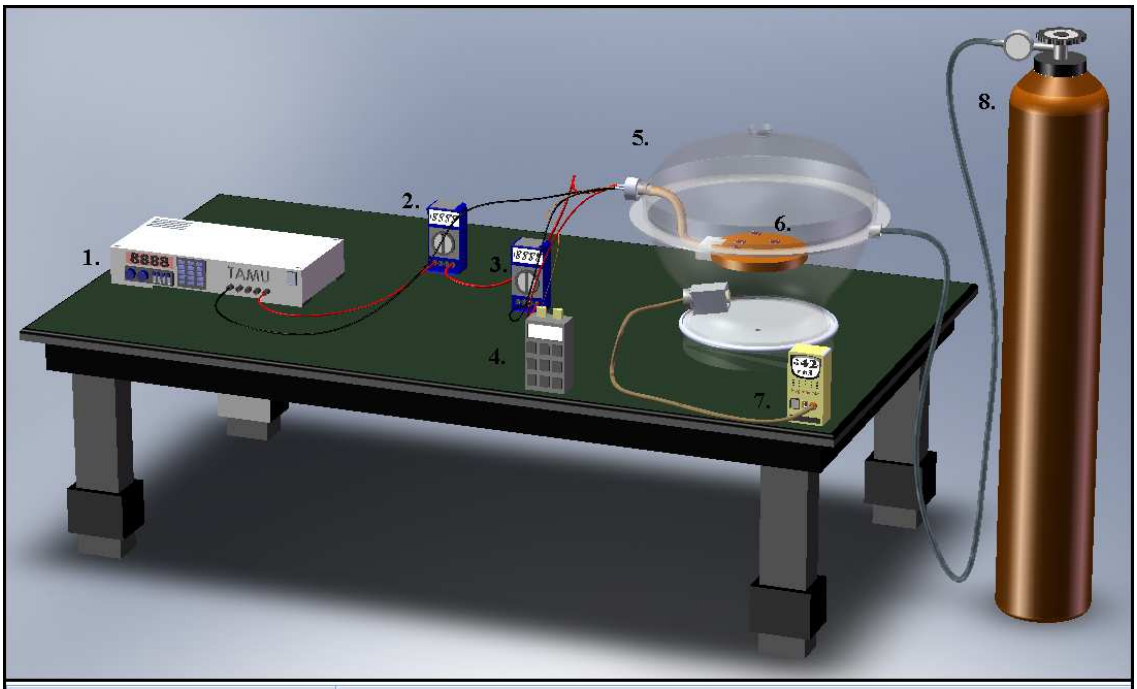

Part Number	Part Name
1.	DC Power Supply
2.	Multimeter (Current)
3.	Multimeter(Voltage)
4.	Thermocouple with Reader
5.	Desiccator
6.	Heater with Substrates
7.	Humidity Sensor
8.	UHP Nitrogen Cylinder

Figure 22: Schematic model of the experimental setup.

The substrates proposed for this research, on which the CNT synthesis takes place, are categorized as Active and Passive substrates. The Active substrates used are the ActivePen™ Arrays from NanoInk Inc. and custom designed PIMTEM chips with inbuilt microheaters. The passive substrates include the passive AFM probes, Sindex™ Chips and bare Silicon wafers.

In the same context, for another experiment, the DPN instrument is used, since it has a climate control chamber along with voltage supply option, specifically designed for the active pens.

2.4 Verification and Evaluation

These equipments make it possible to visualize and characterize the samples for various depositions and results. Several equipments can be used in accordance to confirm the same.

2.4.1 XPS Instrument

A Kratos Axis Ultra Imaging X-ray Photoelectron Spectrometer, equipped with dual aluminum-magnesium sources is used for this spectroscopy. It is located at the Material Characterization Facility (MCF) in the Chemical Engineering Department at Texas A&M University. The XPS technique is described in section 1.5.3. The Figure 23 shows this instrument.

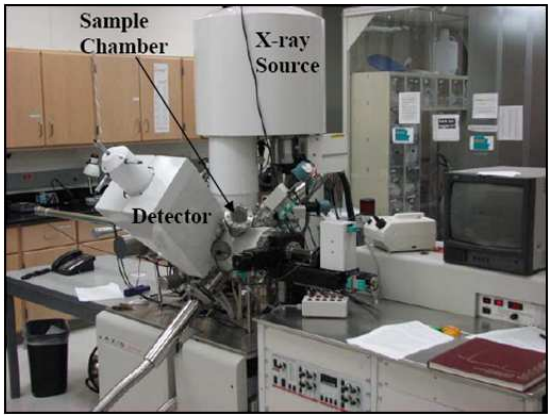

Figure 23: Kratos Axis Ultra Imaging XPS.

2.4.2 Raman Spectroscopy Instrument

JY Horiba LabRam IR Raman/FTIR Spectrometer, in conjunction with the JY Open Electrode CCD detector for excitation laser wavelengths of 633 and 785 nm at the MCF, Chemical Engineering at Texas A&M University is used for the purpose. It is shown with the respective parts labeled in Figure 24.

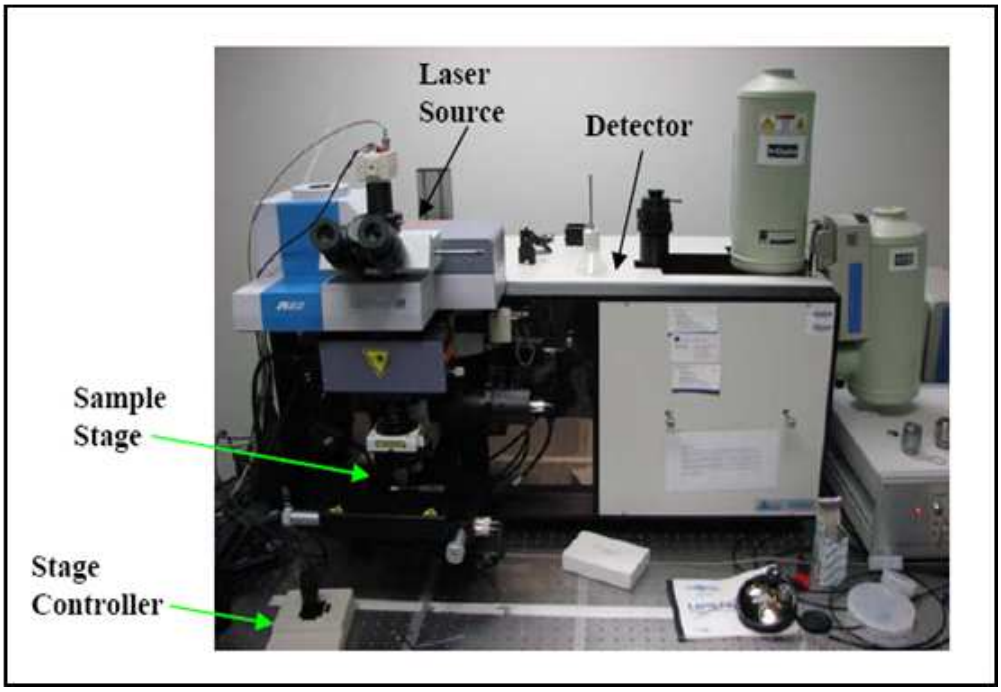

Figure 24: JY Horiba LabRam IR Raman Spectrometer.

2.4.3 Scanning Electron Microscope

JEOL 6400 is a software-oriented, analytical-grade SEM, is capable of acquiring and digitizing images. Acceleration voltages from 0.2 to 40kV, a magnification range of

10 to 300,000 X. This is located at the Microscopy and Imaging center, Texas A&M University. (seen in Figure 25, left image)

Figure 25: The JEOL 6400 (left) and the FEI Strata (right) Scanning Electron Microscopes.

The FEI Strata (Figure 25, right image) is the latest SEM available at MIC, which provides a resolution even better than the JEOL 6400. This was used to obtain high resolution images, in case the resolution obtained by JEOL 6400 was not sufficient.

2.4.4 Transmission Electron Microscope

JEOL 2010 TEM with an inbuilt Electron Diffraction unit, operating at 200 kV was used for this microscopy, located at the Microscopy and Imaging center, Texas A&M University. It is capable of obtaining images at a very high resolution up to a few nanometers. This microscope is shown in Figure 26.

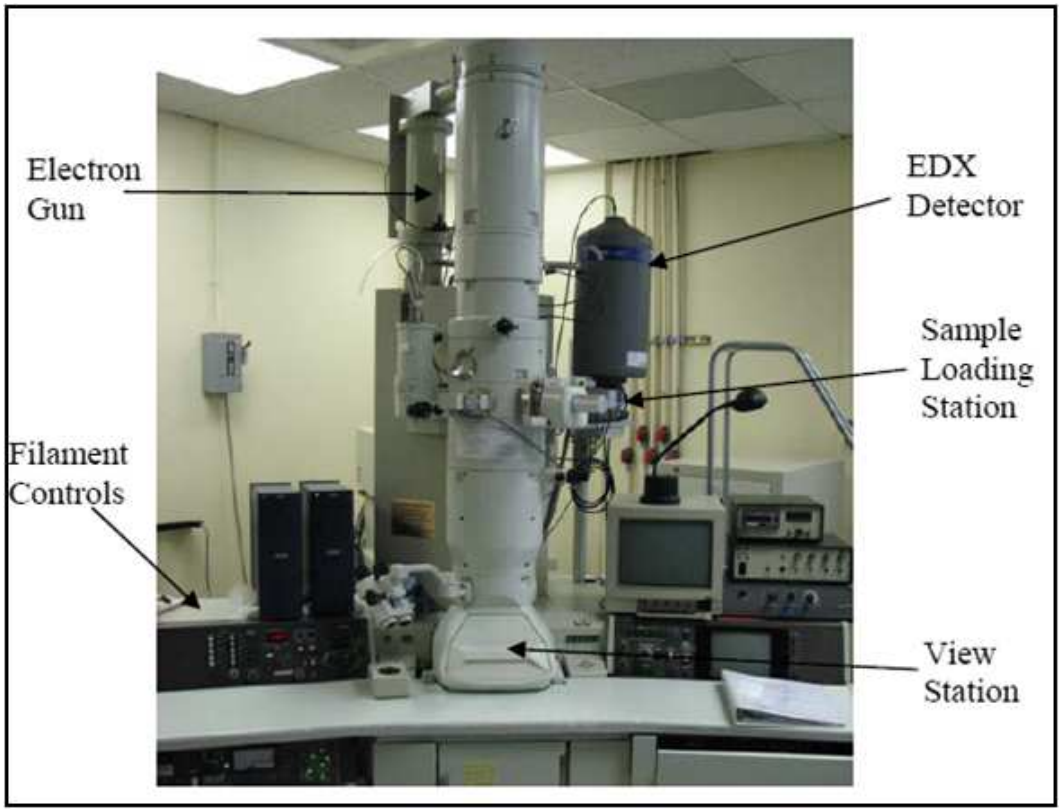

Figure 26: JEOL 2010 Transmission Electron Microscope.

CHAPTER III

EXPERIMENTAL PROCEDURE

3.1 Sample Preparation

3.1.1 Fullerene Deposition

It has been demonstrated experimentally that Carbon Nanotubes (CNT) can be synthesized with Fullerene as the source for carbon, where the synthesis temperature is ~500 °C (Morjan *et al*., 2004)**.** For the available substrates (Active and Passive probes, PIMTEM Chips, Silicon wafers and Sindex Chips), multiple methods of Fullerene depositions were used.

Method I - The Thermal Denton evaporator was used as described in the previous section for thermally deposition of Fullerene on the substrates. These substrates were mounted onto glass slides using a double sided stick tape and these glass slides were clipped to the target plate on the roof of the Denton Evaporator using the available clamps. A small amount of C60 fullerene powder (Manufactured by Nano-C Inc., Westwood, MA) was placed inside the metallic boat at the bottom of the depositor. The metallic boat was electrically heated at a pressure of 1 mTorr to a temperature of 550 ◦C to enable sublimation of the fullerene powder. By adjusting the respective settings on the machine, the deposition rate by sublimation was estimated to be ∼20 nm/s for a total deposition time of 10 s. The substrates when taken out of the evaporator were visibly different from the clean ones confirming the presence of fullerene. The fullerene

thickness was estimated to be ~200 nm at the end of the vapor deposition process using a Profilometer.

Method II - In another method of deposition, Fullerene solution was obtained by dissolving solid fullerene into an organic solvent (Toluene), in 1:1 ratio by weight. The solution thus obtained was heated for 5 minutes at 70◦C and ultrasonicated to ensure homogeneity. This uniform concentrated solution of Fullerene is directly deposited on the substrates. In case of the Active and Passive pens some of the solution is taken in a syringe (without needle), and the plunger of the syringe is very softly pressed so that a small droplet protrudes out of the syringe nozzle. With the syringe rested horizontally, the substrate (Active pen array) is then horizontally moved towards the nozzle until the array is just dipped in the protruding droplet. This contact is maintained for ~10 minutes. For the PIMTEM chips and Silicon wafers, the syringe is used to put a drop on the surface, or, the substrate is fully dipped into the solution for 5-10 minutes. These substrates are dried either at room temperature or by heating on a hotplate at 50 ºC for 15 minutes.

3.1.2 Metal Catalyst Preparation

Metals known to catalyze CNT synthesis were used for the experiment. Nickel chloride ($NiCl_2$), Cobalt Chloride ($CoCl_2$) and Palladium Chloride ($PdCl_2$) were prepared by mixing the solid powder into De-Ionized water with minimal heating for uniformity, to yield a 0.05 M solution (Li *et al*., 20010. Sodium Hydroxide (NaOH) was used in the

preparation of the PdCl2, since it doesn't form a direct solution with water but is soluble in alkali hydroxide solutions.

3.1.3 Passive Pen Bulk Deposition

After obtaining a uniform solution of the metal catalysts, the passive pen, which is already coated with a 200 nm thick layer of fullerene, is held in a clean pair of tweezers, and is immersed in the metal catalyst solution. The pen is kept immersed for ~10 Seconds, after which it is removed and dried very softly by flowing pure Nitrogen gas in order to avoid the washout of the deposited fullerene. This pen is then ready to be a substrate for the experiment.

In another way of pen preparation, some of the catalyst solution is taken in a syringe (without needle). The syringe is rested horizontally with the help of a clamp and the plunger if the syringe is very softly pressed so that a small droplet protrudes visibly out of the syringe nozzle. The passive pen (already coated with fullerene) is then horizontally moved towards the nozzle until the array is just dipped in the protruding droplet. This contact is maintained for ~10 seconds. This process is repeated for different pens with different salt solutions. The pen is then ready to be used as a substrate for the experiment.

3.1.4 Active Pen and Passive Pen Inkwell

An Inkwell™ is used for localized deposition of chemical solutions on to scanning probe tip arrays using dip pen techniques (Banerjee *et al*., 2005). A syringe is

used to deposit a very small quantity of these solutions (50 – 100 nL) onto a reservoir of Inkwell. This solution then flows into the corresponding wells pertaining to the capillary action of the micro channels. This inkwell is mounted onto the substrate holder, which is then positioned below the Active pen array in the AFM platform.

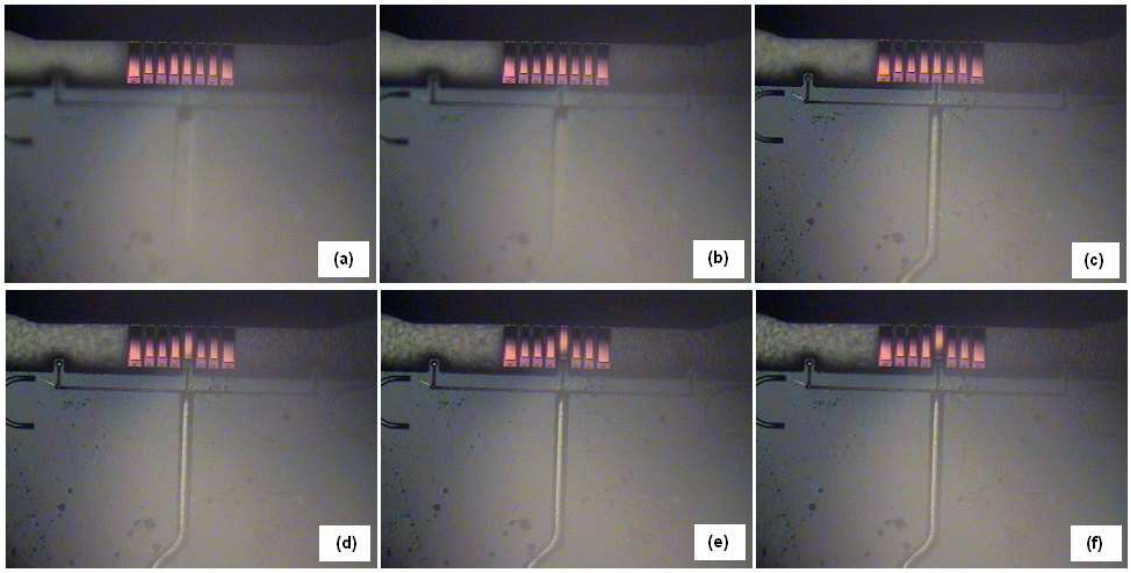

Figure 27: Sequence of images showing the inkwell dipping (coating) operation for a scanning probe tip in the ActivePen™ array.

The active pen array is aligned vertically over the inkwell in such a way that particular well filled with the fullerene solution is exactly below the pyramid probe of the cantilever which is to be dipped in Fullerene solution. Through the interfacing software, this probe tip is brought down in the Z-direction in small steps of 5 μm, until the tip is properly dipped into the well. This is confirmed by the visible deflection of the cantilever in the video window of the interfacing software (seen in Figure 27). At this instant, the pyramid probe is in contact with the solution in the well. This instant is

schematically shown in Figure 28. After ~10 seconds, the tip is lifted up again, and this process is performed/repeated with all the tips in the array. The inkwell dip ensures the deposition over a localized area, which presents the laser signal in the optical lever from being compromised.

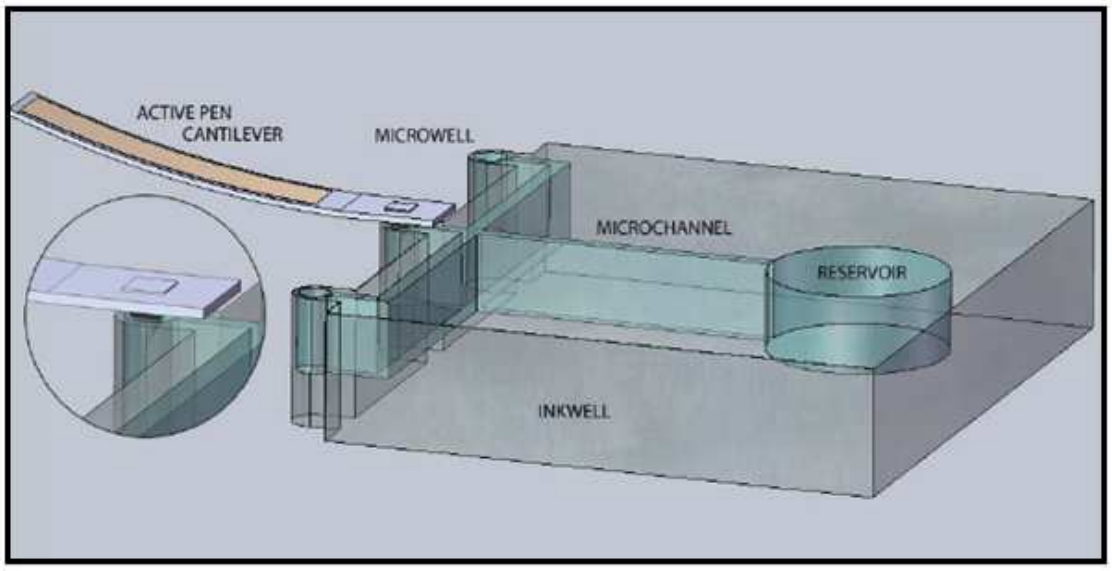

Figure 28: A schematic showing a microcantilever with the pyramid probe dipped into a microwell of the Inkwell.

The process is possible for one individual cantilever at a time. To coat multiple pens, the process is repeated for each of the cantilever.

3.1.5 PIMTEM Chips Bulk Deposition

An Eppendorf tube was used to deposit a small quantity (~1 mL) of the metal catalyst solution on the fullerene coated chips. This was allowed to dry and then used as the substrate for the experiment. The figure below shows overview of a PIMTEM Chip

bulk deposited with the PdCl2 metal Catalyst. As seen, the thickness of the catalyst is maximum at the center and then reduces as it reaches the edges of the chip. On the other hand, some of the PIMTEM chips were also sputter coated with Gold-Palladium (60 - 40%) target for a time duration of 1 minute. Basically the sputter coater is used on samples after the experiment to use under SEM for better resolution, but since it contains some amount of Palladium, we decided to try it.

3.1.6 DPN Pen Preparation (Double Dipping)

The DPN pens (SiN3 AFM tip – 0.58 N/m, Veeco) were coated with metal salt solutions using the double dipping procedure recommended by NanoInk, Inc. This procedure involves immersing the tip of the AFM probe into the “ink” solution for 5 – 10 seconds. This is followed by blowing off any of the excess solution clinging to the pen by using ~ 10 psi of compressed nitrogen gun. The angle of the nitrogen gun was maintained at approximately 20 degrees with respect to the cantilever, to prevent any damage to the probe. Next, a small quantity of deionized (DI) water was heated to its evaporation temperature. At this point a visible layer of water droplets is formed on the bottle which contains the DI water. This evaporation was exposed to the surface of the probe by suspending the probe above DI water for a period of ~40 seconds. The probe was removed and left to air dry for approximately 5 minutes; then the entire procedure was repeated to ensure proper and uniform coating of the “ink.” The ‘pen’ at this stage is ready for performing the DPN operation (or “writing”).

3.1.7 Substrate Patterning Using DPN Pens

Dip Pen Nanolithography is used for the controlled deposition of the catalysts on the fullerene coated PIMTEM and Sindex Chips. The 'DPN Pens' are used for the pattering of the catalysts on the metal surface. For an efficient DPN process, the relative humidity in the environment controlled chamber was kept at ~44%. The humidity level was monitored and controlled through the E-Chamber Climate control interfacing software. This confirmed the claims of previous studies into meniscus formation in DPN (Schwartz 2002; Weeks *et al*., 2005). During writing, the tip speed of the pen was maintained at 1 μm/s. Square patterns ranging from 150 nm to 5 μm were attempted for each metal salt. The interface software of Nscriptor™ provides a CAD-extension, which provides basic CAD features within the limitations of the controller of the DPN machine. The Figure 29 shows a screenshot of a pattern in the INKCAD™ software window. The reference squares are visible in the background in faint blue color. These reference squares have a side of 1 μm.

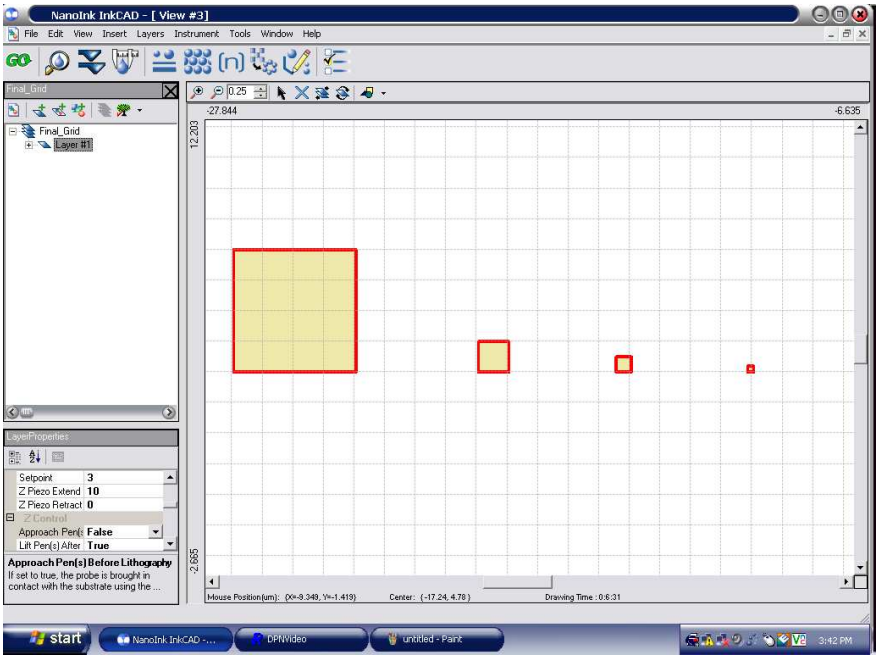

Figure 29: A snapshot of the InkCAD window with the CAD Pattern. The faint squares in the background are 1 µm in size.

To verify DPN patterning, a Lateral Force Microscopy (LFM) scan with dimension bigger than the pattern was performed on the same surface. LFM scans were performed at a faster rate of 10 µm/s to prevent deposition while 'reading'.

The Figure 30 shows a high resolution verification scan. The original image is black and white and has been given a blue shade for a better contrast and lighting.

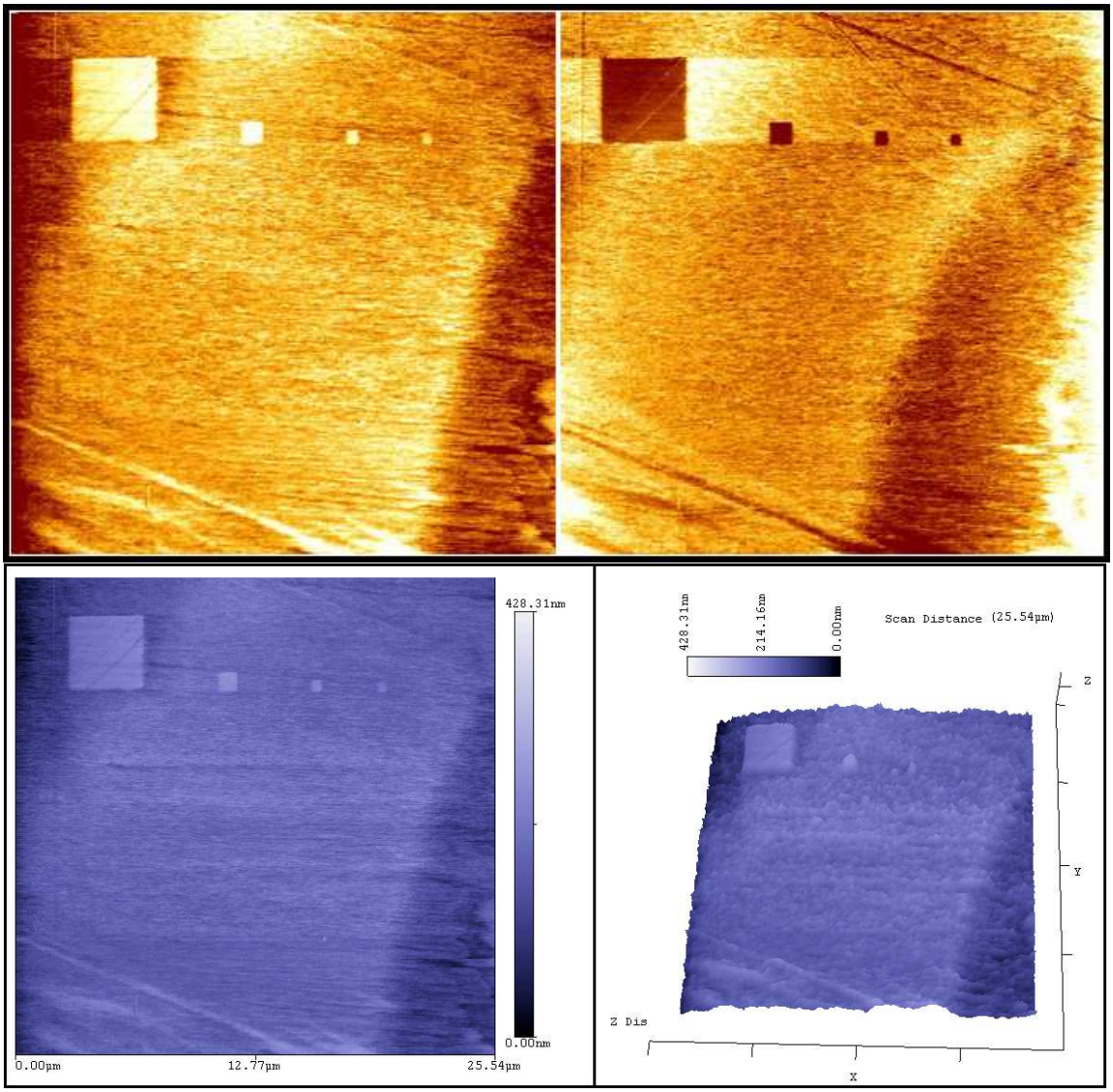

Figure 30: Top: Lateral Force Microscopy scans of the deposited pattern in forward (left) and reverse (right) directions.
Bottom: Left – LFM-forward scanned image of the deposited pattern showing the squares 4 µm, 1 µm, 500 nm and 200 nm respectively. Right – 3 dimensional LFM image to indicate the heights of the depositions.

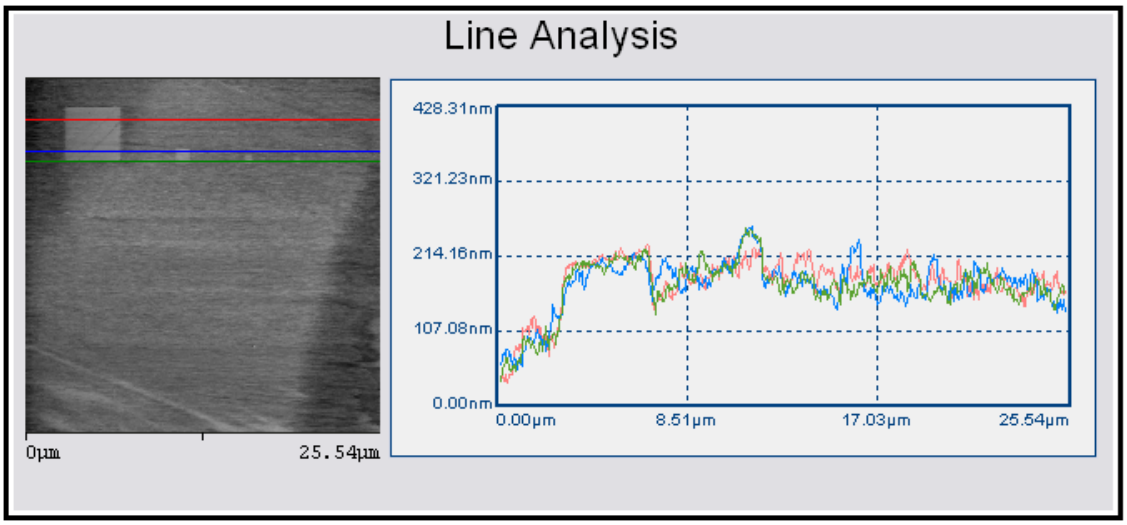

Figure 31: A line analysis of the same image in 2D, showing a X-Z axis plot. Note the colors of the graph and the corresponding positions in the LFM image.

A line analysis of the same scanned pattern is shown in Figure 31 which displays these depositions in a 2Dimensional format from a front- side view, providing the XZ plot.

3.2 Synthesis Experiment

3.2.1 Synthesis on DPN Nscriptor

Inkwell dipping was performed using the active pens. This procedure was repeated sequentially for all the eight microcantilevers. Of the eight microcantilevers in the Active Pen array, three of the scanning probe tips were dipped into NiCl2 solution, three were dipped in CoCl2 solution and two were dipped in PdCl2 solution. Performing the dipping operation using the microwells helps to constrain the area over which the catalyst is deposited in each scanning probe tip. After accomplishing the dipping of the scanning probe tips into the catalyst precursor solutions, the Inkwell was dismounted,

and the environmental chamber was closed. The humidity was recorded. The recorded value indicated that the ambient moisture and air was in contact with the probe tips. Hence, Nitrogen was passed into the chamber, and the relative humidity was monitored. When the humidity dropped to ∼1% RH after a small duration (10 – 30 minutes depending on the ambient humidity), indicating that the environmental chamber was filled with nitrogen, the synthesis experiments were performed sequentially for each cantilever. Initially, the current supply to an individual microheater (at the base of a microcantilever) was set at 25 mA. The current was increased in the steps of 2–3 mA, until the limiting value of 50 mA was attained for the supply current (the software setting limited the supply current to this value). This resulted in a heat spreader of the microcantilever attaining a temperature of ∼400 ◦C, while the scanning probe tip reached a temperature of ∼350 ◦C (temperature data was obtained using infrared microscopy measurements). The supply current to the microheater at the base of each microcantilever was maintained at 50 mA for a period of 5 min and the power was then switched off. This procedure was repeated sequentially for all the scanning probe tips, before dismounting the probe array. The probe array is now ready for characterization. The low synthesis temperature provides several advantages. It has been reported that lower synthesis temperatures yield a narrower distribution of the diameters (and correspondingly the chirality) of the synthesized CNT (Robertson, 2007). Also, lower synthesis temperatures can enable easier integration with conventional microelectronics manufacturing and packaging processes (e.g. CMOS processes).

3.2.2 Synthesis at Ambient Conditions

This was performed using the custom setup which was setup as seen in Figure 32. The metal salt precursors were prepared in an aqueous solution as mentioned above. Initially, each catalyst was deposited as a bulk layer on separate fullerene coated chips with the aid of a syringe (Bulk deposition as explained above). Later on, for the same setup, patterned depositions were made on the fullerene coated PIMTEM and Sindex chips using the DPN process as explained in the precious sections.

Figure 32: Photograph of the experimental apparatus for synthesis at ambient conditions.

The catalyst precursor solution was allowed to dry at room temperature after dispensing it on the fullerene coated chips. In an initial attempt, heater connections were made across the bond-pads of one of the heater per chip. The connections were made using thin gage electrical wires onto the bond-pads. The apparatus was placed in a

dessicator and connected to nitrogen supply from a pressurized cylinder. The experiments were performed in an inert atmosphere by passing the nitrogen into the dessicator. A humidity sensor was also placed inside the dessicator. The relative humidity in the air was recorded at the beginning before passing nitrogen gas. After a duration of ~10 to 30 minutes (depending on the ambient humidity), the humidity was found to be 3.0% inside the dessicator. At this stage, current was passed through the microheaters in the chip. The temperature was read on the thermocouple reader, connected to a wire thermocouple with one end placed on the sample. However, the chips were damaged when they reached a temperature of ~300 °C due to stress concentration. Since this low temperature was incompatible for CNT synthesis, external MINCO heaters were therefore used in this process. The external heaters were connected in a parallel assembly as discussed above. The chips were then placed on the MINCO heater assembly for direct contact heating. The free end of this thermocouple was placed on the heater apparatus to monitor the temperature and ensure that a target temperature in excess of 500 °C was reached. The temperature of the heaters was then raised slowly in steps of 10 °C per minute until the temperature reached 510 °C. It has been reported that lower synthesis temperatures yield a tighter distribution of the diameters (and correspondingly the chirality) of the synthesized CNT (Robertson, 2007). The heater was maintained at this temperature for 15 minutes and the power supply was then cutoff, along with the flow of nitrogen, and the samples were taken out from the setup for characterization and evaluation.

Both the experiments were performed at room temperature with the heated zone being localized only to specific portion of samples.

The experimental settings and parameters were optimized to obtain successful synthesis of CNT.

3.3 Conductivity Measurements

The conductivity of synthesized nanotubes was measured using the Dry and Wet Methods.

3.3.1 Dry Method

The Dry method was performed by devising a simple circuit on an AFM platform as described in section 1.8. A sample holder was connected to the DC power supply and the electrical connection was monitored using a multimeter. The substrate was placed on this holder. Electrically conductive AFM probes (Tap300E-10, Manufacture by NanoAndMore Inc, Lady's Island, SC) were used to complete the circuit through a cable connecting the other terminal of the battery and the tip holder. A voltmeter was connected across the setup for voltage measurement. The AFM controller was used for the movements of the probe.

3.3.2 Wet Method

In the wet method an “electrolytic cell” apparatus was used. Common salt – Sodium Chloride solution in de-ionized water was used as the electrolyte. The substrate

with CNTs served as one electrode and another regular copper wire was used as the complementary electrode. The setup is shown in Figure 33.

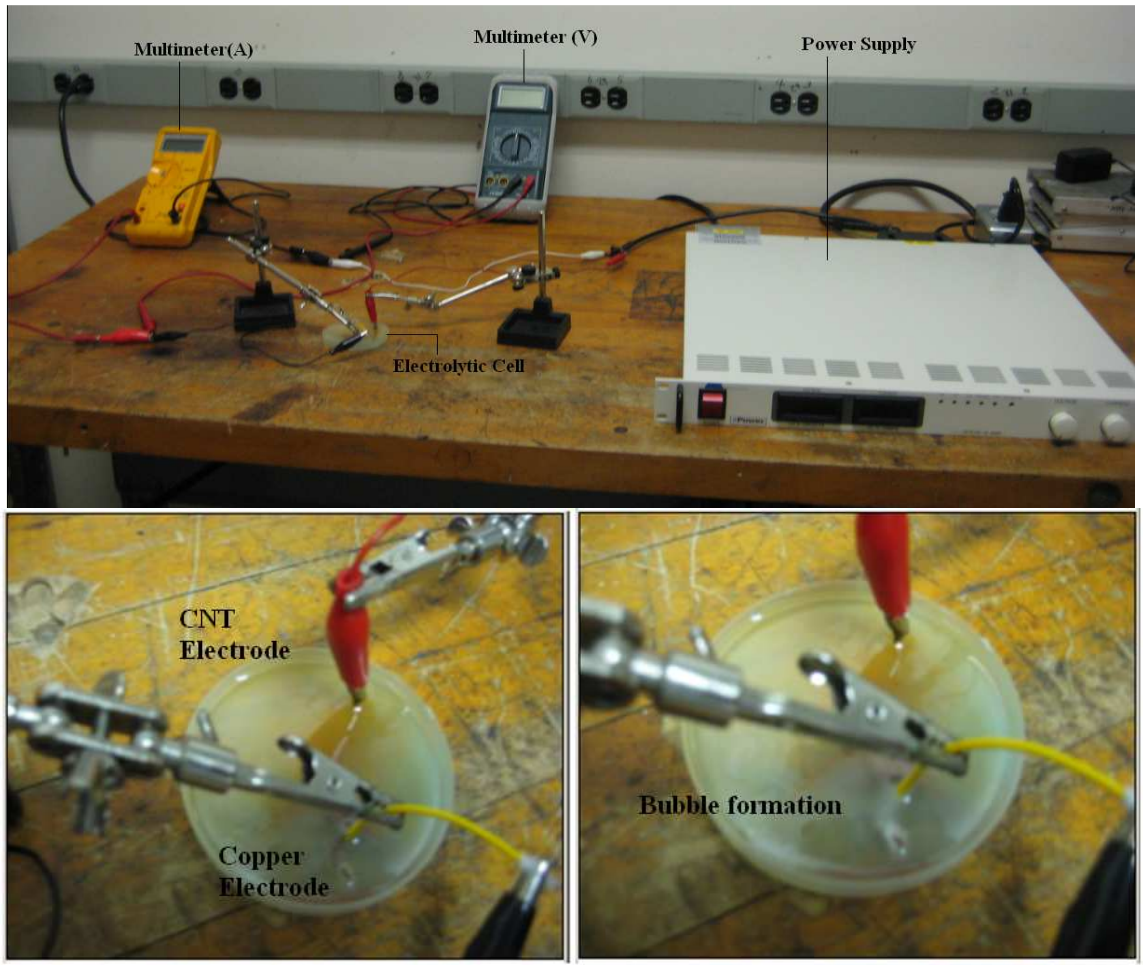

Figure 33: Top - Experimental setup for conductivity measurement using the wet method. Bottom – bubble formation is seen at the copper electrode in the right image.

Current was passed through the electrodes using a DC power supply. At a voltage of 1.4 V, bubble formation was seen indicating dissociation. Hence voltages lower than these were then used for the measurements. Starting at 0V, the supply voltage was incremented by 0.2 V to reach a final value of 1.4 V and the corresponding current

measurements were noted. Same procedure was followed using a bare electrode for comparison of measurements between a bare electrode and substrate electrode.

3.4 Uncertainty Analysis

As mentioned earlier, we use the following relation to calculate the diameter of the CNTs:

$$d = \frac{248}{\omega}$$

Where, d = Diameter of the CNT in nm.

ω = Raman Shift in the RBM region in cm^{-1}

The Raman spectroscopy instrument captures the intensity of the inelastically scattered light to obtain the Raman spectra. This recording of intensity peaks is digitized (or discretized) into regular intervals. Thus the RBM peak location has an uncertainty corresponding to the minimum discretization interval used for recording the peak signal.

To address this uncertainty in peak location, we specify the diameters of the CNT with a corresponding uncertainty. This uncertainty for diameter measurements is calculated using the Kline and Mc-Clintocks method (Kline and McClintock, 1953).

$$\frac{\Delta d}{d} = \sqrt{\left(\frac{\Delta w1}{w1}\right)^2 + \left(\frac{\Delta w2}{w2}\right)^2 + \cdots + \left(\frac{\Delta wn}{wn}\right)^2}$$

Where, d = quantity to be calculated.

Δd = uncertainty in the quantity to be calculated.

$w1, w2, \ldots . wn$ = variables involved in measurement of d.

$\Delta w1, \Delta w2, \ldots . \Delta wn$ = uncertainty in the variables measurements.

Typically the peak location varied from to ± 0.01 cm^{-1} to ± 0.05 cm^{-1}.

3.5 Evaluation and Characterization

3.5.1 X-Ray Photoelectron Spectroscopy

The bulk samples were chemically characterized with x-ray photoelectron spectroscopy (XPS) in order to verify the composition of the deposition before the synthesis experiment was performed. This was mostly performed for the bulk deposition PIMTEM and SINDEX Chips, and the active pens. In case of the DPN patterned samples, the deposited quantity was very small and did not provide adequate signal for analysis. A basic survey for binding energies between 1,100 and 0 eV was obtained using either the Mg source with the anode operating at 12 mA and 15 kV or the mono Al source operating at 10 mA and 12 kV (used during a period when the Mg source was out of commission). The fullerene content was explicitly recognized by scanning the C 1s binding energy region between 295 and 275 eV.

3.5.2 Scanning Electron Microscopy

Direct visual imaging was carried out using JEOL 6400 SEM. Spot size used was 11 – 14. Acceleration voltage used was 15 KV. Increasing the spot size value improves clarity of the image at the expense of a additional noise generation. Different images were obtained at various magnifications ranging from 10 to 40,000 X, after which loss in resolution was observed.

To achieve images at higher magnifications, the FEI Strata was used (the author acknowledges help of Tom Stephens at Microscopy and Imaging Center, Texas A&M University). Automatic spot size was used with an accelerating voltage of 10 KV. This microscope allowed images to be obtained at magnification up to 200,000X with adequate resolution. This microscope was used only on selective samples due to the high usage and operator costs involved.

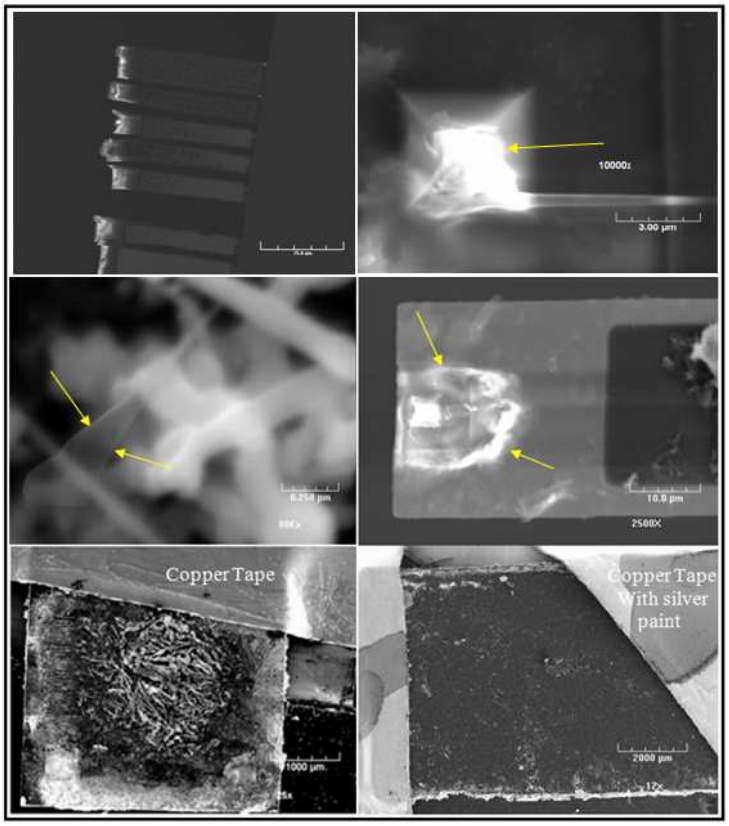

Figure 34: SEM images showing charge trapping effects and the remedies that were developed in this study. Top left: Distortion of cantilevers causing damage to an active probe array. Middle Left: Vibration of an individual nanotube. Top and Middle Right: too much illumination in the charge trapped area (arrow indicates charge trapping). Bottom: samples mounted using Copper tape, sputter coating and silver paint to minimize charge trapping.

Charge trapping is observed in case of non conductive substrates. It causes the sample to heat up and to vibrate due to constant exposure to electrons as seen in the left Figure 34. This makes it difficult to resolve individual tubes, or to obtain higher magnifications in some of the specific cases. As a remedy to this, a commercially available copper conductive tape was used to connect the surface of the substrate to the sample holder to enable proper 'grounding' of the trapped charge. The sample holder is connected to ground internally in the microscope. Sometimes a conductive silver paint is used on the edge of tape and the samples are used to enhance the conductivity. For a considerable better resolution, sputter coating was performed on the sample for 2 minutes using a Au-Pd Target (60-40%). This coats the sample surface and the holder surface with a nanoscopic layer. Since this deposited layer is beyond the microscope resolution, it is not expected to affect the SEM image drastically. However, this enables better resolution of the features in the SEM image.

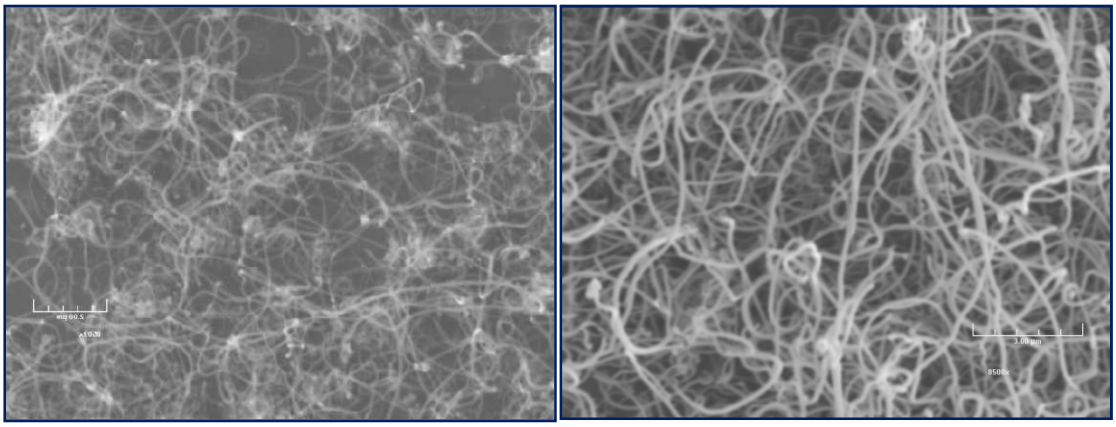

Figure 35: SEM image of a sample before and after sputter coating.

The Figure 35 shows SEM of the same sample before and after the sputter coating at the same magnification, approximately taken at the same spot. After sputter coating, higher magnifications are achieved without much loss in resolution. However, sputter coating should be performed with extra caution since thicker coating will affect the measurement of CNT diameter in the SEM images.

The measurements performed in this study are obtained mostly without sputter coating taken to ensure that all the measurements are performed with minimal user generated errors.

EDS units built into both of the above mentioned SEM's were also used to get the elemental composition of the samples.

3.5.3 Transmission Electron Microscopy

TEM imaging of the PIMTEM chips was difficult, since the diced chip were bigger than the TEM holder. Ultrasonication was tried for many PIMTEM chips to remove CNTs/CNFs in a solution for subsequent deposition onto the TEM grids. These attempts were not successful. Finally we were able to image passive probes by direct mounting without the carbon grid. Even this proved difficult to image since the tubes hanging out of the cantilever were observed to vibrate due to charge trapping. The optimal accelerating voltage used to minimize cantilever vibrations and obtain sufficient clarity was 15 KV. Electron Diffraction patterns were also attempted using the Silicon/Lithium EDX detector, exposing the samples for 50 seconds.

3.5.4 Raman Spectroscopy

After completing CNT synthesis on the metal salt samples, the CNTs synthesized on the substrates were characterized using Raman spectroscopy (at both 633 and 785 nm wavelength laser excitations). Although variations in samples required different scan parameters, typical settings were as follows:

Scan Range: 0 to 2,000 cm^{-1}

Microscope Obj: 50x

Exposure time: 1 s – 5 s (Depending on signal strength)

Accumulation #: 3 (for spectra with high noise w.r.t. signal i.e. weak signals)

: 1 (for spectra with strong signals)

Grating: 300

Confocal Hole: 150 μm

Filter: D 0.6, D 0.3, D--.

Same settings were used for the spectroscopy before and after the experiment for accurate comparisons.

3.5.5 Resonance

In some cases, where SEM, TEM measurements were not possible, and Raman spectra was used to confirm the presence of CNT in the samples. The Nscriptor was used to calculate the mass of carbon nanotubes/fibers that formed on the cantilever using resonance method as explained in section 1.5.3. These measurements were done in the AC (Alternating Contact) mode, which gives the drive/resonant frequencies of the

cantilevers. The measurements were obtained before depositions as well as before and after the experiment. The resonant frequencies were noted (as described in section 1.5.3) section, the respective masses were calculated.

Multiple readings were obtained while noting the frequencies, so as to ensure that the values obtained from the software were consistent.

CHAPTER IV

RESULTS AND DISCUSSION

XPS analysis was performed on the samples before the synthesis experiment was performed. These was done for confirming the deposition of the Fullerene on the substrates. Spectra taken are displayed in Figure 36, and show a peak around binding energy of 285 eV, confirming presence of Fullerene (Reinke and Oelhafen, 2005).

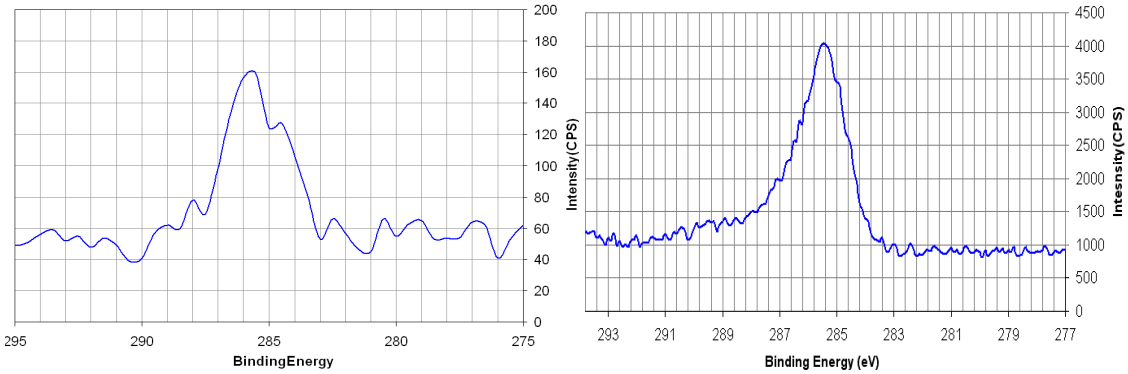

Figure 36: XPS Spectra shows a peak at ~285 eV confirming fullerene deposition.

The following section discusses the results obtained after the synthesis experiment, data analysis and characterization, using the techniques mentioned in the previous sections. The results are arranged in a chronological order.

4.1 Active Pen Results (Method I)

The temperatures reached using the active pens as substrates were of the order of 350 – 400 ºC. All 3 catalysts were used and deposited on the fullerene coated tip using Method I.

4.1.1 Raman

The following images show the Raman data from the experiments with Active pens as substrates and Method I for deposition. As discussed in the characterization section, we look for the presence of RBM, D and G peaks to confirm the synthesis of CNT. The Figure 37 shows spectra after using the noise reduction feature of the acquisition software.

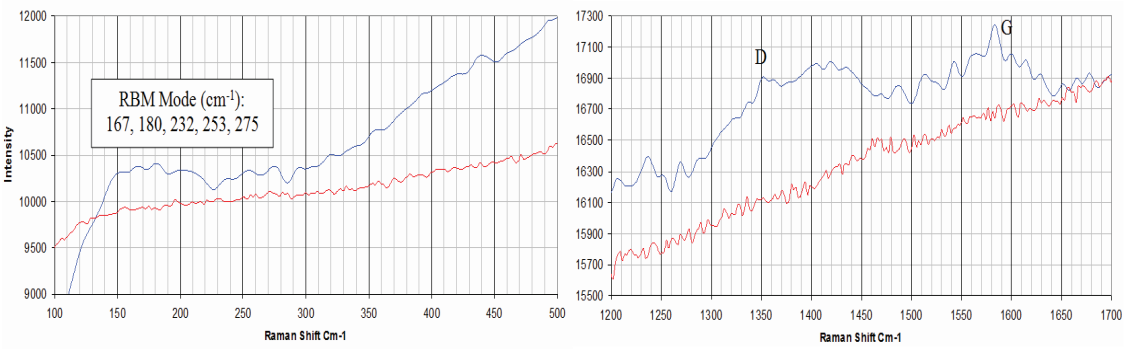

Figure 37: Micro-Raman spectra in the RBM mode, and D and G mode of the fullerene-coated scanning probe tip (dipped in PdCl2*)*, before (red) and after (blue) the synthesis experiment.

As seen in the spectra, the peaks for G and D band are clearly visible in the prescribed frequency regions at ~1350 cm^{-1} and 1582 cm^{-1} it can be argued that since the G band has a higher intensity than D band, purely SWCNT are synthesized. The D and G bands ~1350 and ~1590 cm^{-1} respectively. Also in the RBM mode peaks at 167, 180, 232, 253 and 275 cm^{-1} are observed indicating diameters of the CNT ranged from 0.9 to 1.5 nm.

4.1.2 SEM

Positive results from the Raman spectra motivated us to do the imaging of the sample. The results of which are shown in the following figure.

Cluster of CNT's are visible on the cantilever as seen in Figure 38. The density seems very low and distribution of the tubes is very narrow. This is expected due the low temperatures maintained during the experiments.

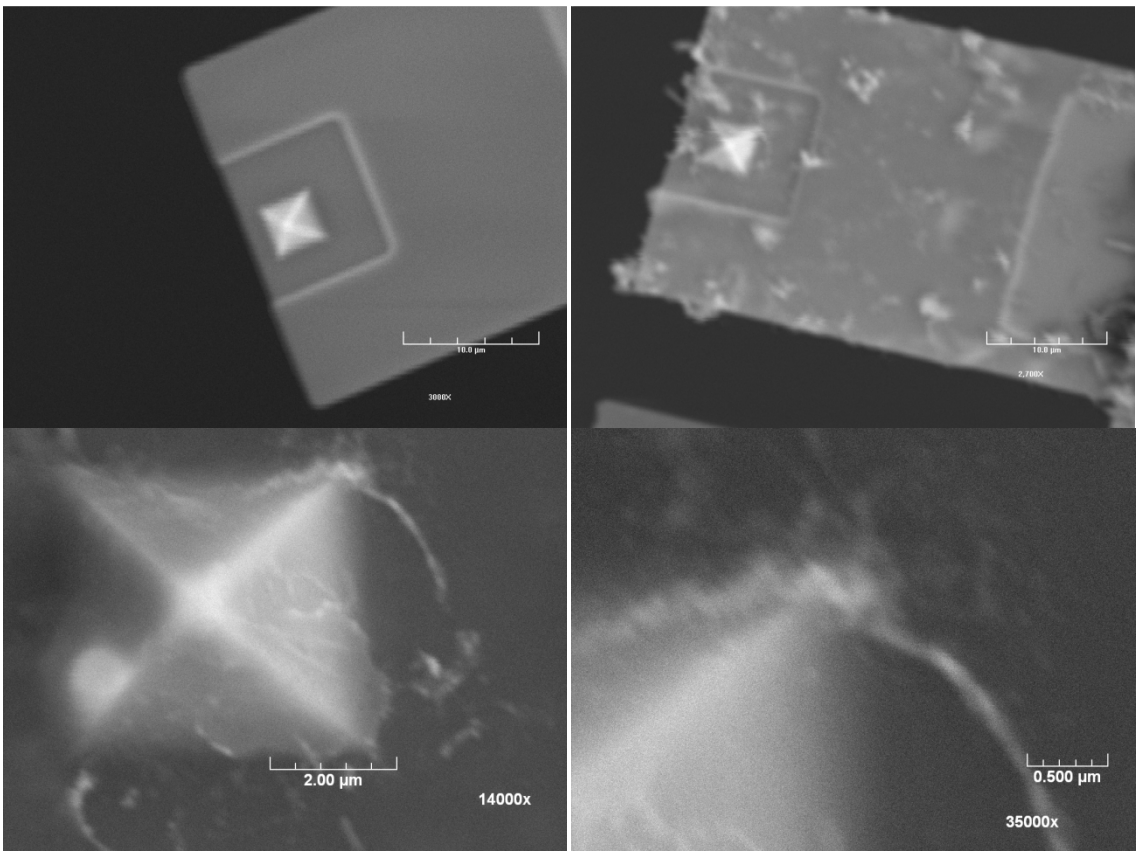

Figure 38: SEM images of a microcantilever before and after the synthesis experiments, at different magnifications. The figure shows carbon nanotube bundles, which appear as hair or wire shaped material synthesized at the base of the scanning probe.

The results shown are from only one of the cantilever, on which PdCl2 was used as the catalyst. The other cantilevers with $NiCl_2$ and $CoCl_2$ as catalysts did not show the expected Raman spectra.

4.1.3 Uncertainty Analysis

Using the Kline and McKlintock method, we calculate the uncertainty as follows:

$$\frac{\Delta d}{d} = \sqrt{\left(\frac{\Delta w1}{w1}\right)^2}$$

Where, d = diameter of the CNT.

Δd = uncertainty in the diameter measurement.

$w1$= Raman shift (166.49, 175.82, 180.48, 229.41, 252.71 cm^{-1})

$\Delta w1$ = uncertainty in Raman shift measurement (±1.165).

$\frac{\Delta d}{d} = \sqrt{\left(\frac{1.165}{166.49}\right)^2}$ (Calculated for all values individually)

$$\frac{\Delta d}{d} = 0.00700, 0.00662, 0.00646, 0.00510, 0.00461$$

Hence, Percentage Uncertainty = 0.7%, 0.662%, 0.646% 0.510%, 0.461%.

Thus the values of the diameters 1.49 nm, 1.41 nm, 1.37 nm, 1.08 nm, 0.98 nm are accurate within 0.7%, 0.66%, 0.65% 0.51%, 0.46% respectively.

4.2 Active Pen Results (Method II)

The temperatures reached using the active pens as substrates were of the order of 350 – 400 ºC. All 3 catalysts were used and deposited on the fullerene coated tip using Method II.

4.2.1 Raman

The Raman spectra obtained from the samples after experiment are shown in the following figures.

The D and G peaks are visible at ~1400 cm^{-1} and ~1600 cm^{-1}. Furthermore, clear single RBM peak is visible at 217.4 cm^{-1} seen in Figure 39.

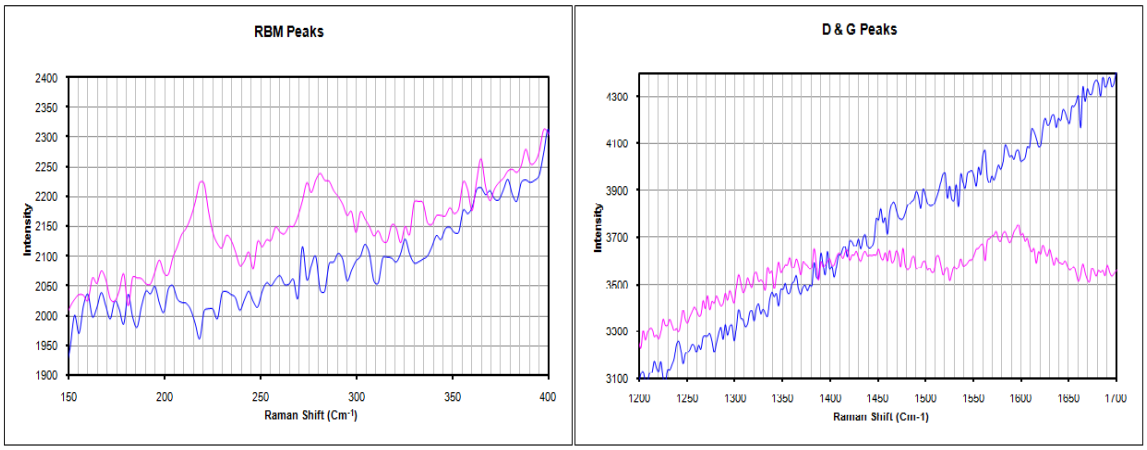

Figure 39: Micro-Raman spectra in the RBM mode, and D and G mode of the fullerene-coated scanning probe tip (dipped in NiCl2*)*, before (faint) and after (dark) the synthesis experiment.

This is an indicative of synthesized CNT's having a single diameter. (Same spectra for different locations on this cantilever were obtained). Note that the peak at ~300 cm^{-1} is because of the silicon substrate (Kolobov 2000).

4.2.2 SEM

SEM imaging of the cantilevers after the experiments were attempted. The results of this imaging are discussed next.

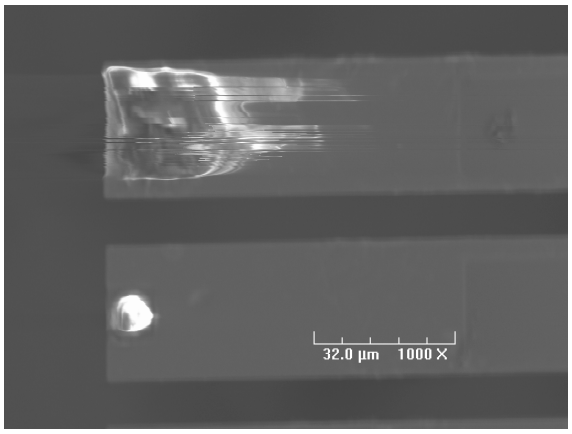

Figure 40: SEM image of the cantilevers taken after the experiment showing charge trapping.

The Figure 40 shows a high amount of charge trapping on the cantilever occurred, thus preventing image acquisitions at higher magnifications. Copper conductive tapes could not be used due to the size of the cantilevers. The electrical connections were grounded, however this did not improve image resolution. Sputter coating was also avoided since it would short the heater connections.

4.2.3 Resonance

Since we were not able to image this sample, we decided to use the resonance concept to measure the change in mass of this cantilever with the aid of DPN machine. Mass measurements at earlier stages were already obtained and were also performed after the experiment. The Table II shows the results.

Table II: Mass of the respective components calculated using Resonance techniques on the DPN platform.

Element	Mass (Kg)
$NiCl_2$ (catalyst)	2.6×10^{-13}
Fullerene Solution	5.5×10^{-14}
Carbon Nanotubes	6.4×10^{-15}

The results shown, again, are from only one of the cantilever, on which NiCl2 was used as the catalyst. The other cantilevers with $PdCl_2$ and $CoCl_2$ as catalysts did not show the expected Raman spectra. We believe these inconsistencies were because of the very low temperatures used for these substrates.

The results from the active pens motivated us to investigate further and carry out more experiments using higher temperatures. Different substrates (passive pens, PIMTEM and Sindex chips) were used for subsequent experiments in place of active pens. This was because of the costs and the fragility involved with active pens, and mounting of the active pens on the SEM and Raman Spectroscopy sample holders was extremely difficult.

4.2.4 Uncertainty Analysis

Using the Kline and McKlintock method, we calculate the uncertainty as follows:

$$\frac{\Delta d}{d} = \sqrt{\left(\frac{\Delta w1}{w1}\right)^2}$$

Where, d = diameter of the CNT (nm).

Δd = uncertainty in the diameter measurement.

$w1$= Raman shift (217.4 cm^{-1})

$\Delta w1$ = uncertainty in Raman shift measurement (±1.165).

$$\frac{\Delta d}{d} = \sqrt{\left(\frac{1.165}{217.76}\right)^2}$$

$$\frac{\Delta d}{d} = 0.00535$$

Hence, Percentage Uncertainty = 0.54 %

Thus, the calculated diameter of 1.14 nm is accurate within 0.54% of the measured value.

4.3 PIMTEM Chip and Si-Wafer Results (Method I)

The initial experiments with the PIMTEM samples were performed at around a temperature of ~450 ºC, and did not provide desired results (Raman and SEM data in the Appendix I). Later, the temperature was increased to 520 ºC, the humidity being a little high ~6%. Even these settings did not yield any results. Finally results were obtained at this temperature of ~520 ºC when relative humidity less than 2%. These results are

presented below. Also beginning with these samples, SEM was done before the Raman, since both the data were confirmative of each other.

4.3.1 SEM

Since the desired results were not seen in this case, other experiments were run at an elevated temperature of ~510 ºC. These settings worked. The results from the first experiment with positive results using Pd as Catalyst are shown below.

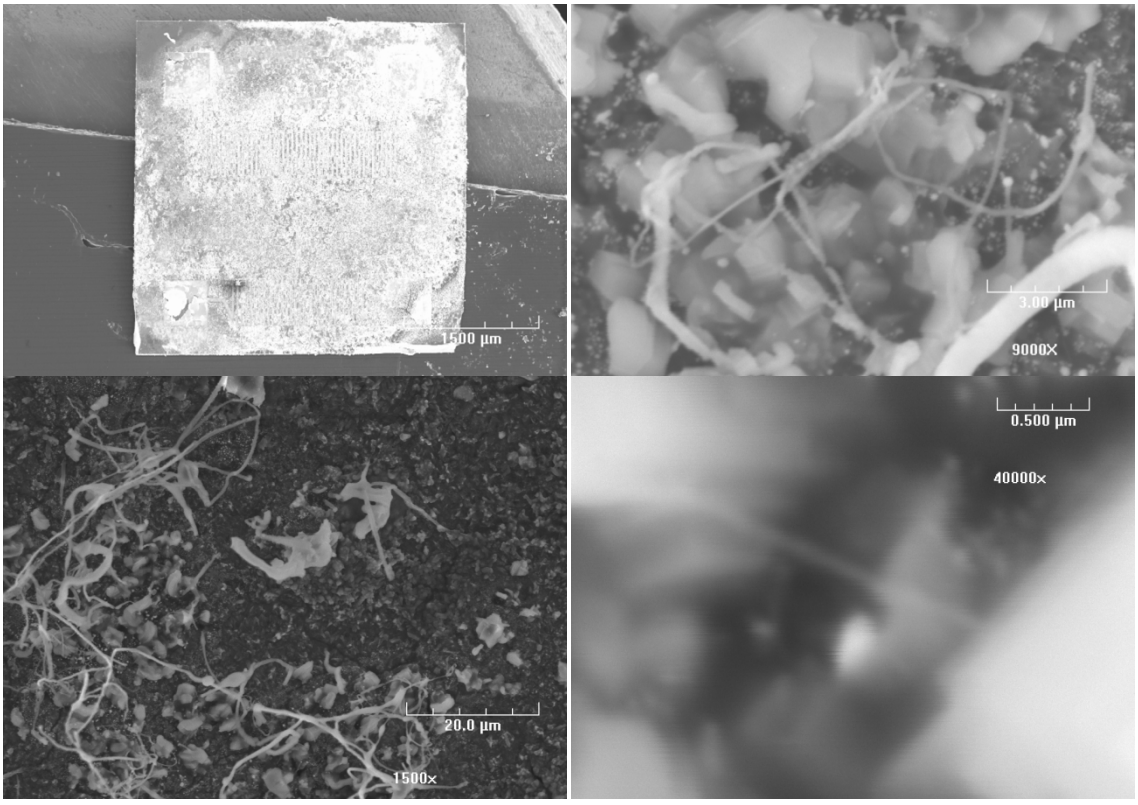

Figure 41: Images from the first experiment (successful with method I and Palladium catalyst) showing samples under SEM at various magnifications.

As seen from the SEM images in Figure 41, Ni and Co catalysts did not produce any useful results, but for the first time, we were able to 'see' tubes with the Pd Catalyst. The tube diameters varied from 50 nm – 1 µm, indicating a mixture of multi-walled carbon nanotubes and carbon fibers, and were distributed throughout the surface.

4.3.2 Raman Spectroscopy

Raman spectra obtained from the samples with the settings mentioned in section 3.5.4, after the experiments with positive results are shown in Figure 42. These are obtained from the experiments which were performed at temperatures of ~520 ºC, and the humidity being less than 2% as mentioned earlier. Spectra obtained from samples with Nickel, Cobalt and Palladium catalysts are presented in the first, second and the last two rows respectively. Each row shows around 2 to 4 spectra taken on different samples with the same catalyst, shown in different color and accompanied by a boxed legend indicating name of the sample, corresponding to its color.

The Raman spectra confirm the results obtained from the SEM. The spectra obtained from Palladium samples show the presence of MWCNT since the D and G bands are of comparable intensity, and D band being intense in some cases. We repeated the experiment with only the Palladium catalysts, to confirm the repeatability. The SEM images are shown in Figure 43.

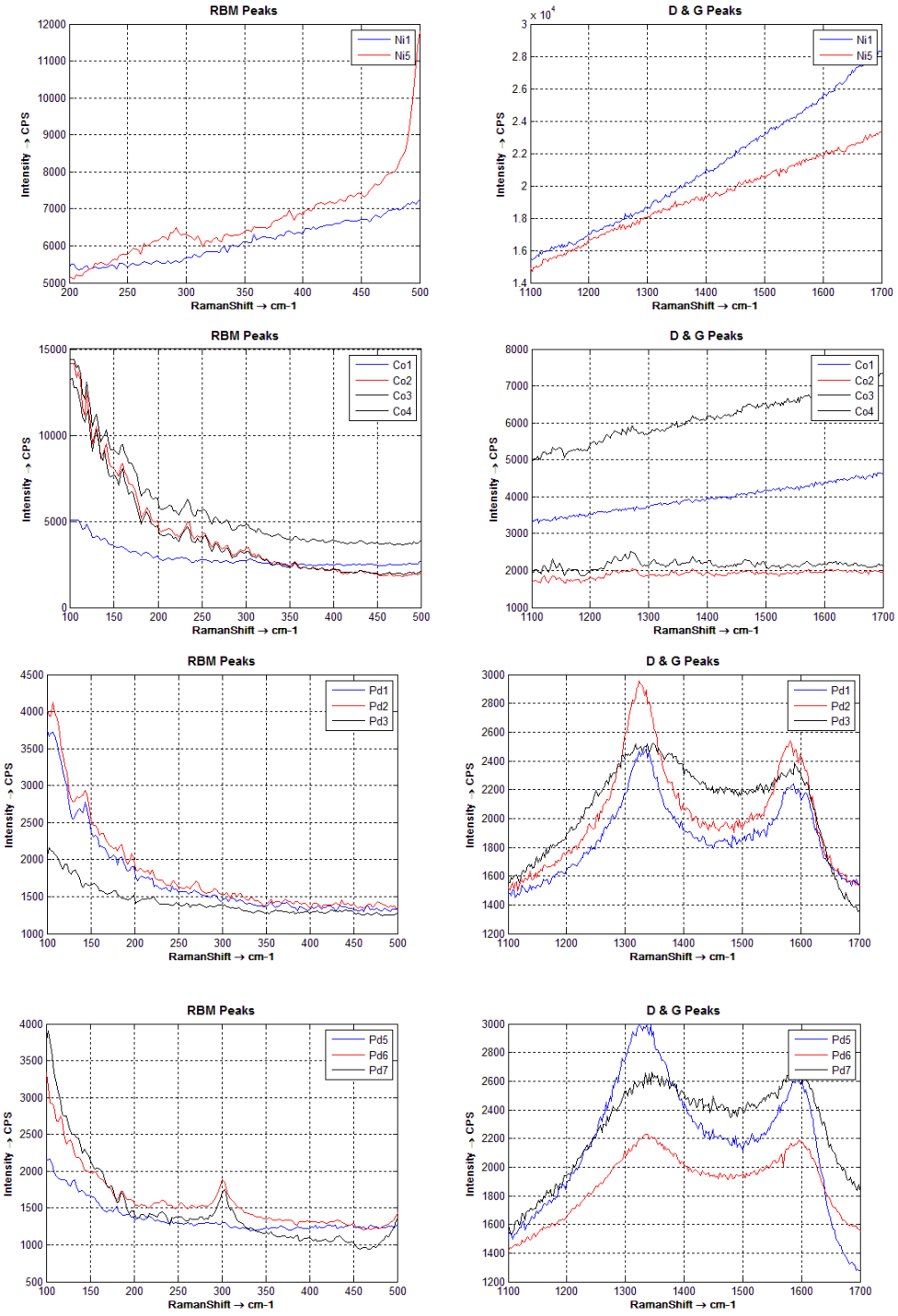

Figure 42: Raman spectra from the experiment. Top Row: samples with NiCl2 catalyst, second row: CoCl2 catalyst, Bottom rows: PdCl2 Catalyst.

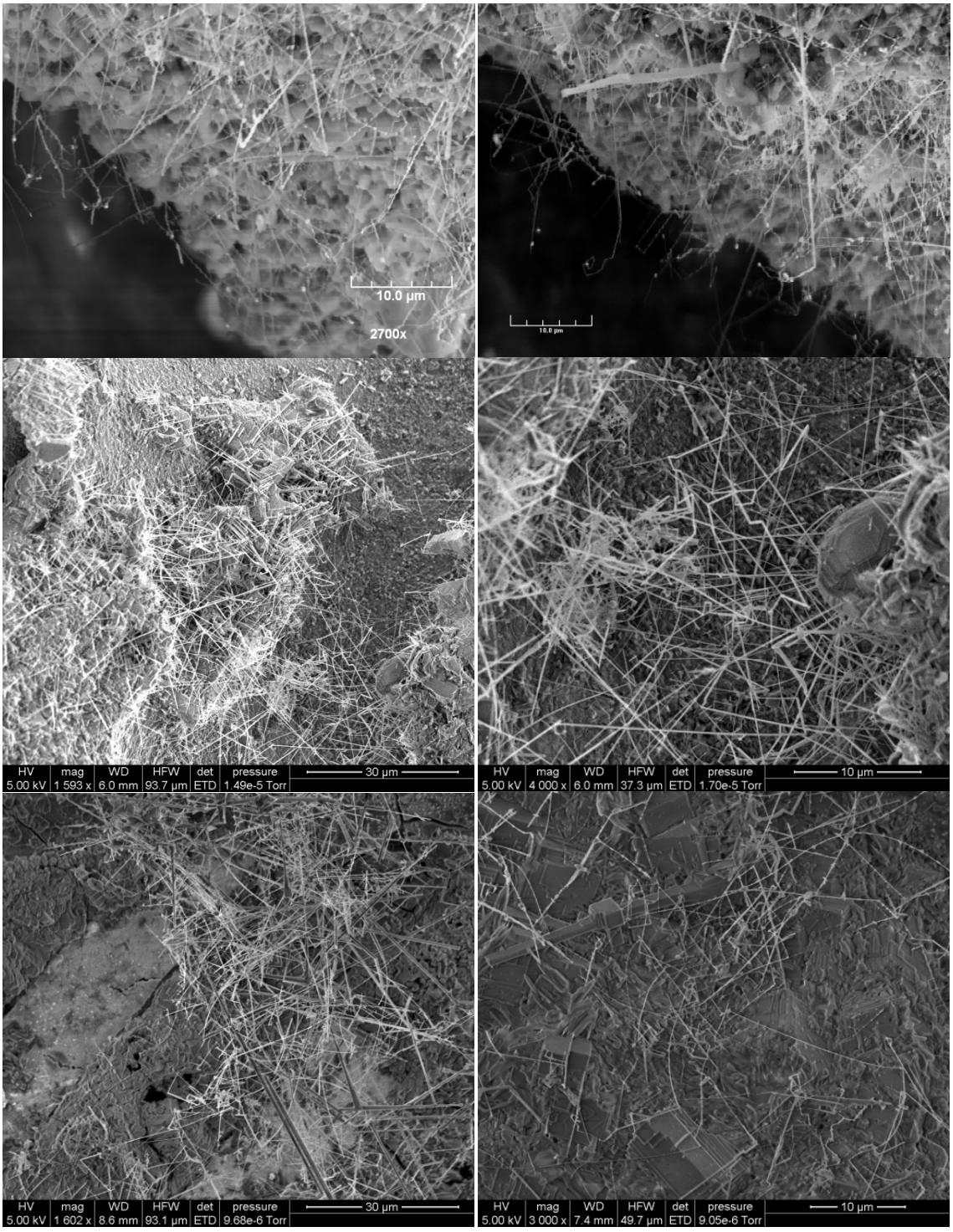

Figure 43: SEM images from the repeated experiments (with method I and Palladium catalyst) at various magnifications, showing straight CNTs.

Shown in Figure 44 are the images of samples on which Au-Pd (60 – 40 %) was sputter coated as the catalyst source on the samples before CNT synthesis.

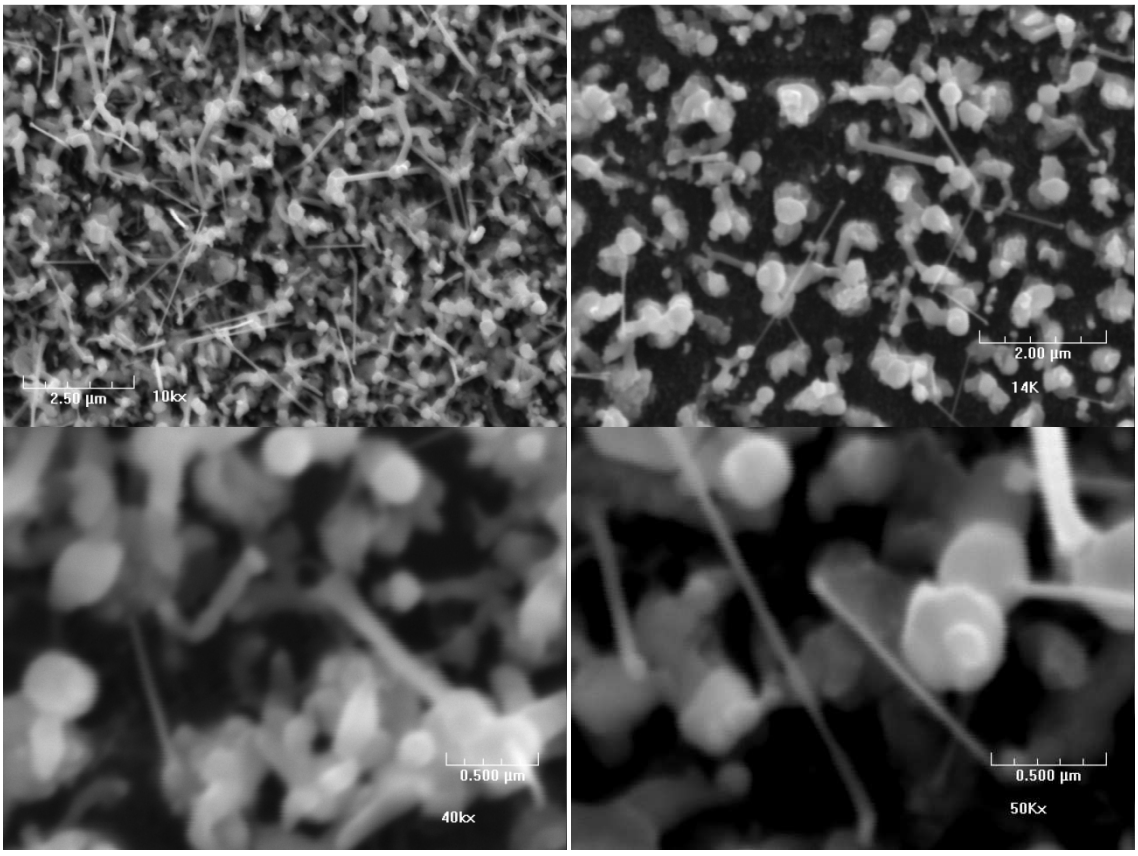

Figure 44: SEM images from the experiments using direct palladium catalyst through sputter coating at various magnifications, showing straight CNTs

Raman data collected from the samples in these experiments is shown below in the Figure 45.

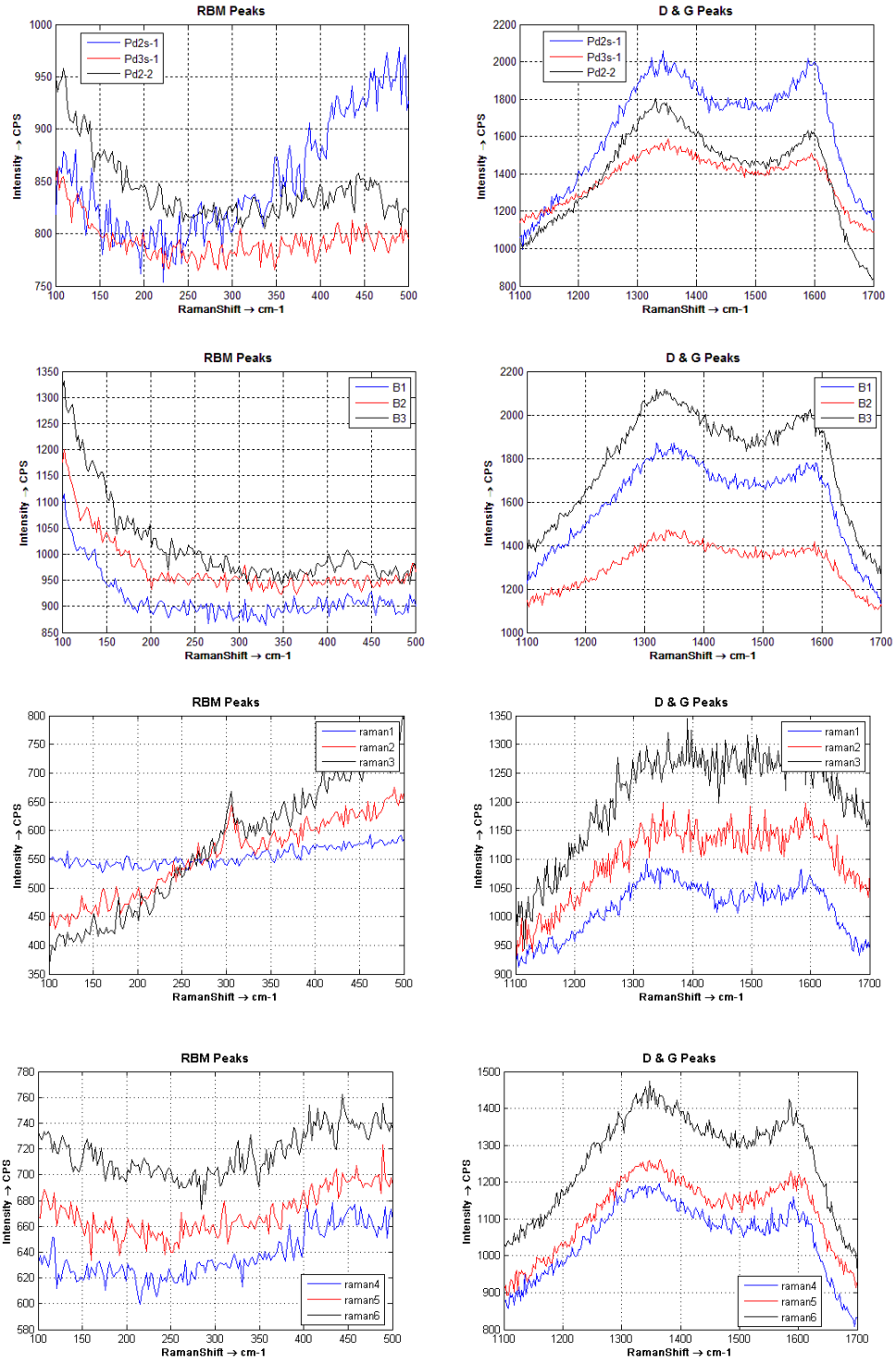

Figure 45: Raman spectra from the method I repeated experiments showing the desired D and G peaks.

4.4 PIMTEM Chip and Si-Wafer results (Method II)

Along with the samples used in Method I with Palladium catalyst, the Silicon wafer samples prepared using Method II also resulted in successful synthesis of CNT, verified from the data obtained from the SEM imaging and the Raman Spectroscopy.

The results obtained from the SEM are presented in Figure 46. Each row shows two images taken either on different samples, or on the same sample at different locations or magnifications. The images in the first two rows are taken on the FEI SEM whereas the images in the last two rows are taken on the JEOL SEM at various magnifications. Smooth and curved CNT are clearly seen on the substrates with diameters ranging from 20 nm to 200nmm.

These results are followed by the results obtained from the Raman Spectroscopy, showing multiple spectra in each row with a boxed legend as mentioned earlier. The spectra show the desired D and G frequency regions along with the RBM region in a few cases, confirming the CNT presence.

4.4.1 SEM

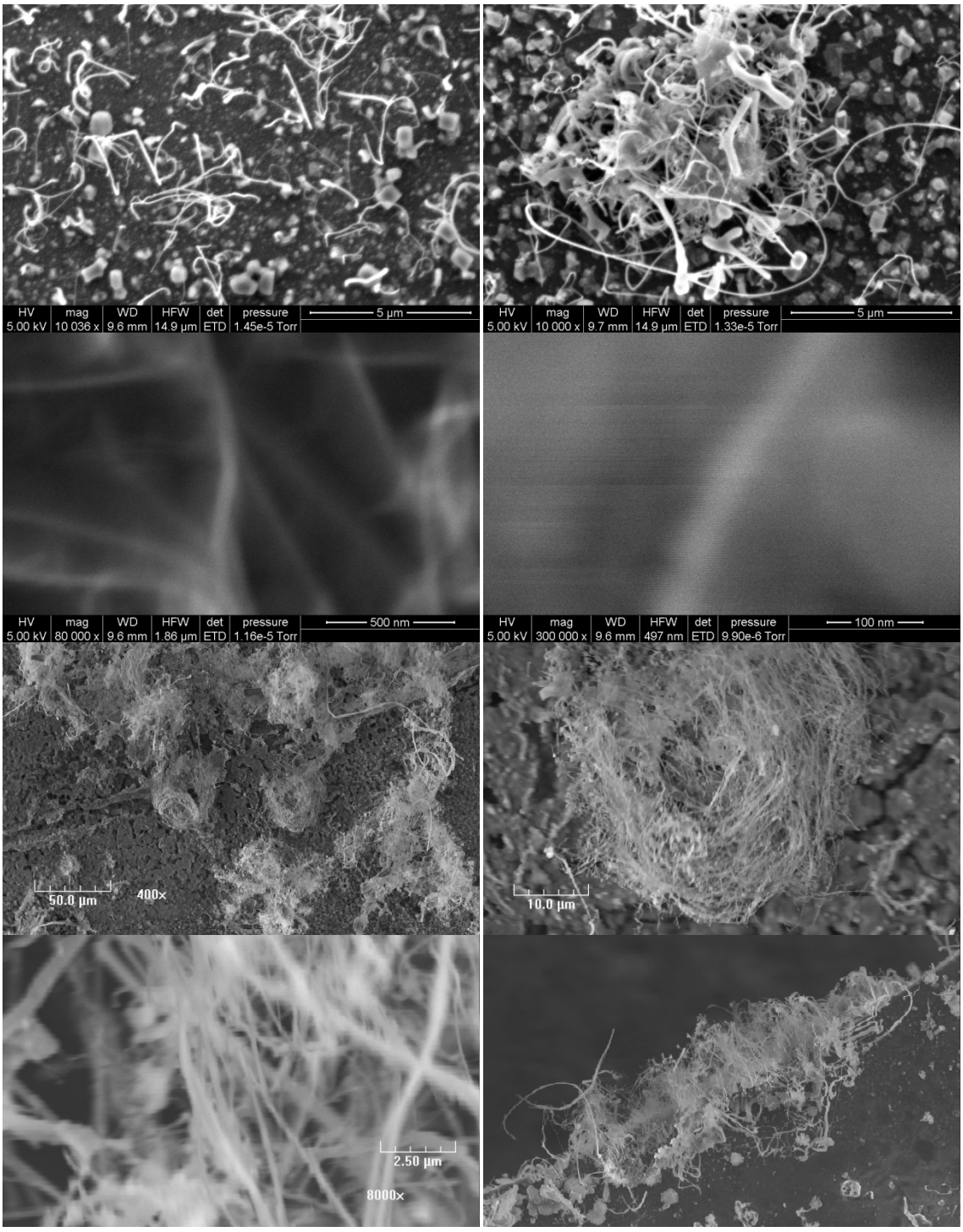

Figure 46: SEM images from the experiments (Pd Catalyst, Method II) at various magnifications, showing smooth and curved CNTs.

4.4.2 Raman Spectroscopy

Raman Spectra from the samples are shown in Figure 47.

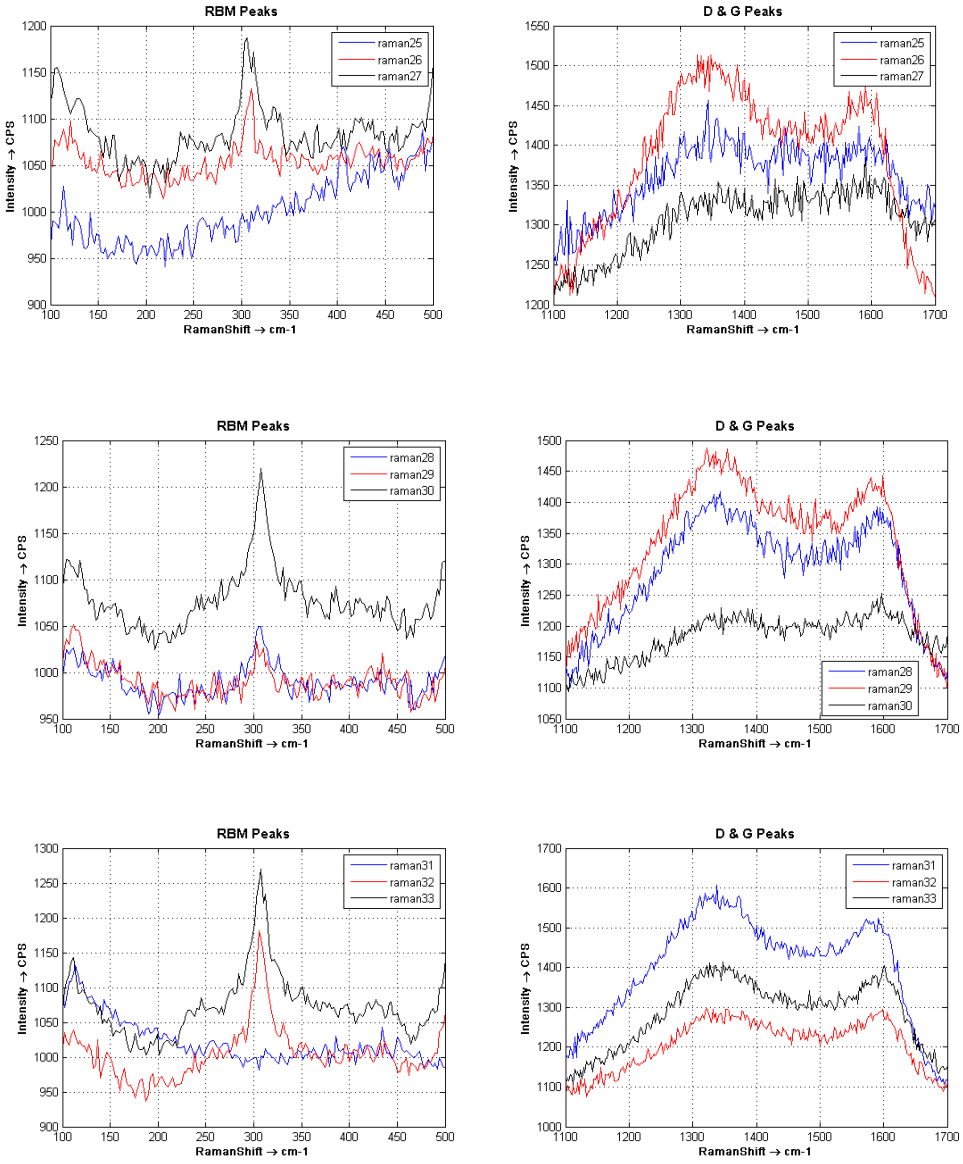

Figure 47: Raman Spectra from the method II repeated experiments showing the desired D and G peaks.

4.5 Uncertainty Analysis

The precision range for any calculations done for CNT diameter measurements for the bulk deposition experiments can be found out using the Kline and McKlintocks method for any particular Raman spectra by taking the uncertainty of the Raman shift as ± 1.165 and using the equations mentioned in section 3.4.

4.6 Patterned Deposition Results

Patterning of Palladium Chloride catalyst solution was accomplished using Dip Pen Nanolithography technique. These depositions were confirmed through LFM scans, with dimensions bigger than that of the deposition. The patterning success using DPN depends on humidity, scanning speed and sample surface roughness. While the first two can be controlled, the third depends entirely on the sample used. Higher the surface roughness, lower the rate of deposition. Owing to this fact, the depositions were mostly successful only on fullerene coated SINDEX chips. The PIMTEM chips recorded high surface roughness values, of the order of 50-100 nm, whereas Sindex Chips Recorded 1-5 nm.

DPN patterning was performed on the bare PIMTEM chips using Ni catalyst at various locations. These locations were recognized with the help of the marker present on the chip. These chips were then subjected to the CVD synthesis process. SEM imaging was performed at the locations where the deposits were made. These locations showed successful synthesis of nanotubes. Figure 48 shows the location of areas where

DPN was performed and the high magnification images at those locations. The images show successful synthesis of CNT at the locations of DPN patterning.

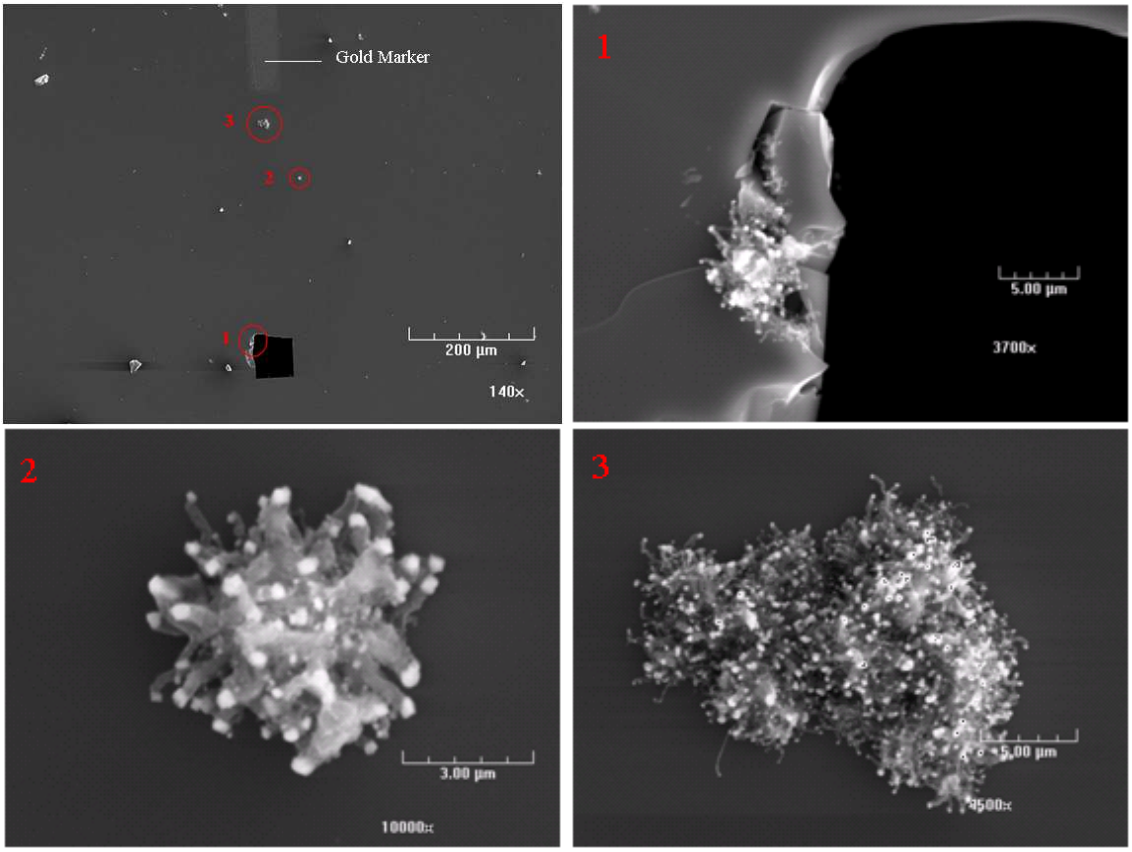

Figure 48: SEM images of the PIMTEM chip showing the patterned deposition locations in red circles, and magnified image of each location showing successful CNT synthesis.

4.7 Passive Probes Results

In these experiments, passive probes were used as the substrates. The initial few runs did not yield any results. We recognized the problem as since the tip is elevated from the heater surface, the temperature might be lower, due to the flow of nitrogen. To avoid this problem, the temperature of the heater was raised to ~570 ºC, so that the

desired elevation will have the temperature around 500 ºC. This worked and the SEM results are shown in Figure 49.

4.7.1 SEM

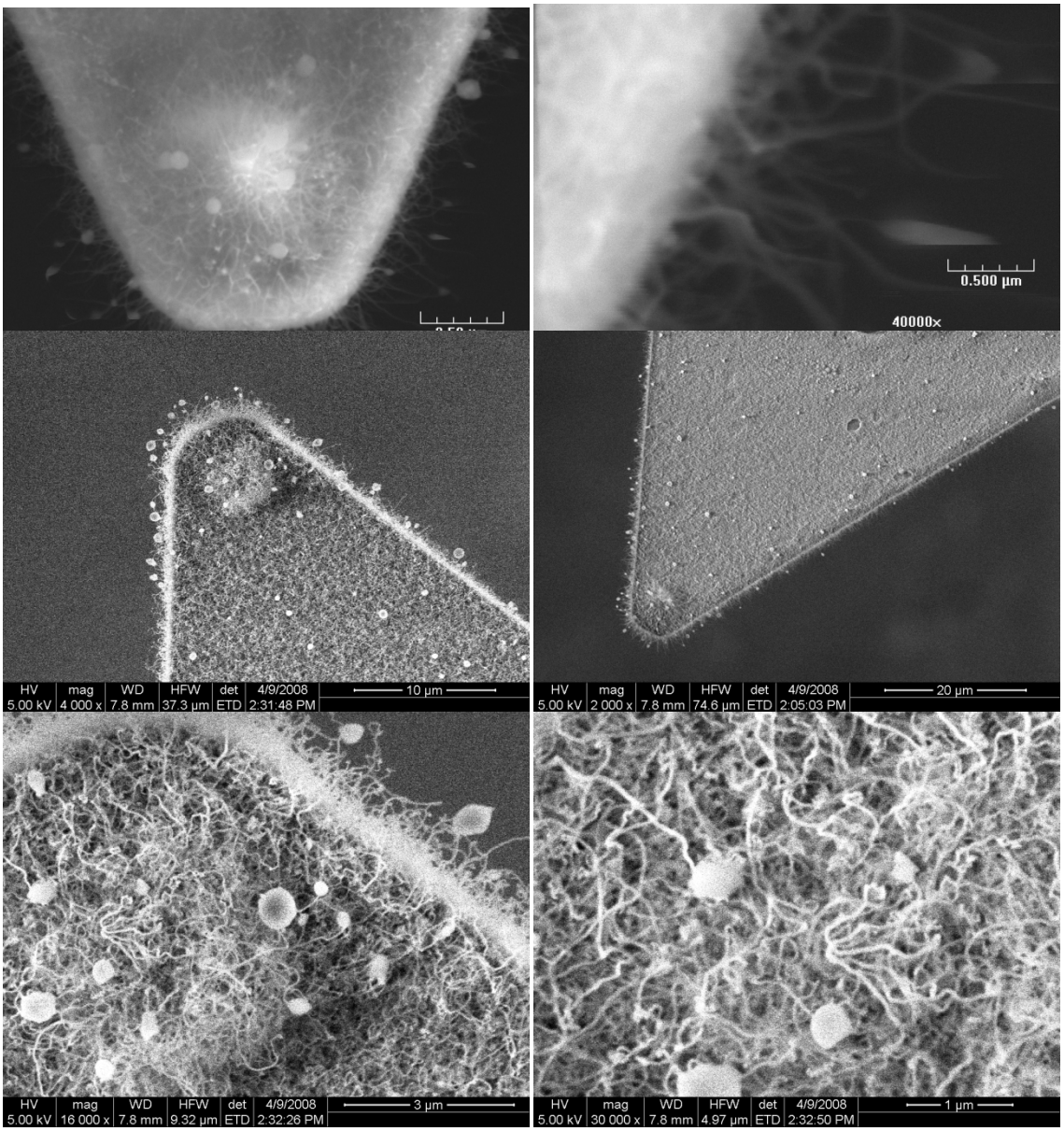

Figure 49: SEM images from the experiments on passive probes as substrates (Pd Catalyst, method I) at various magnifications.

The diameter of the tubes was found to be ranging from 20 nm – 200 nm. The nodules seen in the above images were identified as Sodium deposits after doing an EDS on these nodules at high magnification. Sodium comes from the Sodium hydroxide pellets that are used to dissolve Palladium in water. The data obtained from the EDS unit is presented in the graph shown in Figure 50. Palladium is not visible in this spectrum since it needs higher excitation voltage, and the voltage was kept minimal to avoid charge trapping in the samples, since none of the samples were sputter coated or silver painted. Charge trapping in the passive probes was seen to cause immediate damage to the tips in previous SEM imaging experiments.

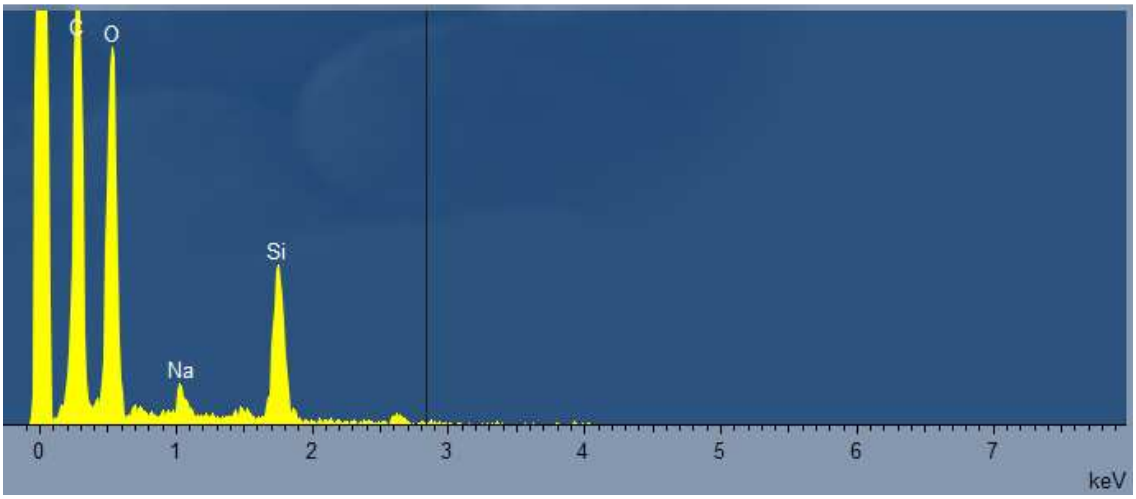

Figure 50: EDS micrograph obtained from the passive probe samples shows Silicon and Carbon presence. The first peak seen at 0 KeV does not mean anything.

4.7.2 Raman

Raman was tried on these samples and the collected data obtained is shown in Figure 51.

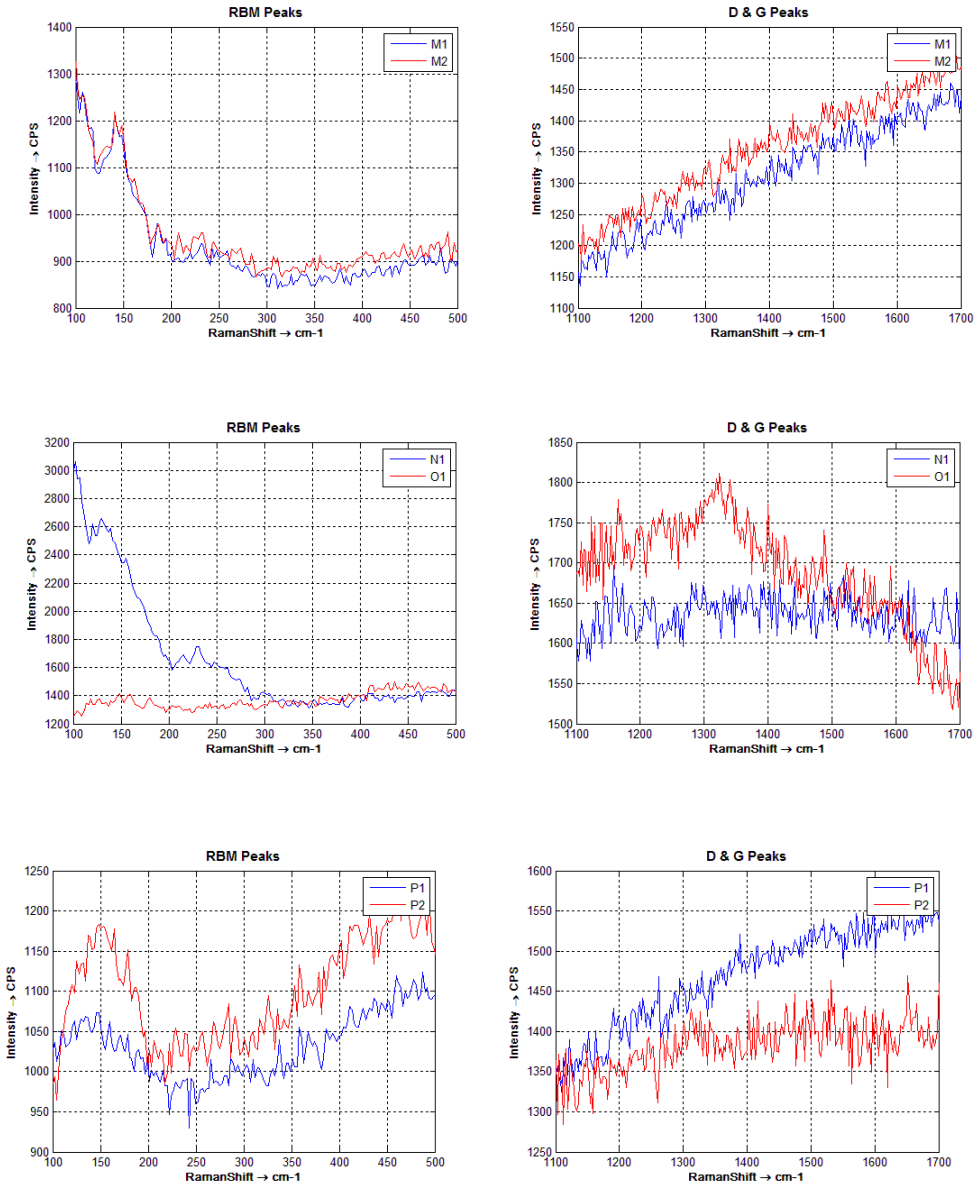

Figure 51: Raman spectra from the passive probe samples.

As seen from these images, distinct CNT spectra was not observed, so a SEM was done performed to verify if handling had damaged the CNT samples. It was seen that at the points where the Raman Spectroscopy was done, the tube layer had ablated

because of the laser intensity. (laser signal at various intensities was tried with the same result). The ablation is shown in Figure 52.

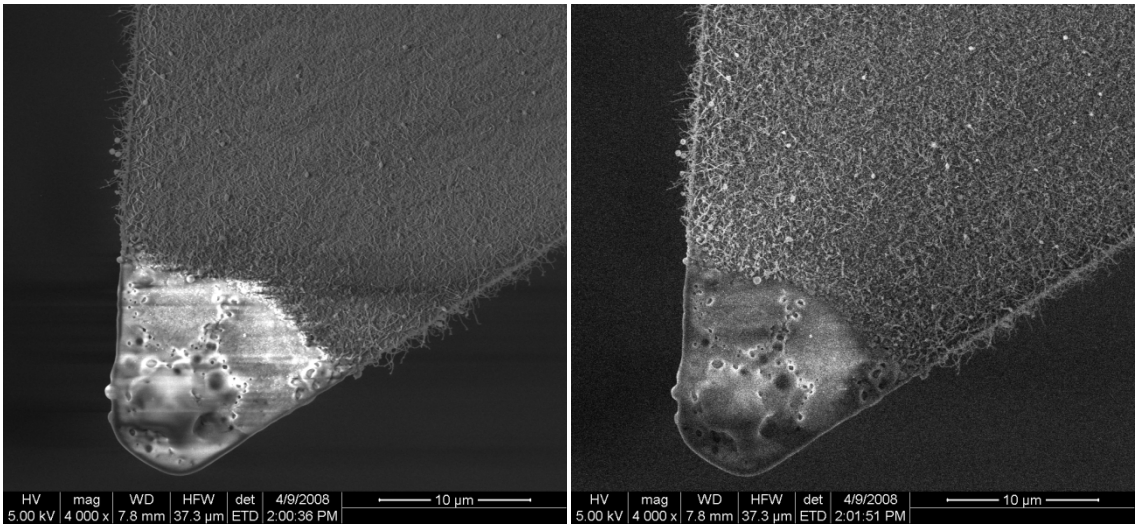

Figure 52: SEM images of the passive probes obtained after doing the Raman Spectroscopy, showing the ablation of nanotubes.

4.8 Conductivity Results

4.8.1 Wet Method

The results obtained from this approach indicated that the electrical conductivity of a sample coated with CNTs shows ~200-300% enhancements over that of the bare sample. These experiments were conducted for the proof of concept, without any precise control (eg. only exposing the CNT coated surface of the electrode and using controlled concentration of the salt solution).

The results obtained from these experiments are discussed next.

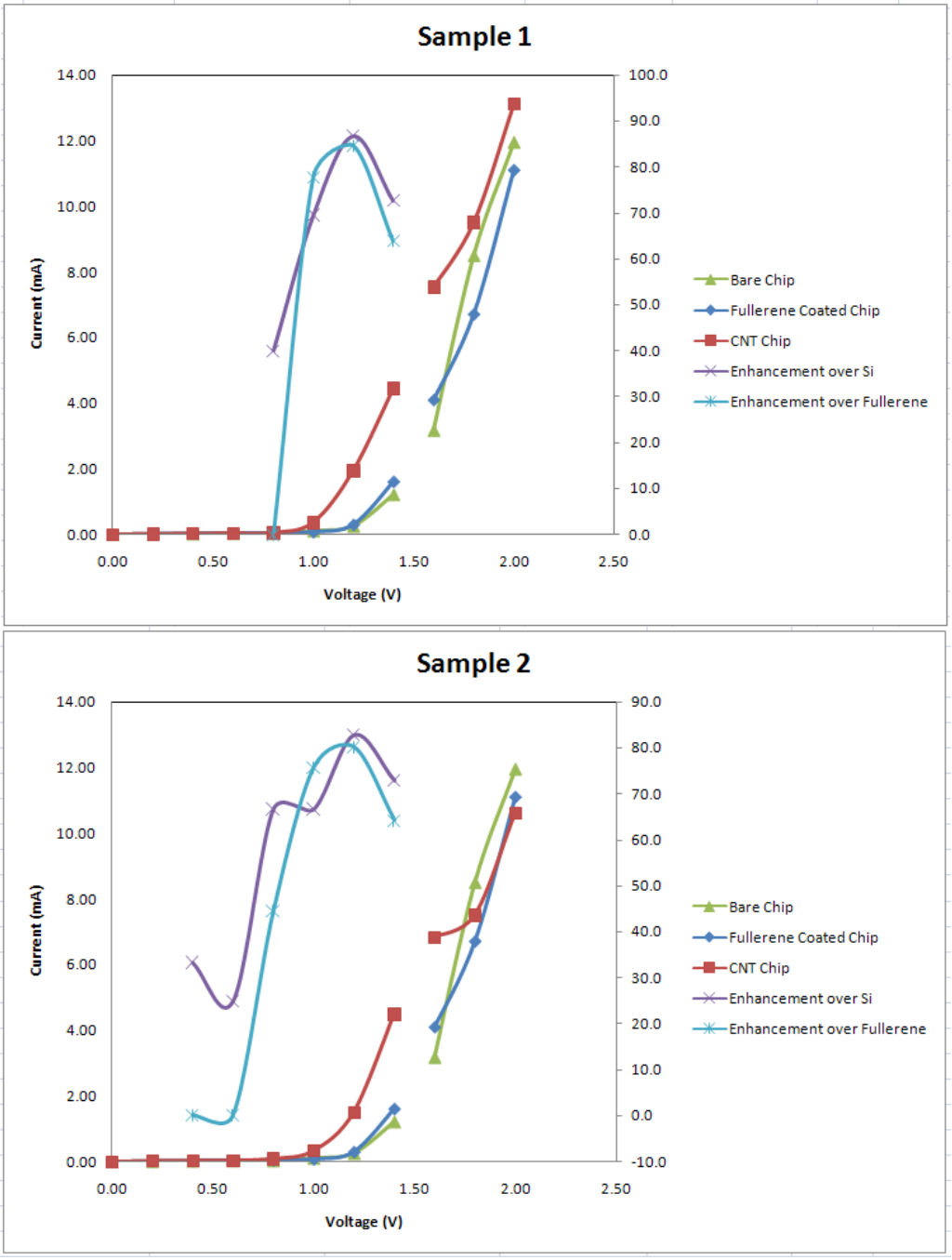

Figure 53: Variation of current w.r.t. voltage for the two samples, showing increased currents for same voltage on the CNT coated Chips.

The graphs presented in Figure 53 show that higher current is obtained for the same supply voltages in case of the CNT coated sample as compared to a bare or fullerene coated sample.

Log plots for the same data are shown in Figure 54 for enhanced clarity. These allow easy identification of the behavior of the CNT coated sample with respect to change in voltage on a logarithmic scale.

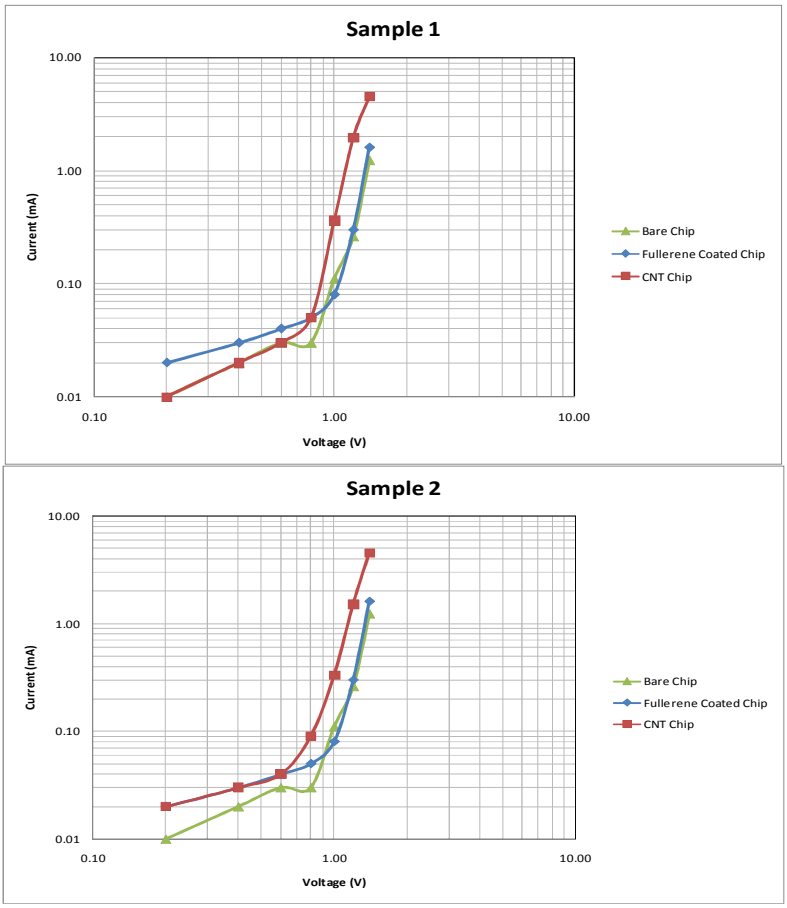

Figure 54: Logarithmic Variation of current w.r.t. voltage for two samples, showing increased currents for same voltage on the CNT coated Chips.

CHAPTER V

CONCLUSION AND FUTURE DIRECTION

Till date, attempts have been made to synthesize Carbon Nanotubes at low temperatures to obtain better quality and other obvious benefits. Literature review shows that synthesis at temperatures as low as 666 ºC (Ren *et al*., 1998) and even 520 ºC (Choi *et al*., 2000) have been achieved**.** Both of these researches were variations of the basic CVD method. In this research, we have demonstrated synthesis temperatures lower than the values reported in the literature. Results from the experiments indicate that we have been able to synthesize CNTs at much lower temperatures, ranging from 350 ºC - 580 ºC. Even though the basic synthesis principle remains the same, the method we have used is different from all the other methods mentioned. Lower synthesis temperatures helps to improve the quality of the resulting CNTs. Temperature values can be used to control and hence improve the growth rate, density, length and crystalline nature of nanotubes (Lee, *et al*., 2001). We don't require any gas flows other than Nitrogen to maintain an inert atmosphere, hence this technique can be used to synthesize CNT in vacuum. This allows us to keep the synthesis apparatus simple, compact and even realize a portable/hand held platform.

We also have various scenarios where we have been able to grow CNT's of a specific type and even specific diameters and hence chirality. More experimentation is needed on these topics, so that dedicated conditions for different types of CNT's can be confirmed. If successful this would be a breakthrough and of great advantage.

As seen in the results sections, in case of deposition using Fullerene solution, the usually smooth and curvy CNT were obtained, whereas in case of thermal vapor deposition technique for Fullerene, straight nanotubes were observed.

The Table III shows a comparison of the popular commercial methods to the novel method developed in this study:

Table III: Comparison of popular commercial methods for CNT synthesis against the novel approach.

	CVD	Arc Discharge	Laser Ablation	New Method
Synthesis Temperature	500°-1000°C	>1000°C	1200°C	300-600°C
Cost	High (~$3000)	High (~$10000)	High	Low (~$100 - $500)
Carbon Source	Liquid or Gas	Solid	Solid	Liquid or Solid deposition
CNT Defectiveness	High	High	Low	Low
Purity	Mixed	Mixed	Mixed	Single chirality possible.
Process gases	Required	Required	Required	Not required
Pressure	Atmospheric	~500 torr	~500 – 600 torr	Atmospheric or vacuum
Orientation	Vertical alignment possible	Random orientation	Random orientation	Vertical alignment possible

We have also demonstrated *in-situ* synthesis of CNT on AFM probes. This can be used to enhance the capability of Dip Pen Nanolithography. We speculate that use of Nanotubes for this process would increase the sharpness of the tips to a considerable extent and hence the accuracy significantly, allowing depositions at far more smaller scales than those possible today, which in turn can be used to enhance the synthesis process developed in this study.

This proves the feasibility for realizing a hand held portable platform for synthesis of CNT with tunable chirality “on demand”.

REFERENCES

Bandow S, Asaka S, Saito Y, Rao A, Grigorian L, Richter E, Eklund P: Effect of the growth temperature on the diameter distribution and chirality of single-wall carbon nanotubes, *Phys. Rev. Lett*. **80**, 3779 - 3782 (1998).

Banerjee D, Amro N, Disawal S, Fragala J: Optimization of microfluidic ink-delivery apparatus for Dip Pen Nanolithography, J Microlith, Microfabric Microsystems **4**, 23014–23021 (2005).

Brief Communications: Carbon nanotubes in an ancient Damascus sabre, *Nature* **444**, 16 Nov. (2006).

Chen G, Warmack R, Thundat T, Allison D: Resonance response of scanning force microscopy cantilevers, *Rev. Sci. Instrum* **65**, 2532-2537 (1994).

Cheung C, Camarero J, Woods B, Lin T, Johnson J, Yoreo J: Fabrication of assembled virus nanostructures on templates of chemoselective linkers formed by scanning probe nanolithography, *J. Am. Chem. Soc.* **125**, 6848–6849 (2003).

Cho Y, Ivanisevic A: SiOx surfaces with lithographic features composed of a TAT peptide, *J. Phys. Chem. B* **108**, 15223–15228 (2004).

Cho Y, Ivanisevic A: TAT peptide immobilization on gold surfaces: a comparison study with a thiolated peptide and alkylthiols using AFM, XPS, and FT-IRRAS, J. *Phys. Chem. B* **109**, 6225–6232 (2005).

Choi Y, Bae D, Lee Y, Lee B, Han I, Choi W, Lee N, Kim J: Low temperature synthesis of carbon nanotubes by microwave plasma-enhanced chemical vapor deposition, *Synthetic Metals* **108**, 159-163 (2000).

Cleveland J, Manne S, Bocek D, Hansma K: A nondestructive method for determining the spring constant of cantilevers for scanning force microscopy, *Rev. Sci. Instrum*. **64**, 403-405 (1993).

Collins P, Avouris P: Nanotubes for electronics, *Scientific American* **283**, 62-69 (2000).

Czerwosz E, Dluzewski P, Dmowskaa G, Nowakowskid R, Starnawskae E, Wronka H: Atomic force microscopy and transmission electron microscopy investigations of catalytic formed nanotubes in C60/C70+Ni layers, *Applied Surface Science* **141**, 350–356 (1999).

Dai H, Rinzler A, Nikolaev P, Thess A, Colbert D, Smalley R: Single-wall nanotubes produced by metal-catalyzed disproportionation of carbon monoxide, *Chem. Phys. Lett.* **260**, 471-475 (1996).

Demers L, Ginger D, Park S, Li Z, Chung S, Mirkin C, Direct patterning of modified oligonucleotides on metals and insulators by dip-pen nanolithography, *Science* **296**, 1836–1838 (2002).

Diegoli S, Hamlett C, Leigh S, Mendes P, Preece J: Engineering nanostructures at surfaces using nanolithography, *Proceedings of the Institution of Mechanical Engineers Part G-Journal of Aerospace Engineering* **221**, 589-629 (2007).

Dresselhaus M, Dresselhaus G, Eklund P: Science of fullerenes and carbon nanotubes (1st ed.). Elsevier Science, Academic Press-New York (1996).

Ebbesen T, Ajayan P: Large scale synthesis of carbon nanotubes. *Nature* **358**, 220-222 (1992).

Eklund P, Holden J, Jishi R: Vibrational modes of carbon nanotubes: spectroscopy and theory, *Carbon* **33**, 959-972 (1995).

Eichhorn V, Stolle C: Automated nanohandling by microrobots(1st ed.). Springer, Verlag-London, (2007).

Guo T, Nikolaev P, Thess A, Colbert D, Smalley R: Catalytic growth of single-walled nanotubes by laser vaporization, *Chemical Physics Letters* **243**, 49-54 (1995).

Iijima S: Helical Microtubules of Graphitic carbon, *Nature* **354**, 56-58 (1991).

Jeroen W. G. Wilder; Liesbeth C. Venema; Andrew G. Rinzler; Richard E. Smalley; Cees Dekker;: Electronic structure of atomically resolved carbon nanotubes: *Nature* **391**, 59-62 (1998).

Jiang Z, Stupp S: Dip-pen patterning and surface assembly of peptide Amphiphiles, *Langmuir* **21**, 5242–5246 (2005).

Jorio A, Saito R, Dresselhaus G, Dresselhaus M: Determination of nanotubes properties by Raman spectroscopy, *Philos Trans R Soc Lond* Part A **362**, 2311–2336 (2004).

Jorio A, Saito R, Hafner J, Lieber C, Hunter M, et al.: Structural determination of isolated single-wall carbon nanotubes by resonant Raman scattering, *Phys Rev Lett* **86**, 1118 (2001).

Journet C, Bernier P: Production of carbon nanotubes, *Applied Physics A* 67, 1-9(1998).

Journet C, Maser W, Bernier P,Loiseau A, Chapelle M, Lefrant S, Deniards P, Lee R, Fischer J: Single-walled carbon nanotubes by the electric-arc technique, *Nature* **388**,756-758 (1997).

Kline J, McClintock A: “Describing the uncertainties in single sample experiments”. Mechanical Engineering **75**, 3–8 (1953).

Kolobov A: Raman scattering from Ge nanostructures grown on Si substrates, *Journal of Applied Physics*, **87**, 2926-2930 (2000).

Kroto H, Heath J, O'Brien S, Curl R, Smalley R: C60: Buckminsterfullerene, *Nature* **318**, 162 – 163 (1985).

Huitink D, Banerjee D, Sinha S: Precise control of carbon nanotube synthesis of a Single chirality, *IMECE2007* **42588**, 1-7 (2007).

Lee C, Jeunghee P, Huh Y, Lee J: Temperature effect on the growth of carbon nanotubes using a thermal chemical vapor deposition, *Chemical Physics Letters* **343**, 33-38 (2001).

Lefrant S, Buisson J, Schreiber J, Wery J, Faulques E, Chauvet O, Baibarac M, Baltog I: RAMAN and SERS studies of carbon nanotubes, *Spectroscopy of Emerging Materials* **165**, 127-138 (2004).

Lee, K. B., Lim, J. H. and Mirkin, C. A. Protein nanostructures formed via direct-write dip-pen nanolithography. *J. Am. Chem. Soc.* **125**, 5588–5589 (2003).

Levin A, Meyer D, Reibold M, Kochmann W, Patzke N, Paufler P: Microstructure of a genuine Damascus sabre, *Cryst. Res. Technology* **40**, 905-916 (2005).

Li Y, Kim W, Zhang Y, Rolandi M, Wang D, and Da H: Growth of Single-Walled Carbon nanotubes from discrete catalytic nanoparticles of various sizes, *Journal of Physical Chemistry* **105**, 11424-11431 (2001).

Lim J, Ginger D, Lee K, Heo J, Nam J, Mirkin C: Direct-write dip-pen nanolithography

of proteins on modified silicon oxide surfaces. *Angew. Chem. Int. Edn* **42**, 2309–2312 (2003).

Louchev O, Laude T, Sato Y, Kanda H: Diffusion-controlled kinetics of carbon nanotube forest growth by chemical vapor deposition, *J. Chem. Phys*. **118**, 7622-7634 (2003).

Morjan R, Nerushev O, Sveningsson M, Rohmund F, Falk L, Campbell E: Growth of carbon nanotubes from C60, *Applied Physics* **78**, 253–261 (2004).

National Geographic News: Legendary swords' sharpness, strength from nanotubes, *Study Says* 16 Nov. (2006).

Ouellette J: Building the Nanofuture with Carbon Tubes, *The Industrial Physicist*, December, 18-21, (2002).

Piner R, Zhu J, Xu F, Hong S, Mirkin C: Dip-Pen Nanolithography, *Science* **283**, 661-663 (1999).

Rao C, Satishkumar B, Govindaraj A, Manashi Nath: Nanotubes, *ChemPhysChem* **2**, 78-105 (2001).

Ren Z, Huang Z, Xu J, Wang J, Bush P, Siegal M, Provencio P: Synthesis of large arrays of well-aligned carbon nanotubes on glass, *Science* **282**,1105-1107 (1998).

Reinke P, Oelhafen P: *In situ* photoelectron spectroscopy investigation of silicon cluster growth on fullerene surfaces, Physical Review **71**, 045420-1 - 045420-8 (2005).

Rivas-Cardona J, Banerjee D: Microfluidic device for delivery of multiple inks for dip pen nanolithography, *J. Micro/Nanolith. MEMS MOEMS* **6**, 0330041-0330049 (2007).

Robertson J: Growth of nanotubes for electronics, *Materials Today* **10**, 36–45 (2007).

Rozhok S, Clifton K, Shen C, Pey-Lih L, Zhifang F, Chang L, Chad A, Mirkin, Richard C: Methods for fabricating microarrays of motile bacteria. *Small* **1**, 445–451 (2005).

Saito R, Jorio A, Filho A, Dresselhaus G, Dresselhaus M, Gruneis A, Cancado L, Pimenta M: First and second-order resonance raman process in graphite and single wall carbon nanotubes, *Jpn. J. Appl Phys* **41**, 4878-4882 (2002).

Salvetat J: Mechanical properties of carbon nanotubes, *Applied Physics Letters* **69**, 255-260 (1999).

Schwartz P: Molecular Transport from an Atomic Force Microscope Tip: A Comparative Study of Dip-Pen Nanolithography, *Langmuir* **18**, 4041-4046 (2002).

Small J, Shi L, Kim P: Mesoscopic thermal and thermoelectric measurements of individual carbon nanotubes, *Solid State Communications* **127**, 181-186 (2003).

Su D, Chen W: Natural lavas as catalysts for efficient production of carbon nanotubes and nanofibers, *Angew Chem Int Ed Engl* **46**, 1823–1824 (2007).

Thomsen C, Reich S, Maultzsch J: Resonant Raman spectroscopy of nanotubes, Philos *Trans R Soc Lond Part A* **362**, 2337–2359 (2004).

Treacy M, Ebbesen T, Gibson J: Exceptionally high Young's modulus observed for individual carbon nanotubes, *Nature* **381**, 678-680 (1996).

Vettiger, P, Despont M, Drechsler U, Dürig U, Häberle W, Lutwyche M, Rothuizen H,

Stutz R, Widmer R, Binnig G: The "Millipede" - more than one thousand tips for future afm data storage, *IBM J. Res. Develop*. **44**, 323–340 (2000).

Vinciguerra V, Buonocore F, Panzera G, Occhipinti L: Growth mechanisms in chemical vapor deposited carbon nanotubes, *Nanotechnology* **14**, 655–660 (2003).

Weeks B, Vaughn M, DeYoreo, J: Direct imaging of meniscus formation in atomic force microscopy using environmental scanning electron microscopy, *Langmuir* **21**, 8096-8099 (2005).

Wilder J, Venema L, Rinzler A, Smalley R, Dekker C: Electronic structure of atomically resolved carbon nanotubes, *Nature* **391**, 59-62 (1998).

Zhao X, Ando Y, Qin L, Kataura H, Maniwa Y, Saito R: Radial breathing modes of multiwalled carbon nanotubes, *Chemical Physics Letters* **361**, 169–174 (2002).

APPENDIX I

EXTRA IMAGES

This section presents a few images from the experiments which did not yield results but were the stepping stones towards successful experiments.

Active Pen Results (Method I - Unsuccessful):

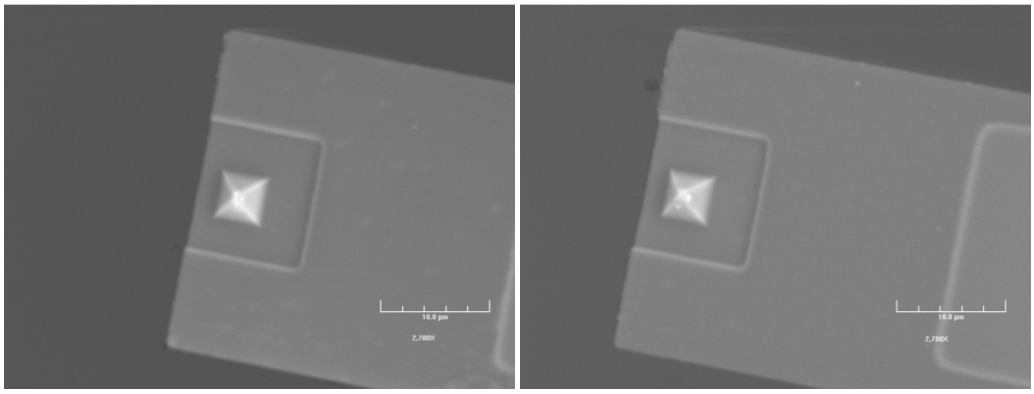

Figure I - 1: SEM images of the cantilever with CoCl2 catalyst.

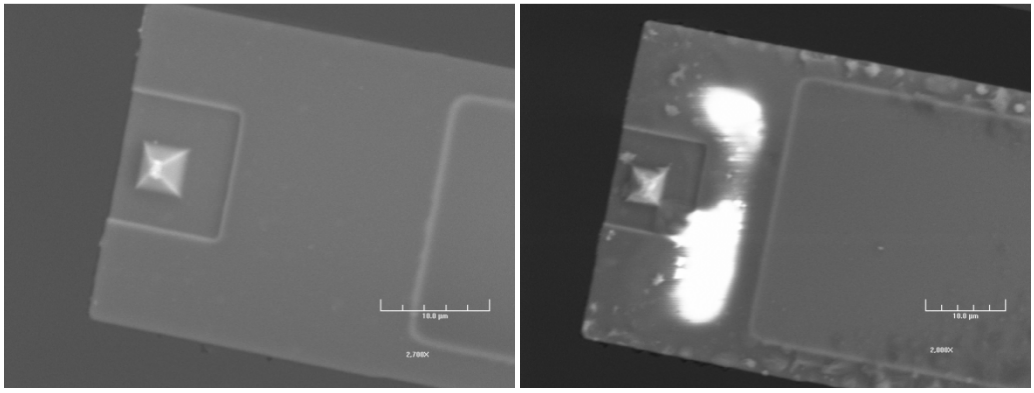

Figure I - 2: SEM images of the cantilever with NiCl2 catalyst.

Active Pen Results (Method II - Unsuccessful):

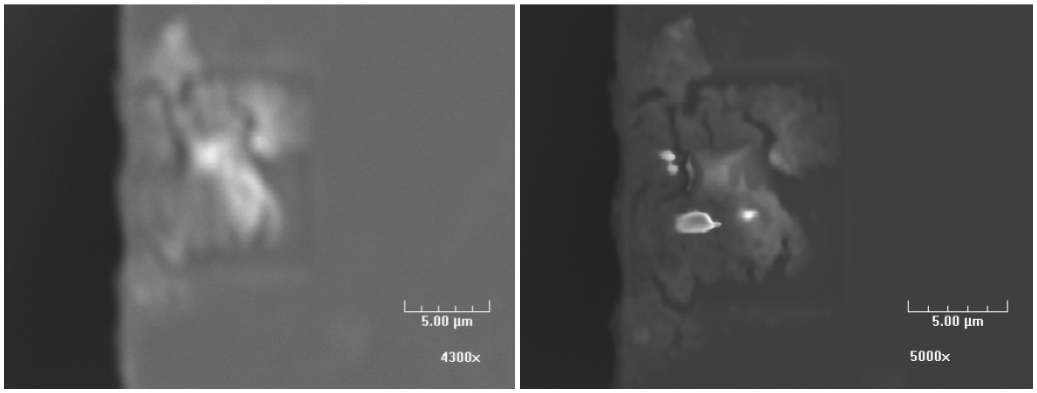

Figure I - 3: SEM images of the cantilever with CoCl2 catalyst.

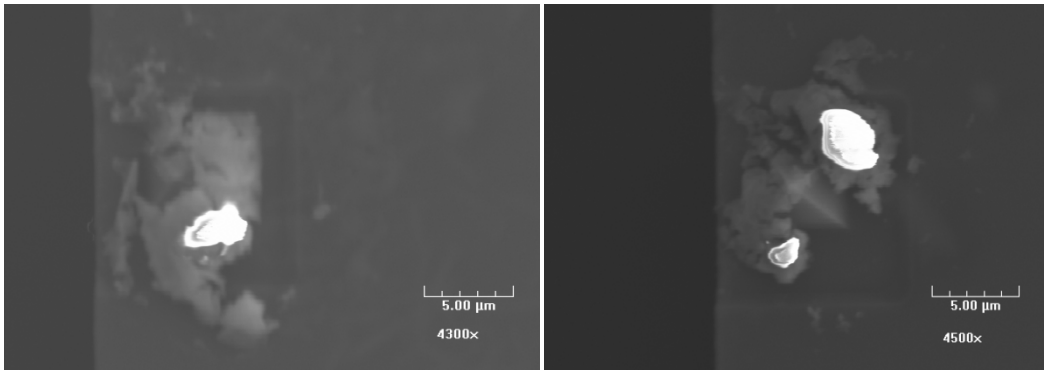

Figure I - 4: SEM images of the cantilever with PdCl2 catalyst.

PIMTEM chips results (Method I – Unsuccessful)

Initial experiments were done with all the 3 catalysts, PdCl2, NiCl2, and CoCl2. This experiment had a temperature of ~450 ºC. The images taken after the experiment are shown below.

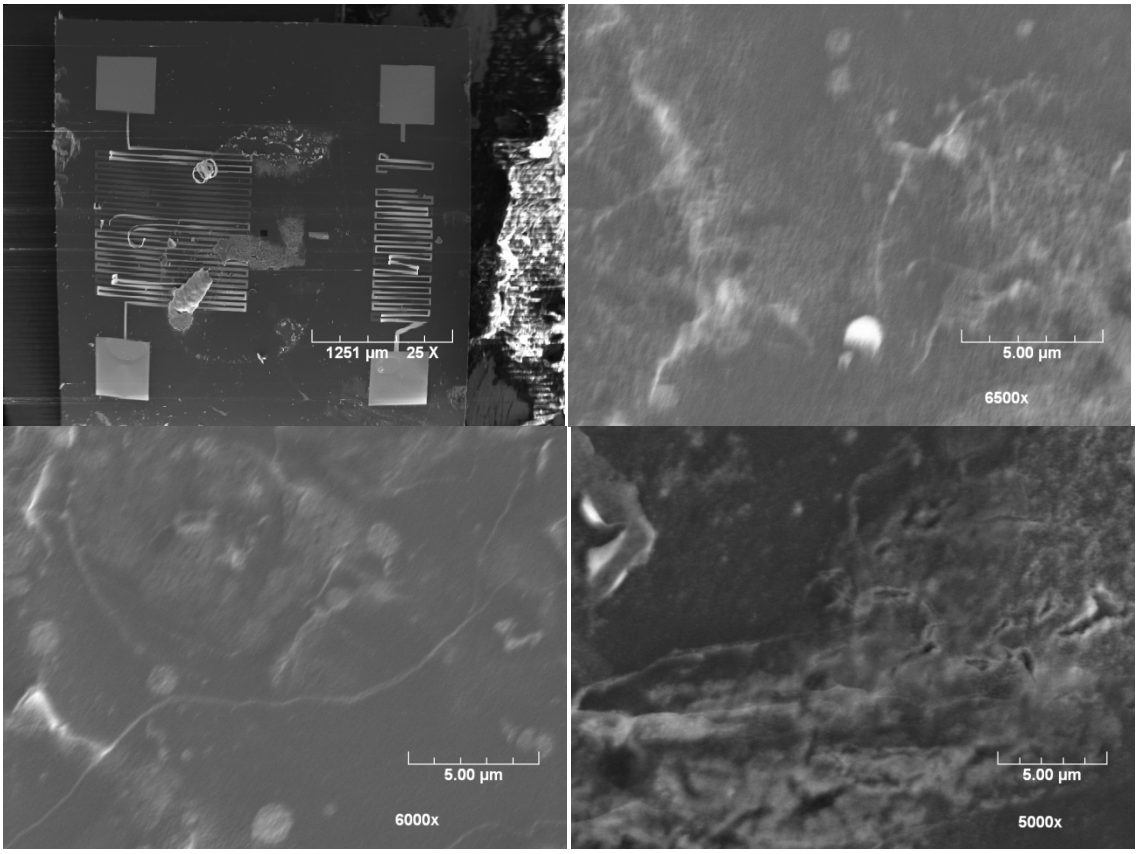

Figure I - 5: SEM images of the cantilever with CoCl2 catalyst.

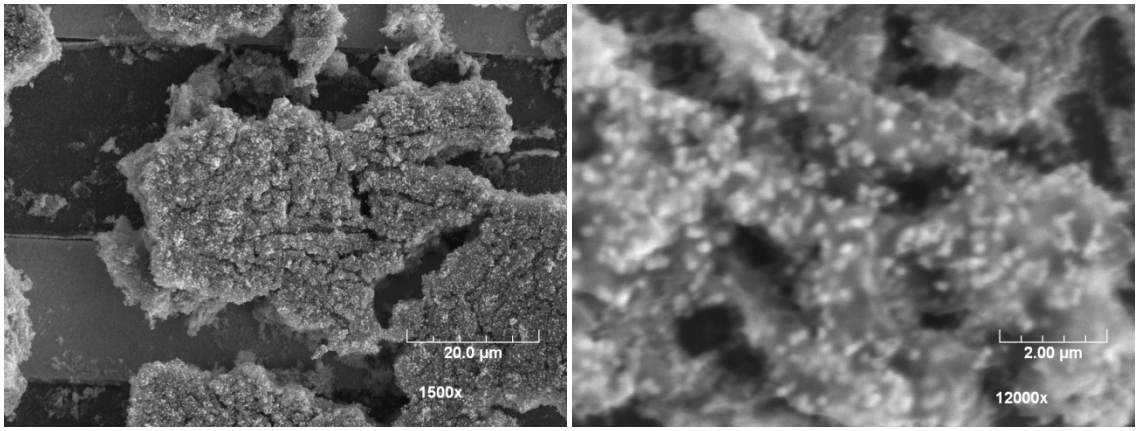

Figure I - 6: SEM images of the cantilever with CoCl2 catalyst.

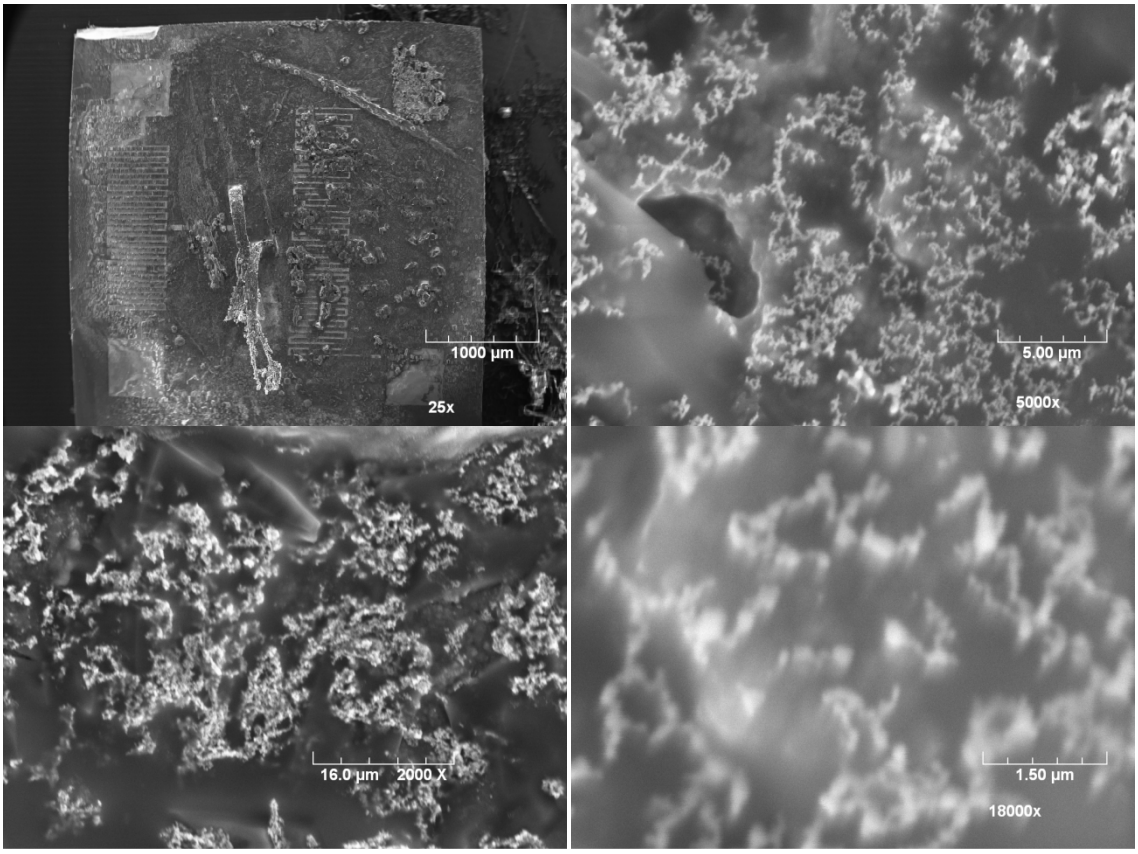

Figure I - 7: SEM images of the cantilever with PdCl2 catalyst.

PIMTEM chips results (Method I – Successful)

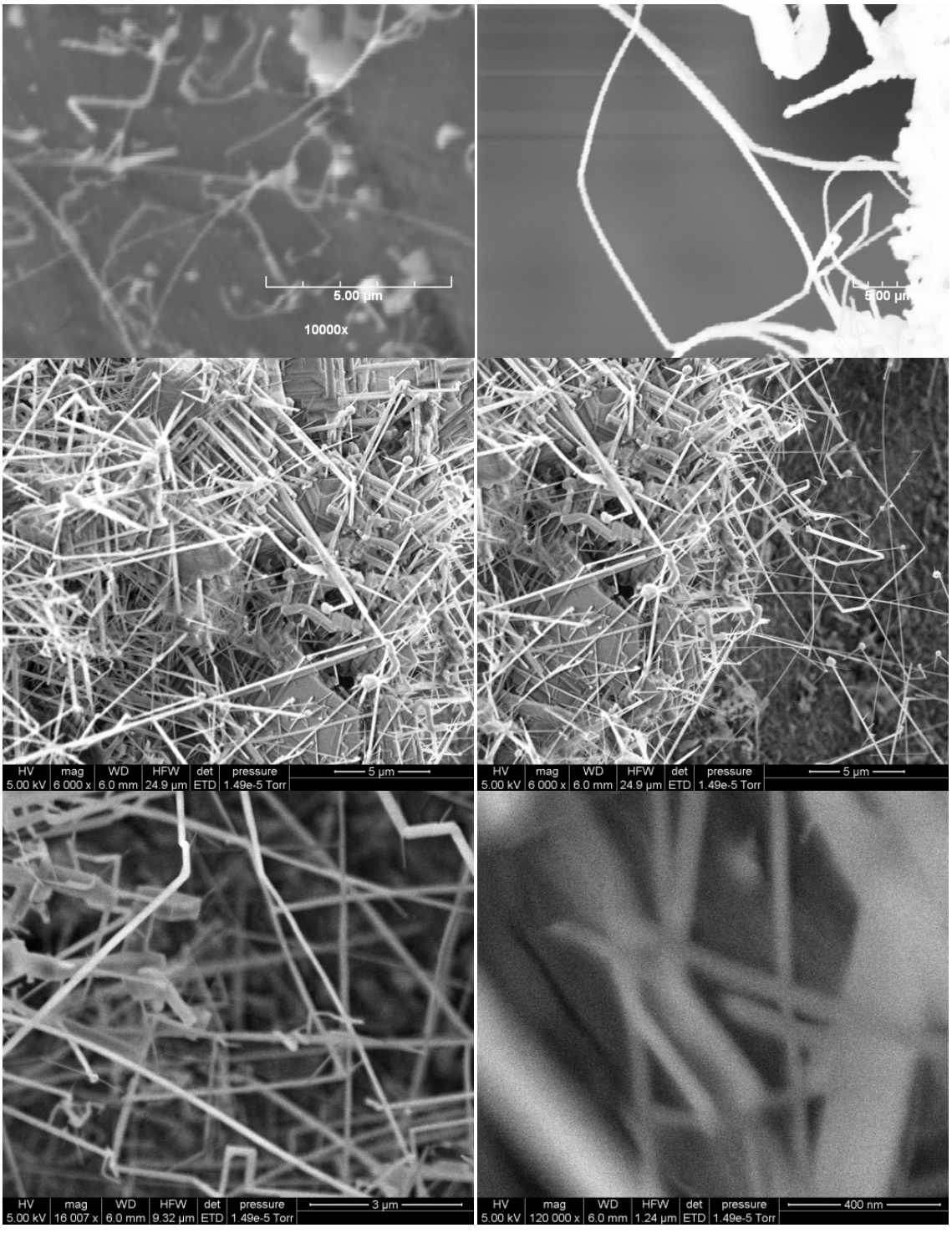

Figure I - 8: SEM images of the cantilever with PdCl2 catalyst (Method I).

Extra results from Raman Spectroscopy are shown below:

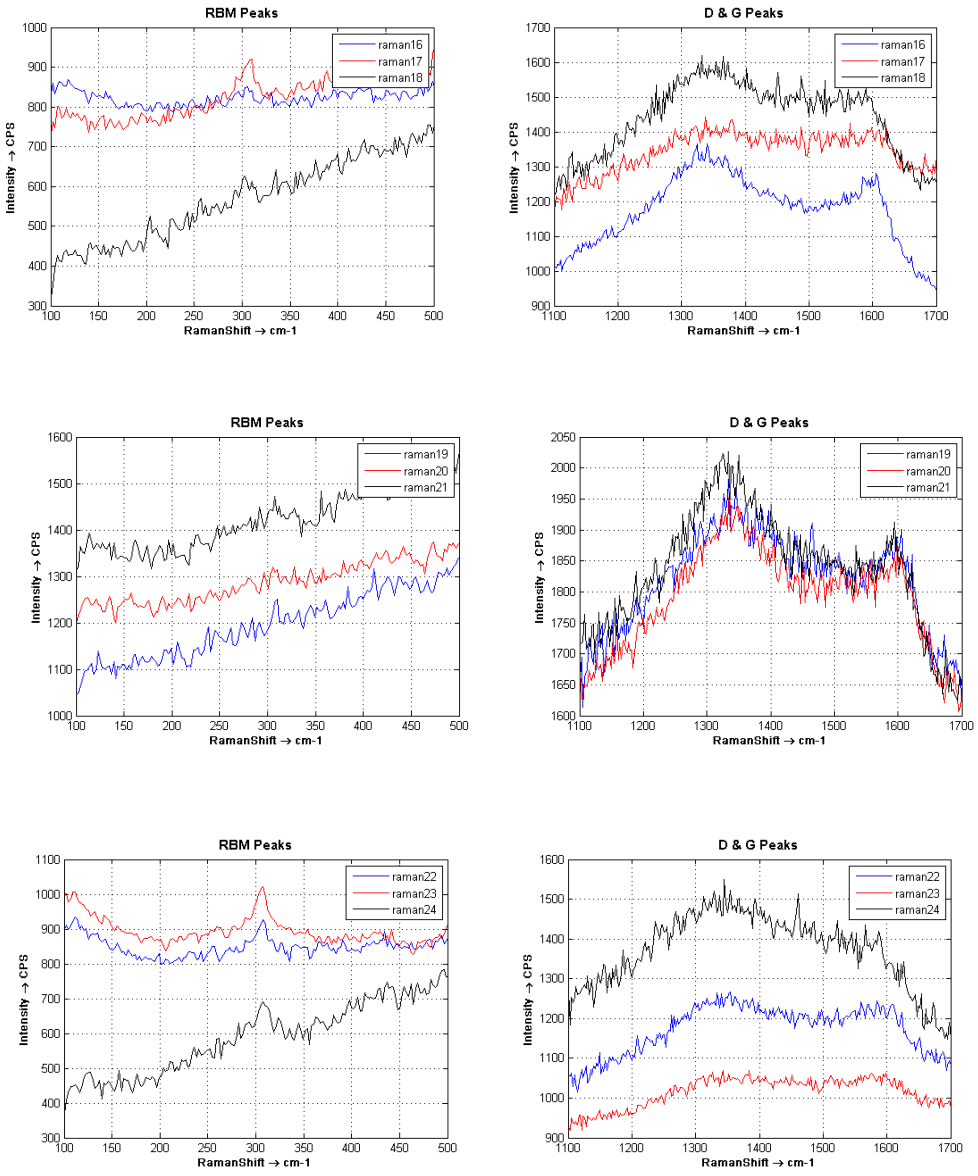

Figure I - 9: Raman spectra of the samples with PdCl2 catalyst (Method I).

PIMTEM chips results (Method II – Unsuccessful)

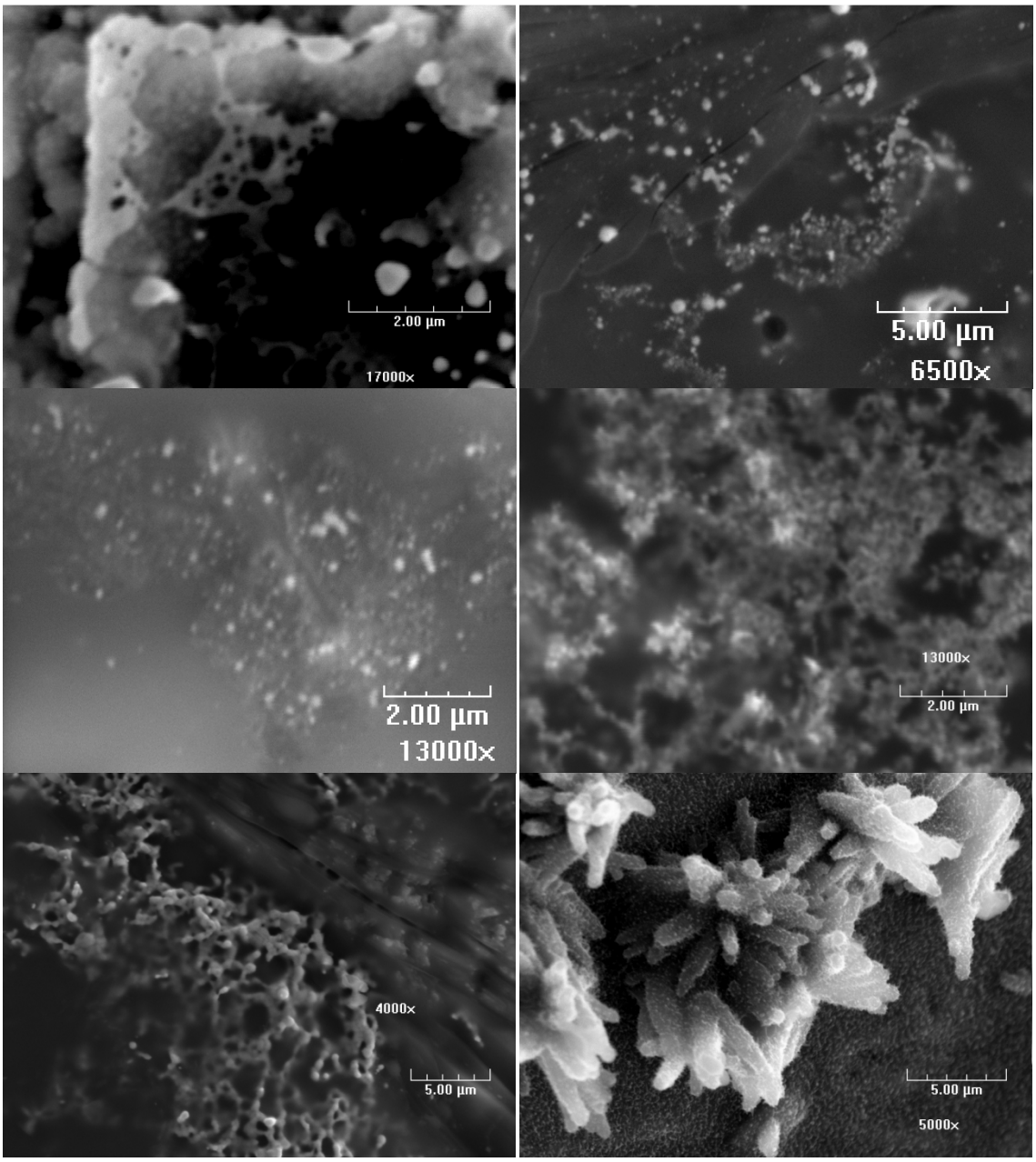

Figure I - 10: SEM Images of the samples with PdCl2 catalyst.

PIMTEM chips results (Method II – Successful)

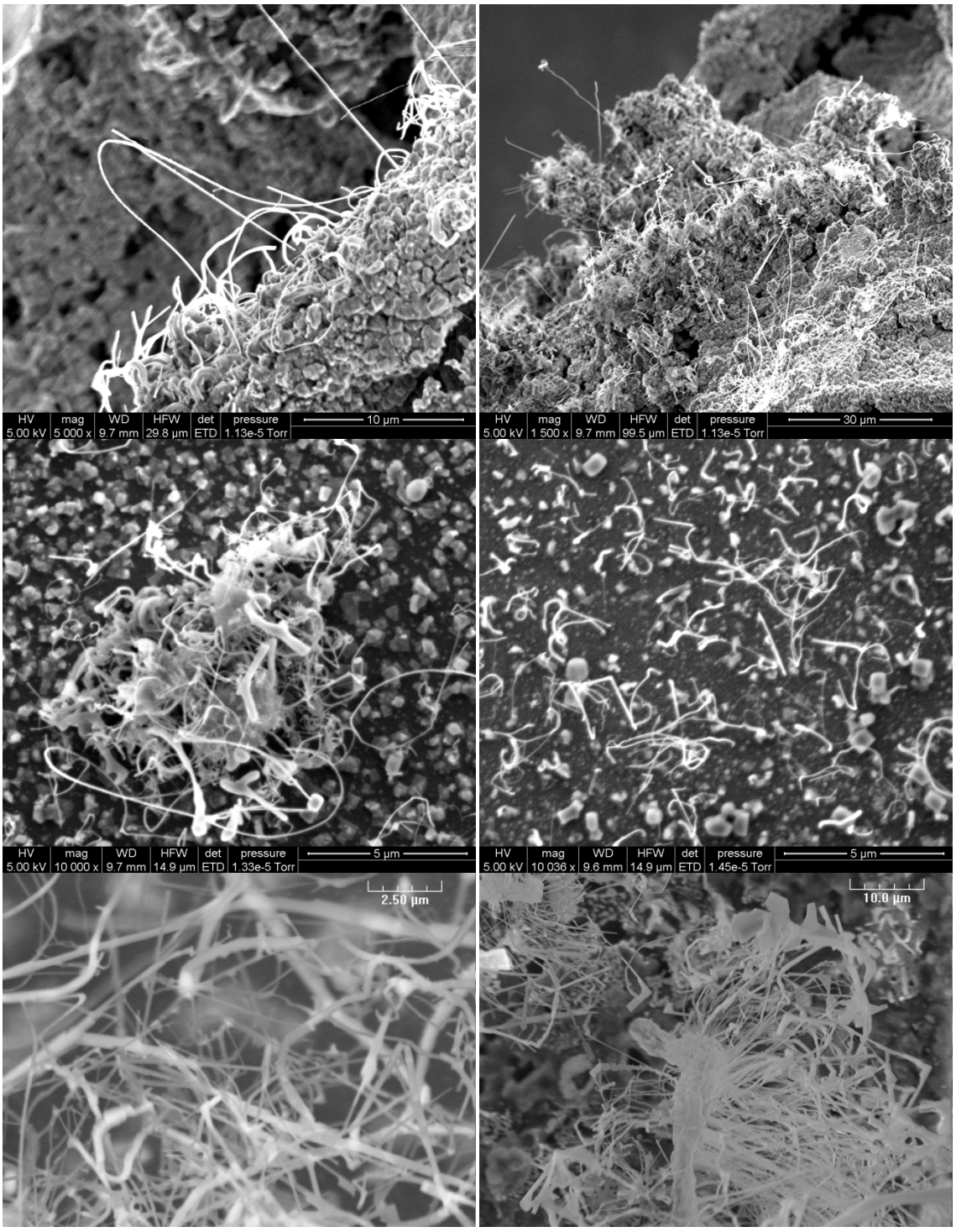

Figure I - 11: SEM Images of the samples with PdCl2 catalyst.

Extra results from Raman Spectroscopy are shown below:

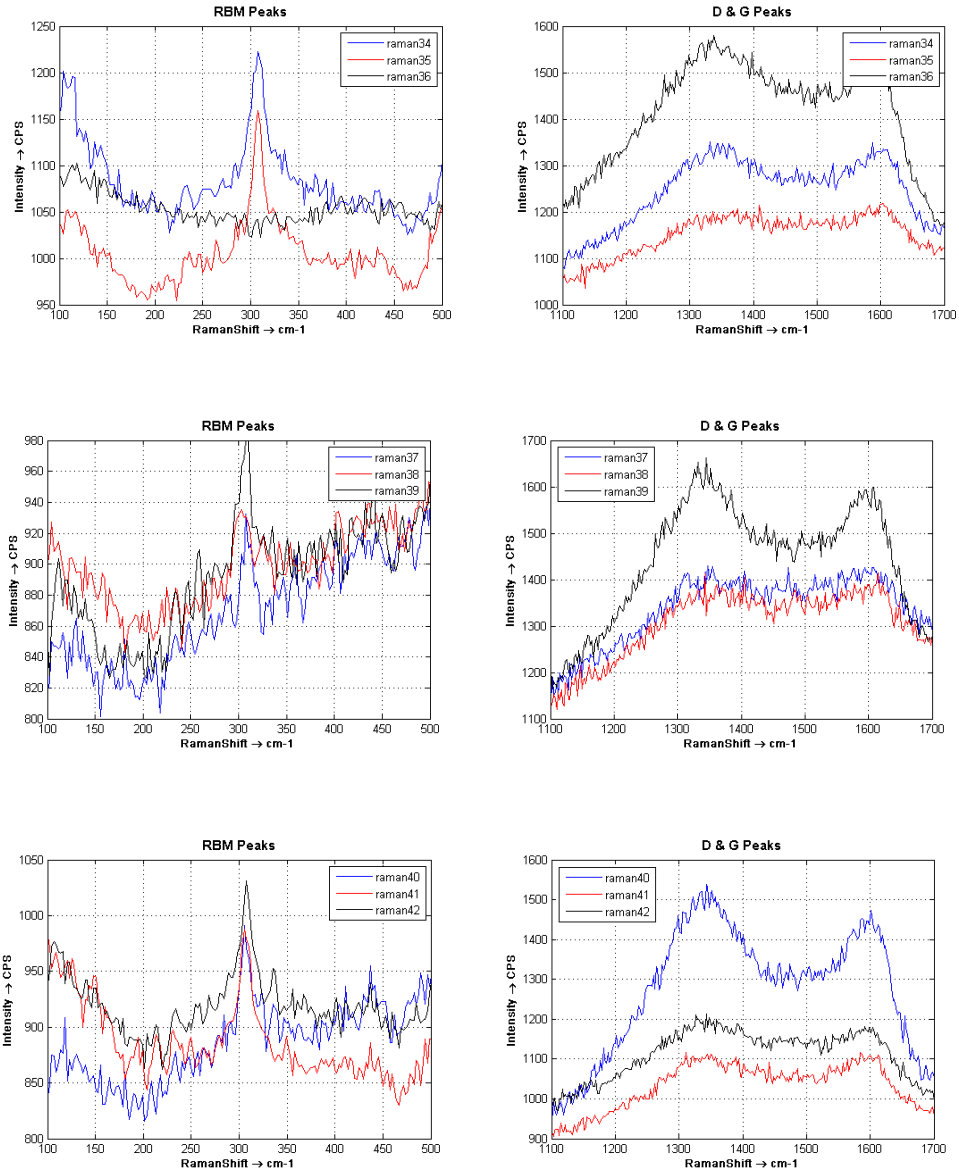

Figure I - 12: Raman Spectra of the samples with PdCl2 catalyst.

Passive Pen Results (Method I and II - Unsuccessful)

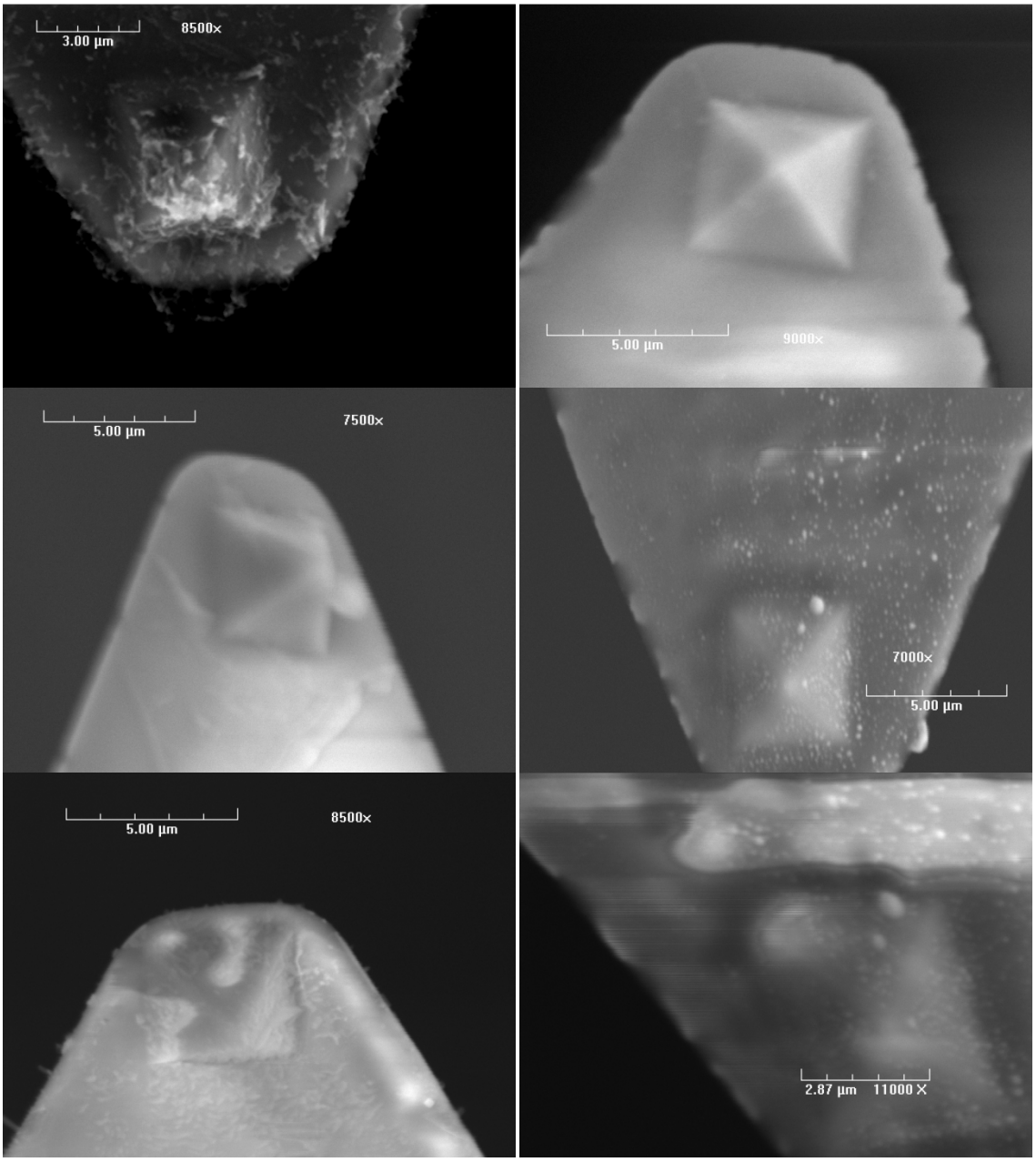

Figure I - 13: Passive pen SEM images - method I.

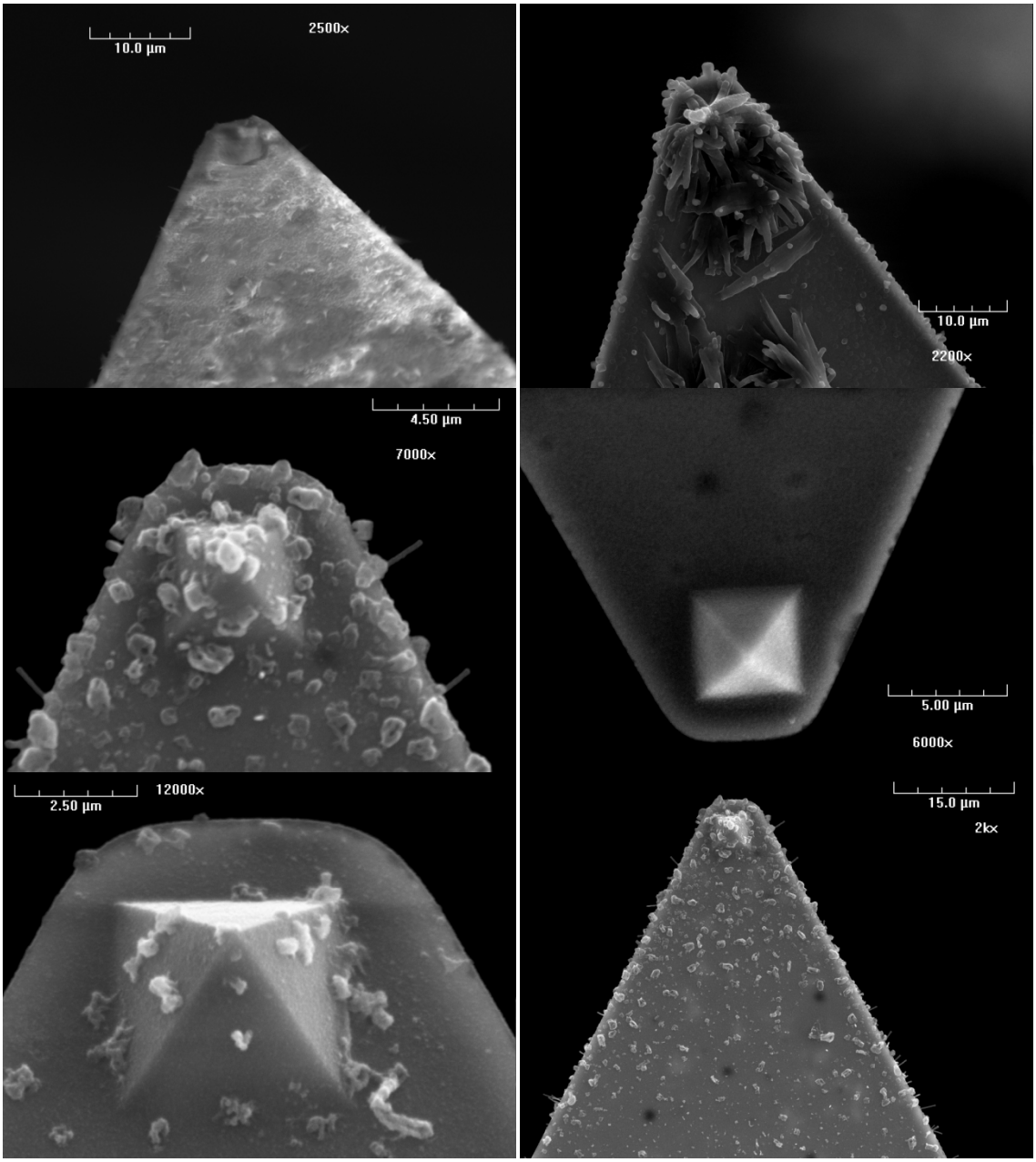

Figure I - 14: Passive pen SEM images - method II.

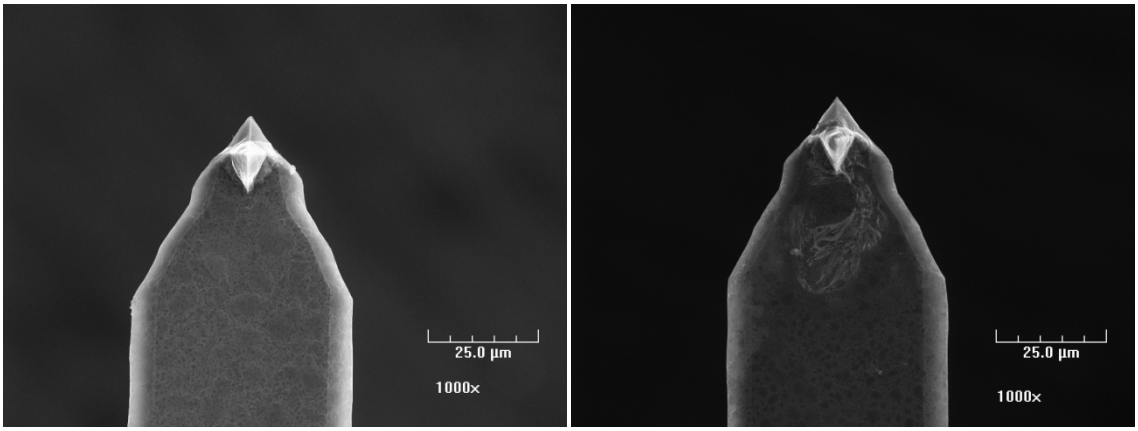

Figure I - 15: Conductive passive pen images – method I.

Passive Pen Results (Method I and II - Successful)

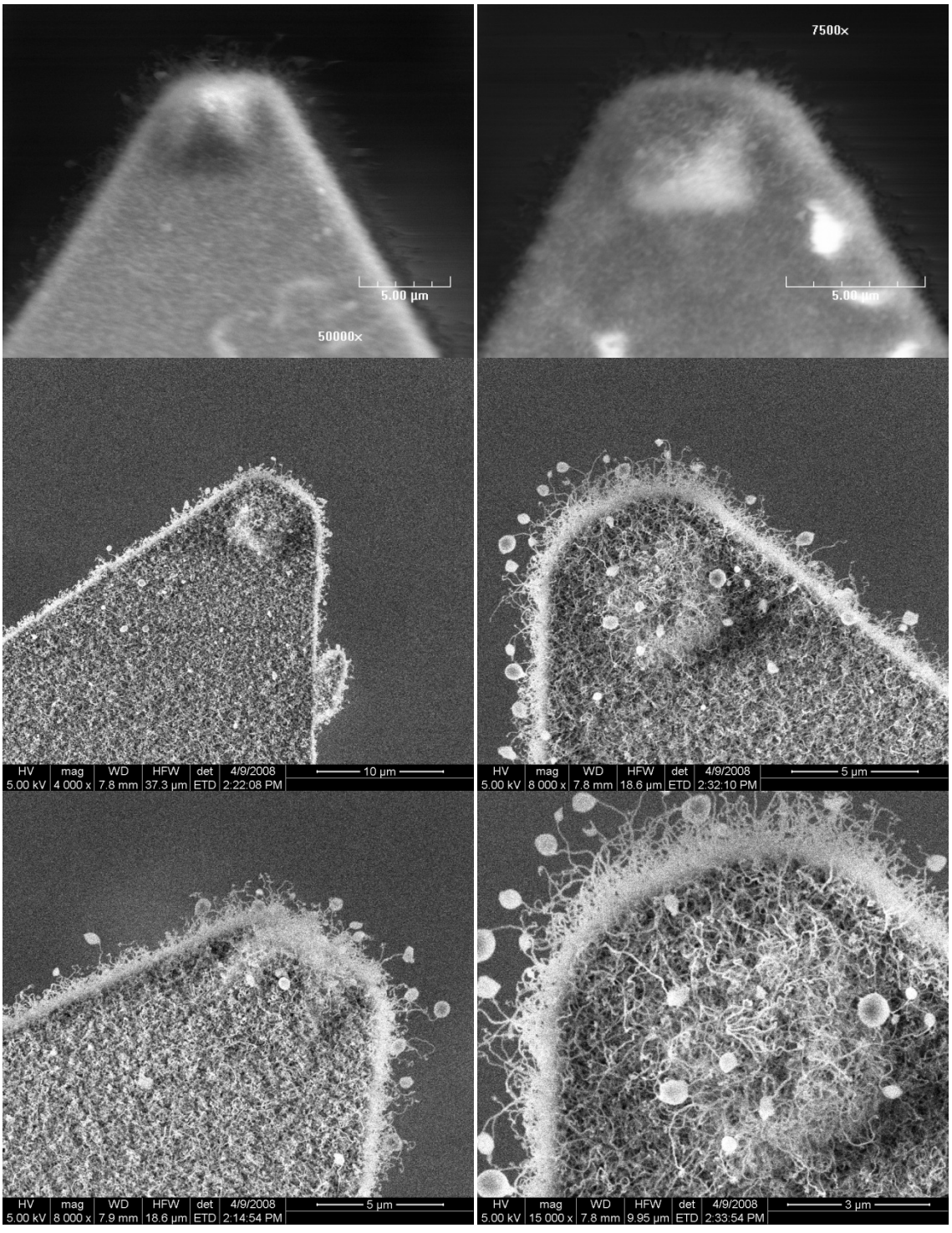

Figure I - 16: SEM images of the cantilevers with PdCl2.

APPENDIX II

MATLAB CODE

The code written to plot the data obtained from the Raman spectroscopy is shown below. The output of Raman spectroscopy is a text file, the data of which lies in the two columns, which form the X and Y coordinate data of the spectra.

```
%%%%%%%%%%%%%%%%%%%%%%%%%%%%%%%%%%%%%%%%%%%%%%%%%%%%%%%%%%%%%%%%%%%%%%%
%ROHIT V. GARGATE%%%%%%%%%%%%%%%%%%%%%%%%%%%%%%%%%%%%%%%%%%%%%%%%%%%%%%%
%Code for plotting data obtained from Raman Spectroscopy
%%%%%%%%%%%%%%%%%%%%%%%%%%%%%%%%%%%%%%%%%%%%%%%%%%%%%%%%%%%%%%%%%%%%%%%
%%%%%%%%%%%%%%%%%%%%%%%%%%%%%%%%%%%%%%%%%%%%%%%%%%%%%%%%%%%%%%%%%%%%%%%
clc
clear all
close all
%%%%%%%%%%%%%%%%%%%%%%%%%%%%%%%%%%%%%%%%%%%%%%%%%%%%%%%%%%%%%%%%%%%%%%%
%%%%%%%%%%%%%%%%%%%%%%%%%%%%%%%%%%%%%%%%%%%%%%%%%%%%%%%%%%%%%%%%%%%%%%%

%Select the INPUT text files from the user interface
[file,path] = uigetfile('*.txt','Select Text files (7 maximum)','MultiSelect','on');

%Value for adding vectors to particular spectra
blue = 0;
red = 0;
black = 0;
magenta = 0;
cyan = 0;
green = 0;
yellow = 0;

%Matrix created using above values to add vector to the main plot and the %subplots.
vectoradd = [blue*[1,1,1,1];...
        red*[1,1,1,1];...
        black*[1,1,1,1];...
        magenta*[1,1,1,1];...
        cyan*[1,1,1,1];...
        green*[1,1,1,1];...
        yellow*[1,1,1,1]];

%Get the Data from the files selected above and store it into Matrices
```

```
num = length(file);
for i=1:1:num
   if num==1
        [A,B]=textread([path,file]);
   else
        [A,B]=textread([path,file{i}]);
   end
  matA(:,i) = A;
  matB(:,i) = B;
end

%Plot the data from the matrices into 3 plots with all attributes
colour=({'blue';'red';'black';'magenta';'cyan';'green';'yellow'});

for j=[1,3,4]
  for i=1:1:num
     if j==1
        subplot(2,1,j);
        axis([100 A(length(A)) -10000 10000]);
        title('Raman Spectra','FontWeight','bold','FontSize',11);
     else
        subplot(2,2,j);
        if j==3
           axis([100  500 -10000 10000]);
           title('RBM Peaks','FontWeight','bold','FontSize',11);
        else
           axis([1100 1700 -10000 10000]);
           title('D and G Peaks','FontWeight','bold','FontSize',11);
        end
     end
     plot(matA(:,i),matB(:,i)+vectoradd(i,j),colour{i});
     grid on;axis('auto y');legend(file);hold on;
     xlabel('RamanShift \rightarrow cm-1','FontWeight','demi')
     ylabel('Intensity \rightarrow CPS','FontWeight','demi')
  end
end

%Make the plot fullscreen for saving a full sized image
 screen=get(0,'screensize');
 if screen(3)==800
    set(gcf,'Units','normalized','Position',[0 0.0467 1.00 0.84])
 elseif screen(3)==1024
    set(gcf,'Units','normalized','Position',[0.00 0.032 1.00 0.92])
 elseif screen(3)==1152
```

```
   set(gcf,'Units','normalized','Position',[0.00 0.032 1.00 0.89])
elseif screen(3)==1280
   set(gcf,'Units','normalized','Position',[0.00 0.032 1.00 0.895])
elseif screen(3)==1400
   set(gcf,'Units','normalized','Position',[0.00 0.032 1.00 0.900])
elseif screen(3)==1600
   set(gcf,'Units','normalized','Position',[0.00 0.032 1.00 0.905])
end

%Specify and save the OUTPUT files
[filename,path] = uiputfile({'*.tiff';'*.*'},'Save as');
saveas(gcf,[pathname,filename],'tiff');

%%%%%%%%%%%%%%%%%%%%%%%%%%%%%%%%%%%%%%%%%%%%%%%%%%%%%%%%%%%%%%%%%%%%%%%%%%%%%%%%
%End
%%%%%%%%%%%%%%%%%%%%%%%%%%%%%%%%%%%%%%%%%%%%%%%%%%%%%%%%%%%%%%%%%%%%%%%%%%%%%%%%
```

This code produces a graph from the output data of Raman spectra. This plot has the full spectrum on the top, while it also shows showing the three frequency regions associated with CNT divided into two different sub-plots in the bottom of the image. The images shown in this thesis report have been cropped so as to show only the bottom two plots.

APPENDIX III

PIMTEM CHIPS FABRICATION PROCESS

Masks (Customer Confidential/Proprietary Information)

Platform_Backside

Equipment type	contact	**Substrate material**	soda lime	**Coating**	chromium
Magnification	1.0	**Field**	bright	**Source**	MX
Length	5 inch	**Width**	5 inch	**Thickness**	0.09 inch
Description					

Platform_Backside 2

Equipment type	contact	**Substrate material**	soda lime	**Coating**	chromium
Magnification	1.0	**Field**	bright	**Source**	MX
Length	5 inch	**Width**	5 inch	**Thickness**	0.09 inch
Description					

Platform_Frontside Mark

Equipment type	contact	**Substrate material**	soda lime	**Coating**	chromium
Magnification	1.0	**Field**	bright	**Source**	MX
Length	5 inch	**Width**	5 inch	**Thickness**	0.09 inch
Description					

Wafer Descriptions (Customer Confidential/Proprietary Information)

P1

Number of wafers	3	**Material**	silicon	**Diameter**	100 mm
Surface finish	double side polish	**Thickness**	275 .. 325 µm	**Orientation**	100
Doping type	p-type	**Quality**	prime	**Resistivity**	1 .. 20 Ω*cm
Initial state	virgin	**Source**	MXF		

Process Sequence (Customer Confidential/Proprietary Information)

Step 1

Layout generation

Status pending

Batch size 1 **Time** 3 hour

Number of items 3

Instructions Die will be arrayed across each wafer, however only 49 die (a block of 7 x 7) will have FIB holes.

Step 2

1X LPG L10 mask

Status	pending				
Batch size	1	**Critical dimension tolerance**	0.5 µm	**Defect density**	0 > 5.0um
Magnification	1	**Mask coating**	chromium	**Mask material**	soda lime
Mask plate dimension	5x5x0.09"	**Min feature size**	3 µm		
Number of items	3				

Step 3

Super low stress silicon nitride LPCVD (50 MPa) — **Side**: both

Status	pending				
Batch size	25	**Excluded materials**	gold (category), copper	**Material**	silicon nitride
Perform clean	yes	**Pressure**	1 atm	**Thickness**	0.11 µm

Wafers

P1 (100 mm) 3 of 3

1 RCA clean with HF dip — both

2 Super Low-Stress LPCVD Silicon Nitride — both

3 Spectrophotometric film thickness measurement — both

Wafers

P1 (100 mm) 2 of 3 (W001, W003)

Step 4

Contact photolithography (Automated) — **Side**: front

Status	pending				
Alignment tolerance	1 µm	**Alignment type**	flat	**Batch size**	1
Magnification	1	**Min feature size**	1 µm	**Perform edge bead removal**	no
Perform hardbake	none	**Perform linewidth metrology**	no	**Perform microscope inspection**	yes
Perform stylus profilometry	no	**Resist thickness**	1.4 µm		

Wafers

P1 (100 mm) 3 of 3

1 HMDS Vapor Prime — both

Material HMDS **Thickness** 100 Å

2 Photoresist Spin Coat ACS200 (AZ 5214E) — front

Material AZ 5214e

3 Photoresist Softbake ACS200 — both

4 Contact flat alignment and exposure — both

Wafer category(s) P1 **Alignment type** align to flat **Mask** Platform_Frontside Mark

5 Photoresist Develop (5214E) — both

Depth 1.4 .. 3 µm **Material** AZ 5214e

6 Microscope inspection — both

Step 5

Ebeam evaporation (CHA)

Side
front

Status	pending				
Adhesion layer material	none	**Adhesion layer thickness**	0 µm	**Material**	titanium
Perform sheet resistance measurement	no	**Thickness**	0.1 µm		

Wafers

P1 (100 mm) 3 of 3

1 Titanium E-beam Evaporation — front

Material titanium

2 Stylus profilometer 1-D step measurement — front

Depth 0 .. 1000 µm

Wafers

Step 6

Lift-Off (PRS 3000), DI Rinse and SRD

Side
both

Status pending

Etchant PRS 3000 **Temperature** 80 °C

Wafers

P1 (100 mm) 3 of 3

Instructions Lift-off titanium

Step 7

Photoresist Spin Coat ACS200 (AZ 5214E)

Side
front

Status pending

Material AZ 5214e **Temperature** 110 °C **Thickness** 3.1 µm

Wafers

P1 (100 mm) 3 of 3

Instructions Spin resist to protect frontside

Step 8

Contact photolithography (Automated)

Side
back

Status	pending				
Alignment tolerance	1 µm	**Alignment type**	flat	**Batch size**	1
Magnification	1	**Min feature size**	20 µm	**Perform edge bead removal**	no
Perform hardbake	none	**Perform linewidth metrology**	no	**Perform microscope inspection**	yes
Perform stylus profilometry	no	**Resist thickness**	10 µm		

Wafers

P1 (100 mm) 3 of 3

1 HMDS Vapor Prime — both

Material HMDS **Thickness** 100 Å

2 Photoresist Spin Coat ACS200 (AZ 9245) — back

Material AZ 9245

3 Photoresist Softbake ACS200 — both

4 Contact flat alignment and exposure — both

Wafer category(s) P1 **Alignment type** align to flat **Mask** Platform_Backside

5 Photoresist Develop (AZ 9245) — both

Depth 4.5 .. 6 µm **Material** AZ 9245

6 Microscope inspection — both

Instructions Pattern backsides

Step 9

Silicon Nitride ICP Etch — **Side**: back

Status pending

Depth 0.1 µm **Etch rate** 0.19 µm/min **Gas** SF6, CF4, He

Material silicon nitride **Temperature** 25 °C

Wafers

P1 (100 mm) 3 of 3

Instructions Etch down 100 nm in silicon nitride to pattern the crystallographic orientation mask for the shallow KOH etch.

Step 10

Photoresist Stripping (Metroline) — **Side**

Status pending

Depth 0.1 .. 10 µm **Etch type** dry isotropic **Material** photoresist (category)

Wafers

P1 (100 mm) 3 of 3

Step 11

KOH Silicon Etch I — **Side**: both

Status pending

Batch size 25 **Depth** 20 µm **Etch rate** 20 µm/hour

Etchant KOH **Material** silicon **Selectivity** silicon dioxide: 600, silicon nitride: 10000, silicon: 1

Temperature 60 °C

Wafers

P1 (100 mm) 3 of 3

Instructions Etch to define the crystal orientation.

Step 12

Photoresist Spin Coat ACS200 (AZ 5214E) — **Side**

Status pending

Material AZ 5214e **Temperature** 110 °C **Thickness** 3.1 µm

Wafers

P1 (100 mm) 3 of 3

Instructions Spin resist to protect frontside

Step 13

Contact photolithography (Automated)

Side
back

Status	pending				
Alignment tolerance	1 µm	**Alignment type**	flat	**Batch size**	1
Magnification	1	**Min feature size**	100 µm	**Perform edge bead removal**	no
Perform hardbake	none	**Perform linewidth metrology**	no	**Perform microscope inspection**	yes
Perform stylus profilometry	no	**Resist thickness**	1.4 µm		

Wafers

P1 (100 mm) 3 of 3

1 HMDS Vapor Prime — both

Material HMDS **Thickness** 100 Å

2 Photoresist Spin Coat ACS200 (AZ 5214E) — back

Material AZ 5214e

3 Photoresist Softbake ACS200 — both

4 Contact flat alignment and exposure — both

Wafer category(s) P1 **Alignment type** align to flat **Mask** Platform_Backside 2

5 Photoresist Develop (5214E) — both

Depth 1.4 .. 3 µm **Material** AZ 5214e

6 Microscope inspection — both

Instructions Pattern open areas for through wafer KOH etch. Align to previous KOH etch.

Step 14

Silicon Nitride ICP Etch

Side
back

Status pending

Depth 0.1 µm **Etch rate** 0.19 µm/min **Gas** SF6, CF4, He

Material silicon nitride **Temperature** 25 °C

Wafers

P1 (100 mm) 3 of 3

Instructions Etch down 100 nm in silicon nitride to pattern the wafer backside for the through wafer KOH etch.

Step 15

Photoresist Stripping (Metroline)

Side
both

Status pending

Depth 0.1 .. 10 µm **Etch type** dry isotropic **Material** photoresist (category)

Wafers

P1 (100 mm) 3 of 3

Step 16

Ebeam evaporation (CHA)

Side
front

Status	pending		
Adhesion layer material	none	**Adhesion layer thickness**	0 nm **Material** titanium
Perform sheet resistance measurement	no	**Thickness**	50 Å

Wafers

1 Titanium E-beam Evaporation — front

Material titanium

2 Stylus profilometer 1-D step measurement — front

Depth 0 .. 1000 µm

Instructions Blanket titanium deposition on the frontsides of wafers W002 and W003.

Step 17

KOH Silicon Etch I

Side
both

Status	pending				
Batch size	25	**Depth**	300 µm	**Etch rate**	20 µm/hour
Etchant	KOH	**Material**	silicon	**Selectivity**	silicon dioxide: 600, silicon nitride: 10000, silicon: 1

Temperature 60 °C

Wafers

P1 (100 mm) 3 of 3

Instructions Etch to frontside.

Step 18

Wafer dicing

Side
both

Status	pending				
Cuts per wafer	16	**Die separation (X-direction)**	2500 µm	**Die separation (Y-direction)**	2500 µm
Resist coat substrate	Yes				

Wafers

P1 (100 mm) 3 of 3

Instructions Dice and leave on frame.

Step 19

Organic clean

Side
both

Status pending

Etchant acetone **Temperature** 25 °C

Wafers

P1 (100 mm) 3 of 3

Instructions Release from dicing tape and rinse any residue away.

Figure III - 1: Images showing the manufacturing process of the PIMTEM chips.

VITA

Rohit Vasant Gargate received his Bachelor of Engineering degree in mechanical engineering from Pune University at Pune, Maharashtra, India in 2005. He entered the mechanical engineering program at Texas A&M University in September 2006 and received his Master of Science degree in December 2008. His research interests include Dynamics, Robotics, Control Systems, Programming and Nanotechnology.

He may be contacted at the Department of Mechanical Engineering, Texas A&M University, College Station, TX 77843-3123.

His email address is rohitvg@tamu.edu.